INAUGURAL – DISSERTATION

zur
Erlangung der Doktorwürde
der
Naturwissenschaftlich-Mathematischen
Gesamtfakultät
der
Ruprecht-Karls-Universität
Heidelberg

Vorgelegt von

Diplom-Chem. **Domnica Cristina Breban**
aus: Bukarest, Rumänien

Tag der mündlichen Prüfung: 20 April 2007

Thema

Provenance and Characterization of Aquatic Actinide Colloids: Interaction of Actinides with Aluminosilicate and Humate Colloids

Gutachter:	Prof. Dr. Thomas Fanghänel
Gutachter:	Prof. Dr. Margot Isenbeck- Schröter

Acknowledgements

The experiments described in this work were performed at the Institute of Radiochemistry (RCM), Technical University München (the radiometric experiments) and Institute of Nuclear Waste Management (INE), Forschungszentrum Karlsruhe (the spectroscopic measurements).

I would like to express my deepest gratitude to Prof. Dr. Jae-Il Kim, the initiator of this research subject, for offering me the chance to work on the topic and to Dr. Maria-Anna Kim, my direct supervisor, who shaped my work through her ideas, scientific guiding and critical advices. They both were my mentors and the accomplishment of this thesis would not have been possible without their help.

Special consideration goes to my doctoral supervisor, Prof. Dr. Thomas Fanghänel (FZK), for providing me the opportunity to work at INE-FZK and for his permanent support. I would also like to thank PD Dr. Petra Panak (INE), for the help during the EXAFS measurements, many valuable discussions (regarding TRLFS and not only) and suggestions for revising the thesis.

I am very grateful to Dr. Andrey Priemyschev (RCM) for sharing with me his experience and knowledge and very good collaboration.

Special thanks are due to the colleagues from the INE-EXAFS group: Dr. Melissa Denecke for the very useful discussions and revision of the EXAFS chapter of the thesis and Drs. Kathy Dardenne and Jörg Rothe for assistance during the EXAFS measurements, data analysis as well as for helpful discussions.

A number of other people contributed to the realization of the present work. Thanks are due to Dr. Christian Marquardt and Dr. Gunnar Buckau from INE, for providing the radioactive standard solutions and the humic acid, as well as to Dr. Alexander Mansel (IIIF Leipzig) for labeling the humic acid. I would also like to thank Dr. Reinhard Klenze (INE) for his very kind assistance regarding the formalities in obtaining the German visa and those at the University of Heidelberg.

It was a chance, a pleasure and great experience for me to be one of the coworkers of the RCM and INE; I would like to thank from all my heart to all people from the two institutes for the very friendly atmosphere and their helpful attitude. I own special thanks to Jörg Aign (RCM), for his patience in answering my numerous technical questions.

ANKA Angstromquelle Karlsruhe is acknowledged for the provision of the beam-time for the EXAFS measurements. The financial support for the Ph.D grant provided by the Helmholtz Association, FZK Germany, is also gratefully acknowledged.

Summary

One of the major uncertainties in the process of actinide migration is due to the limited knowledge about the mechanism of formation and stability of the actinide colloids. During the formation of hydroxy-aluminosilicate (HAS) colloids as kernels of natural aquatic colloid, trace actinide ions may be incorporated and become colloid-borne species.

The present work investigates the behaviour of actinides (An) of different oxidation states in the process of aquatic colloid formation, e.g. at the generation of aluminosilicates (HAS) by co-nucleation of Si and Al in absence or in presence of natural humic acid (HA). The study comprises three parts.

The first part of the work concentrates on the interaction of tri-, tetra-, penta- and hexavalent actinide ions with HAS colloids. The HAS colloids are synthesized through heterogeneous nucleation of Si and Al in the pH region 4 to 9 at room temperature and atmospheric pressure. Si concentration is maintained either below or above the saturation concentration of amorphous silica ($2x10^{-3}$ M). In the former case 10^{-3} M Si is mixed with 10^{-5} M Al and Si is present in solution as monosilicic acid. In the latter case, 10^{-2} M Si is mixed with 10^{-4} M Al and polysilicic acid prevails in solution. The following tracer nuclides are introduced in the co-nucleation process: ^{241}Am(III), ^{234}Th(IV), ^{237}Np(V) and ^{233}U(VI). Colloids are separated from solution and precipitate by sequential filtration and ultrafiltration. Definition of the optimum conditions for the formation of colloid-borne actinide species is ascertained by radiometric assay, determining the actinide fraction in the colloidal phase as a function of pH, conditioning time, concentration and concentration ratio of the involved components. Several methods are further applied for the appraisal of the chemical binding state of actinides in the HAS colloids as well as of Al in aluminosilicate solutions: TRLFS (time resolved laser fluorescence spectroscopy), EXAFS (extended X-ray absorption fine structure) spectroscopy and ligand displacement method (using EDTA as competing ligand). The radiometric and spectroscopic results show that the co-nucleation of An with Si and Al forming HAS colloid-borne actinides is more favourable with increasing pH, and concentration of Si and Al, parameters favouring the element hydrolysis. Accordingly, Np does not interact with the HAS colloids in its non-hydrolysis pH range ($\leq$ 9), whereas maximum incorporation of An(III, IV, VI) into the colloidal phase is observed for HAS generated from polysilicic acid in the pH range

7-9. Under these conditions, the desorption experiments show that the Al-O-Si binding as well as well as the Th(IV)/U(VI)-HAS colloid binding are EDTA resistant, whereas Am(III)-HAS colloid binding is not EDTA resistant. The affinity for conucleation with HAS (Th(IV) ~ U(VI) > Am(III)) appears to be higher for the elements with higher tendency toward hydrolysis. The less hydrolyzing tendency of Am(III) might be also the reason of its discrimination against Al(III), Th(IV) and U(VI) at the co-nucleation with polysilicic acid.

The second part of the work further concerns the behaviour of An(III, IV, VI) at the interaction with humate colloids. In addition to actinide activity measurements, ^{14}C-labelled natural humic acid is used in order to facilitate the tracing of humic colloids behaviour. The conditions of colloid formation are investigated by radiometric assay as a function of pH (6.6-7.8), time, concentration of HA (0.6-8 mg/L), Al ($1x10^{-5}$-$1x10^{-4}$ M) and An ($5x10^{-8}$-$1x10^{-5}$ M). Formation of humate-colloid-borne An species appears to be very efficient for trace amount of actinides at HA concentration close to the average level encountered in natural waters (approximately 5 mg/L), as long as the proton exchange capacity of HA for complexation of Al species is not exceeded. The generation of humate-colloid-borne species is distinctively favored for the non-hydrolyzed ionic species. Accordingly, due to the higher hydrolysis tendency of Al(III), its ionic species have lower tendency to complex with humic colloids. Among the An(III, IV, VI) present at tracer concentration, the less hydrolyzing Am(III) shows higher affinity for formation of humate-colloid-borne species in the neutral pH range and for HA concentration at the average level of natural waters. Generation of humate-colloid-borne An(IV, VI) is enhanced by increasing HA concentration or decreasing the An/HA concentration ratio.

The third part of the work follows the conditions for formation of colloid-borne An(III, IV, VI) in the mixed system containing the competing HAS and humic colloids. The simultaneous presence of HAS and HA generally enhances the stability region (in respect with pH and Si/Al concentration) of the colloid-borne An species. The formation of mixed HAS-humic colloids with synergic binding appears to be responsible for the stable incorporation of An into the colloidal phase, as ascertained for Cm(III) by TRLFS. Such a synergic effect is assumed to be related to the two different and complementary mechanisms exhibited by the HAS and HA colloids in binding the actinides. Formation of mixed HAS-humic colloid-borne An could be expected under environmental conditions favouring the presence of partially hydrolyzed An species, interacting with both HAS and HA.

Zusammenfassung

Eine der größten Unsicherheiten im Migrationsprozess der Actiniden ergibt sich aus den begrenzten Kenntnissen bezüglich des Bildungsmechanismus und der Stabilität der kolloidalen Actinidspezies. Während des Kolloidbildungsprozesses von Hydroxyalumosilikaten (HAS), welche Vorstufen für natürliche aquatische Kolloide darstellen, können Actinidionen inkorporiert und so als Kolloidspezies transportiert werden.

Diese Arbeit beschäftigt sich mit dem Verhalten von Actiniden (An) unterschiedlicher Oxidationsstufen während des aquatischen Kolloidbildungsprozesses, d.h. der Bildung von Alumosilikaten durch Si(IV) und Al(III) Kopolymerisation sowohl in Ab- als auch in Anwesenheit von natürlicher Huminsäure (HA). Die Arbeit umfasst drei Teile.

Das erste Teil befasst sich mit den Wechselwirkungen von tri-, tetra-, penta- und hexavalenten Actinidionen mit HAS-Kolloiden. Die HAS-Kolloide werden durch Kopolymerisation von Si und Al in einem pH-Bereich zwischen 4 und 9 bei Raumtemperatur und Atmosphärendruck synthetisiert. Hierbei werden Si-Konzentrationen entweder unter- oder oberhalb der Sättigungskonzentration von amorphem SiO_2 ($2x10^{-3}$ M) verwendet. Im ersten Fall werden 10^{-3} M Si zu einer 10^{-5} M Al-Lösung gegeben. Dabei liegt das Si in der Lösung als Monokieselsäure vor. Im anderen Fall werden Konzentrationen von 10^{-2} M Si und 10^{-4} M Al verwendet, wobei Polykieselsäuren in der Lösung dominieren. Folgende Nuklide werden dem Kopolymerisationsprozess zugesetzt: ^{241}Am(III), ^{234}Th(IV), ^{237}Np(V) und ^{233}U(VI). Die Kolloide werden durch Filtration und anschließende Ultrafiltration von der Lösung getrennt. Die optimalen Bedienungen für den Bildungsprozess der kolloidalen Actinidspezies werden durch radiometrische Untersuchungen bestimmt. Dabei werden die Actinidfraktionen in der kolloidalen Phase unter verschiedenen Kombinationen von Parametern wie pH-Wert, die Konditionierungszeit, die Konzentration und das Konzentrationsverhältnis der Komponenten bestimmt. Verschiedene Methoden werden für die Untersuchung des chemischen Bindungszustands der Actiniden in den HAS-Kolloiden sowie von Al in den Alumosilikaten verwendet: TRLFS (zeitaufgelöste Laserfluoreszenzspektroskopie), XAS (Röntgenabsorptionspektroskopie) sowie die sog. „Ligandenaustauschmethode“ (mit EDTA als Ligand). Die radiometrischen und spektroskopischen Ergebnisse deuten daraufhin, dass die HAS-Kolloidbildung durch

Kopolymerisation von An mit Al und Si mit zunehmendem pH-Wert und zunehmenden Si- und Al-Konzentrationen favorisiert wird. Diese Parameter begünstigen auch die Elementhydrolyse und die Polymerisationsreaktion. Np zeigt keine Wechselwirkungen mit den HAS-Kolloiden für pH < 9 (unterhalb des Hydrolysebereichs). Die maximale Inkorporation von An (III, IV, V) in die HAS-Kolloide aus Polykieselsäure wird dagegen für pH-Werte zwischen 7 und 9 beobachtet. Unter diesen Bedingungen zeigen die Desorptionsversuche mit EDTA, dass sowohl die Al-O-Si-Bindungen als auch die Th(IV)/U(VI)-HAS-Kolloidbindungen in Anwesenheit von EDTA stabil sind. Im Gegensatz dazu erfolgt für Am(III) eine Desorption von den HAS-Kolloiden. Die Affinität zur Kopolymerisation mit HAS (Th(IV) ~ U(VI) > Am(III)) ist für Actinide mit einer starken Neigung zur Hydrolyse deutlich höher. Die schwächere Tendenz des Am(III) zur Hydrolyse kann auch ein Grund für das unterschiedliche Verhalten im Vergleich zu Al(III), Th(IV) und U(VI) bei der Kopolymerisation mit Polykieselsäure sein.

Der zweite Teil der Arbeit beschäftigt sich mit dem Verhalten der An (III, IV, VI) bei der Wechselwirkung mit Huminkolloiden. Zusätzlich zu den Messungen der Actinidaktivitäten wird ^{14}C-markierte Huminsäure verwendet, um das Verhalten der Huminkolloide leichter zu verfolgen. Die Bedingungen für die Kolloidbildung werden durch radiometrische Versuche als Funktion des pH-Wertes (6.6-7.8), der Zeit und der HA (0.6-8 mg/L), Al ($1x10^{-5}$-$1x10^{-4}$ M) und An ($5x10^{-8}$-$1x10^{-5}$ M)-Konzentration untersucht. So lange die maximale Protonenaustauschkapazität der HA für die Komplexation mit Al-Spezies nicht erreicht ist, lässt sich die Bildung der actinidhaltigen Huminkolloide anhand der Aktivität der Actinidionen sehr effektiv im für natürliche Grundwässer relevanten Konzentrationsbereich (ca. 5 mg/L) detektieren. Die Bildung von kolloidalen An-Humatspezies ist im Falle von nicht hydrolysierten ionischen Spezies klar favorisiert. D.h., wegen der höheren Tendenz von Al(III) zur Hydrolyse ist die Tendenz zur Komplexbildung mit Huminkolloiden weitaus geringer. Ein Vergleich der An(III, IV, VI), die in Tracerkonzentrationen vorliegen, zeigt, dass Am(III) die höchste Affinität für die Bildung von actinidhaltigen Huminkolloiden aufweist. Die Tendenz zur Hydrolyse ist insbesondere im neutralen pH-Bereich deutlich geringer. Die An(IV, VI)-Huminkolloidbildung wird entweder durch höhere HA-Konzentrationen oder ein kleineres An/HA – Konzentrationsverhältnis erhöht.

Im dritten Teil der Arbeit werden Bedingungen zur Bildung von An(III, IV, VI)-Kolloiden in gemischten Systemen untersucht, die sowohl HAS als auch Huminkolloide

enthalten. Die gleichzeitige Anwesenheit von HAS und HA haben generell einen stabilisierenden Einfluss auf die Pseudokolloidbindung von An (bezüglich pH-Wert und Si/Al-Konzentration). Die Bildung von stabilen ternären An-HA-HAS-Kolloiden, wie sie für Cm(III) durch TRLFS nachgewiesen wurden, führt bezüglich des Einbaus der Actiniden in die kolloidale Phase zu einem synergistischen Effekt. Solche synergistische Effekte sind durch unterschiedliche komplementäre Mechanismen bei der Wechselwirkung von An mit HAS und HA-Kolloiden zu erklären. Die Bildung von stabilen ternären An-HA-HAS-Kolloiden tritt vorwiegend unter für Grundwässer relevanten Bedingungen auf, und ist somit auch in natürlichen Systemen zu erwarten, wo ebenfalls partial hydrolysierte An-Spezies vorliegen, welche Wechselwirkungen sowohl mit HAS als auch mit HA zeigen.

Contents

1. Introduction

Aquatic colloids are omnipresent in natural waters [1, 2, 3] and composed of inorganic elements with different oxidation states via oxo-bridging [4] or inorganic-organic composites in which ubiquitous humic acid is normally involved [5, 6, 7]. Their chemical composition, number density and particle size distribution vary depending on the geochemical conditions of their provenance. Hence, in natural systems the particle size distribution has been generally observed between 1nm and up to 100 nm, but very often below 50 nm [8, 9]. For this size range, the typical number density has been reported to vary between 10^8 to 10^{14} particles/L water [5, 10]. Regardless of their composition, aquatic colloids have been recognized to play a significant carrier role in the migration of trace contaminants including radionuclides in aquifer systems [10, 11]. Several investigations have demonstrated that low soluble, surface reactive radionuclides could travel much farther and much faster than anticipated from traditional solute transport models taking into account the thermodynamic solubilities [12, 13, 14]. In all cases the enhanced radionuclide transport has been attributed to the association of contaminants with the mobile colloidal phase. As highly charged cations, actinides manifest strong tendency towards hydrolysis/poly-nucleation and complexation, and hence, high potential for incorporation into aquatic colloids [9, 10]. Numerous studies have concentrated on the actinide interaction with aquatic colloids [15-21], however the process for formation of aquatic colloid-borne actinides is still not well understood, a key issue being the stability of such colloids [7]. Therefore, the appraisal of colloid-borne actinide generation is necessary for a possible prediction of the colloid-facilitated migration of actinides which is a requirement for the long-term safety analysis of nuclear waste repositories.

Hydroxyaluminosilicate (HAS) colloids are known to be kernels for a variety of aquatic colloids [10, 22-24], as Al and silicic acid are always present in natural water and may undergo co-nucleation via oxo-bridging to form stable water-soluble composites [1]. In the course of HAS-colloid formation, trace elements are easily integrated in the co-nucleation process and become colloid-borne species. This process has been recently investigated for tri-and tetravalent actinides [25-28].

The present work is a continuation of this series and pursues the behavior of actinides of higher oxidation states (penta-, hexavalent) and aspects regarding the stability

of the HAS-colloid-borne actinides, (III to VI). For a better approach to the complex natural conditions, the formation of HAS-colloid-borne actinides is further analyzed in the presence of humic acid (HA). As humic acid is an ubiquitous component of natural waters and has a strong affinity to complex metal ions of higher charges ($z \geq 3+$) [7, 9, 29], its impact on the formation of HAS colloids and hence of HAS-colloid-borne actinides is expected to be significant. The selected actinides are Am(III), Th(IV), Np(V) and U(VI). Am, Np and U are actinides of most concern from radiological point of view, due to their long-lived isotopes and large abundance in the spent fuel to be disposed. Due to its stable oxidation state, Th(IV) is taken as a model element to characterize the behaviour of redox sensitive actinides like Pu, U and Np which may be reduced to the tetravalent state at low redox potential in the near field of a nuclear repository [30, 31].

2. Natural and actinide aquatic colloids: literature

Colloidal systems are heterogeneous systems, containing very small particles which can remain for an indefinite period in dispersed state in solution. The range of colloidal particle size is commonly defined between 1 and 1000 nm in diameter.

2.1 Theory of aquatic colloid formation [1, 2, 32].

2.1.1 Colloid generation

There are two general ways in which aquatic colloids may be formed: by building up particles from molecular or atomic units, or by breaking down particles from the solid matrix, processes termed respectively condensation and dispersion:

Elements with high oxidation state (≥ 3), such as Al(III), Si(IV) or actinides, tend to minimize their positive charge by hydration, hydrolysis and polymerization. This process includes formation of a supersaturated solution, the release of supersaturation by formation of nuclei or by condensation upon nuclei already present, followed by growth to larger particles. The reverse process for colloid formation, namely dispersion, involves weathering of the solid material in contact with the water, which can be either physical fragmentation of non-cemented grain-size particles or geochemical alteration or both, followed by suspension of detached particles in the liquid phase. These processes are illustrated schematically in Fig. 2.1.

Under certain conditions, nanoparticles can thereby be stabilized in the colloidal phase, a process which is not completely understood. Theoretical considerations concerning colloid generation and stability relevant to the present experimental investigations are conceptually summarized in the followings.

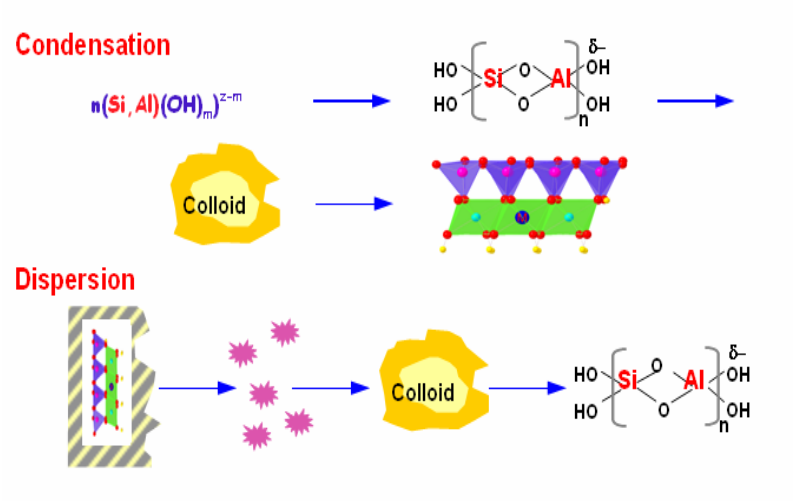

Fig. 2.1 General pathways for the formation of inorganic aquatic colloids such as aluminosilicate colloids [25].

Colloidal interface free energy

The behavior of colloids is governed primarily by their large interfacial area. The interface is defined as the boundary between the adjoining bulk phases that comprise the colloid system, e.g. liquid/solid in the case of aquatic colloids. Within each bulk phase forces acting on a molecule from all directions are balanced. The molecules at the interface interact simultaneously with molecules from both liquid and solid phase. Since forces of attraction are greater between the molecules on the solid phase than between those of the liquid phase, the molecules at the interface are attracted more strongly towards the solid phase. The energy input, required to compensate for this imbalance of intermolecular forces, is the origin of the colloidal free energy. The high reactivity of colloids (activated solid state) originates from the tendency to minimize the free energy.

The questions are, where does this activation energy come from, what kind of energy transfer occurs at deactivation, which mechanisms inhibit complete deactivation, so that the colloidal state, although thermodynamically unfavorable, persists over a long time span and how can the underlying parameters be controlled ? Theoretic thermodynamic and kinetic approaches which are helpful to conceive appropriate experiments to answer these questions are summarized in the followings.

Formation of colloids through condensation

Spontaneous growth of particles out of their solution requires formation of nuclei. The free energy of the formation of a nucleus, ΔG, consists of the energy gained from making bonds and the work required to create a surface as expressed in thermodynamic terms:

$$\Delta G_j = -4 \pi r^3 k_B T \ln S /3V + 4 \pi r^2 \gamma \qquad (2.1)$$

where r is the radius of the nucleus, V the molecular volume, k_B the Boltzman constant, T the absolute temperature, S the supersaturation (the ratio of the actual concentration and solubility equilibrium concentration), and γ the interfacial energy ($\gamma = r k_B T \ln S / 2V$).

Fig. 2.2 shows the free energy of formation of a spherical nucleus as a function of its size, calculated for different supersaturation ratios (a/a_0). The height of the maximum, ΔG^*, is the activation barrier to the nucleation process of nuclei of radius r_j. The activation energy, ΔG^*, as well as the size of the critical nucleus decreases with increasing supersaturation.

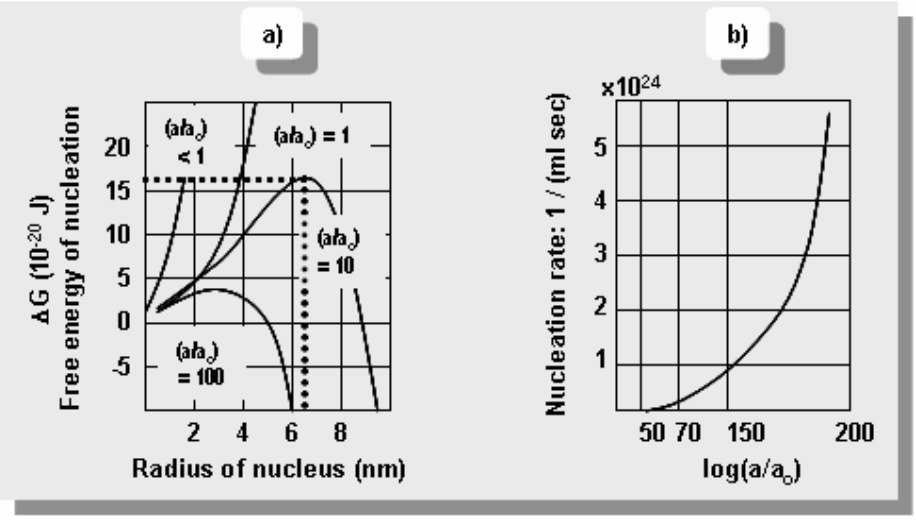

Fig. 2.2: (a) Free energy of nucleus formation calculated as a function of the radius for different supersaturated ratios (Eq.1). The maximum ΔG* is the activation barrier to the generation of nuclei of radius r_j; (b) Nucleation rate calculated as a function of the critical supersaturation [25].

Introduction of foreign solid surfaces for catalyzing the nucleation process, by reducing the energy barrier is the principle of heterogeneous nucleation, the predominant process of the formation of colloids and crystals in natural waters. If the foreign substrate is similar to the product of nucleating components, the interfacial energy between the two solids is smaller than the interfacial energy between the product and the solution and nucleation may take place at lower supersaturation on a solid substrate than in solution. The temperature affects also the critical supersaturation ratio, which decreases with increasing temperature.

The rate of the formation of nuclei, V_1, may be expressed as:

$$V_1 = A \exp(-\Delta G^* / kT) \qquad (2.2)$$

where A is the factor related to the efficiency of collisions between ions and molecules. Accordingly, the rate of nucleation is controlled by the interfacial energy, the supersaturation, the collision frequency efficiency and the temperature.

The rate of particle growth is determined by the rate of diffusion of substance from supersaturated volumes within the bulk towards those particles which are surrounded by thin envelopes of solution in equilibrium with the solid. It may be expressed by the general equation

$$V_2 = A (\ln S)^n \qquad (2.3)$$

where A and n are adjustable parameters.

The relative rates of the 2 processes, nucleation and growth which compete both for the material in the supersaturated solution, determine the number and the size of the particles. At high supersaturation, the nucleation rate may be very fast and most of dissolved mass is transformed in critical nuclei, leaving little material available for further crystal growth. A large number of small particles may be formed. Formation of low number of big size particles is favored at low supersaturation. Inhomogeneity of the system with volumes of different degrees of supersaturation results in particles of various sizes (polydisperse system).

Colloidal electric double layer

Most substances acquire a surface electric charge when brought into contact with a polar (e.g. aqueos) medium, possible charging mechanisms being ionization, ion adsorption and ion dissolution. The ionization of functional groups depends on the nature of the mineral and on the pH, and leads to positively or negatively charged species at low pH and high pH, respectively. A net surface charge can further be acquired by the unequal adsorption of oppositely charged ions. In natural aquatic media, the surfaces carry more often a negative charge. The surfaces which are already charged (by ionization) show high tendency to adsorb ions of opposite charge, which may cause even a reversal of the surface charge. If surfactant ions are present, their adsorption will usually determine the surface charge. In addition to specific adsorption, the net particle charge of some solids may arise from the preferential dissolution of some ions, from lattice imperfections at the solid surface or by isomorphic replacements within the lattice.

The surface charge influences the distribution of the nearby ions in the polar medium. The counter-ions are attracted by the oppositely charged solids. In the same time, these ions have the tendency to diffuse away from the surface toward the bulk phase where their concentration is lower. The net result of the two processes is an equilibrium distribution of ions in which their concentration gradually decreases with increasing distance from the solid surface. Simultaneously there is a deficit of co-ions in the vicinity of the surfaces due to the electrostatic repulsions and a gradually increase of their concentration with increasing the distance from the solid surface. The result is the generation of an electric double layer (EDL) at the solid-liquid interface. EDL consist of three regions with distinct dielectric behavior (Fig. 2.3):

1) the Stern layer, a layer with preferentially orientated water molecules in contact with the boundary, where the ions are specifically adsorbed without their hydration shell.

2) the outer Helmholtz layer, a region with both free water molecules and molecules attached to hydrated ions and defined by the closest approach of a hydrated ion to the surface.

3) the Gouy-Chapman diffuse layer is the region where the concentration of the counterions decreases with increasing distance from the interface.

The electric potential at the surface, Ψ_0, or the electric potential in the Stern plane, Ψ_δ, are not accessible by direct experimental measurements but the surface potential can be calcu-

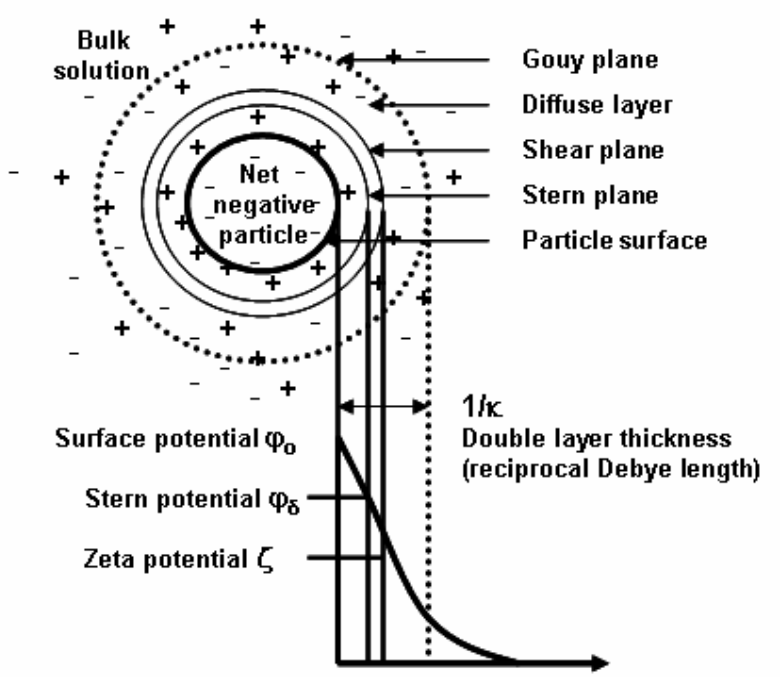

Fig. 2.3 Colloidal electric double layer at the solid-liquid interface.

lated from the experimentally determined surface charge. The hydrodynamic immobile liquid addering to the particle surface is separated from the mobile liquid by a shear plane, which has non-zero mobility relative to the surface. The electric potential in the shear plane is reflected by the potential gradient across the mobile part of the double layer, the elektrokinetic potential (zeta potential), ζ.

$$\zeta = 4\pi\sigma_0 d / \varepsilon \qquad (2.4)$$

where σ_0 is the charge at particle surface, d is the thickness of the mobile part of the EDL and ε is the dielectric constant of the medium.

The double-layer thickness is given by the reciprocal Debye length:

$$1/\kappa = (\varepsilon R T / 8\pi F^2 c z^2)^{1/2} \qquad (2.5)$$

where F is the Faraday constant, c and z are the concentration and the valence of the electrolyte, respectively. Increasing ionic strength decreases the thickness of the double layer and reduces the electrokinetic potential.

2.1.2 Colloid stability

Brownian motion of colloids

Water molecules in permanent thermal movement hit the colloidal particles from opposite sides. The smaller the particles, the less balanced is the molecular bombardment and the more intensive will be the movement. A consequence of the Brownian movement is the diffusion of colloidal particles. The first Fick's law gives the the mass, dm, transferred across an area O, in the time interval dt, as a result of the concentration gradient, dc/dx, when a certain phase is dispersed along the x axis.

$$dm/dt = - D O (dc/dx) \quad (2.6)$$

where D is the diffusion coefficient. The diffusion coefficient depends on the properties of the dispersed phase and of the dispersing medium. For colloidal particles D is related to the friction coefficient, B, between the particles and the dispersing medium by the expression $D = k_B T/B$. The magnitude of B depends on the dimensions and shape of the particles. For spherical particles having a radius r, when the viscosity of the medium is η, the diffusion coefficient becomes:

$$D = k_B T / 6\pi\eta r \quad (2.7)$$

The Brownian motion is the reason of the frequent collisions between the colloidal particles. Depending upon whether the interaction forces between the particles during such collisions are attractive or repulsive, the colloids will agglomerate or stabilize (elaborated below).

Colloid stability: DLVO theory

The quantitative description of the interaction between particles of like charge is given by the generally accepted DLVO (Derjaguin, Landau, Vervey und Overback) theory. According to the theory, the particle interaction is modeled as two spheres approaching each other until their diffuse layers inter-penetrate, the potential energy of interaction,

E, being calculated as the sum between the electrostatic repulsive energy (E_R) and van der Waals attraction energy (E_A). The electrostatic energy E_R, (conventionally considered positive) is approximately an exponential function of the interparticle distance (d) with a range of the order of the thickness of the double layer ($1/\kappa$); the attractive energy E_A (considered negative) decreases with an inverse power of the interparticle distance. The potential energy of interaction can be described by the following equation (simplified and valid only for thick plate particles, e.g. clay tactoids):

$$E = E_R + E_A = (64\ c\ R\ T\ \Gamma^2\ /\kappa\ )\ (e^{-\kappa d}) - (K\ /\ 2\ d^2) \qquad (2.8)$$

where K is a constant depending on the nature of the dispersing medium, the particle thickness and its chemical composition, and Γ is defined as follows:

$$\Gamma = [(\exp(z\ F\ \Psi_\delta/2RT)) - 1]\ /\ [(\exp(z\ F\ \Psi_\delta/2RT)) + 1] \qquad (2.9)$$

Two general types of potential energy curves are presented in Fig. 2.4**:** in a) $E_R > E_A$ and the total potential energy curve shows a repulsive energy maximum, whereas in b) the van der Waals attraction (E_A) predominates at any inter-particle distance. The maximum in the energy curve is an energy barrier. If the potential energy maximum is large compared to the thermal energy of the particles (RT), the system should be stable; otherwise the system should agglomerate. The height of the energy barrier to agglomeration of colloids depends on the magnitude of Ψ_δ (and ζ) and upon the repulsive forces (i.e. upon $1/\kappa$). The higher the elektrokinetic potential, the higher is the repulsion between the solid particles and the stability of the colloidal system increases. The DLVO theory to explain stabilization of colloids has been extended and may include besides electrostatic and van der Waals forces, also steric forces (generally repulsive) as well as bridging forces (attractive) induced by adsorbed long-chain polymer.

Colloid stability: kinetics

Colloid stability depends on an energy barrier and is therefore also a question of kinetics and rates of agglomeration. In the kinetics of agglomeration process rapid and slow agglomeration are distinguished. In the case of rapid agglomeration the energy barrier is

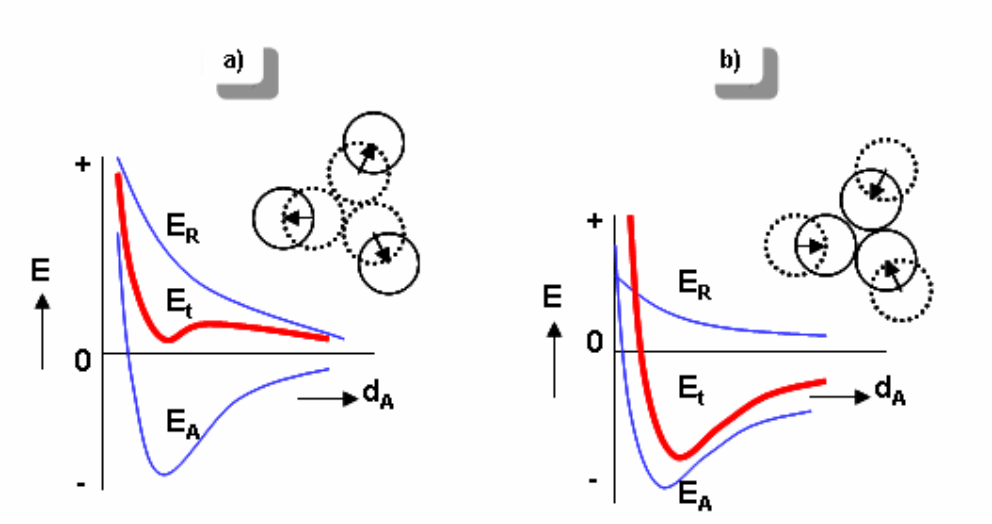

Fig. 2.4 Potential energy of particle-particle interaction (E_t) calculated as the sum of the electrostatic repulsive Energy (E_R) and the van der Waals attractive energy (E_A) (Eqs. 2.8 and 2.9): (a) $E_R > E_A$: particle repulsion and colloid stabilization; (b) $E_A > E_R$: particle attraction and colloid agglomeration

absent or too small to hinder particles from coming into contact (critical electrolyte concentration). In this case every collision leads to irreversible agglomeration. In this case the decrease in time of the particles concentration (N = number of particles / cm^3) in a monodisperse suspension due to collisions by Brownian motion is represented by

$$-dn/dt = k_p N^2 \qquad (2.10)$$

where k_p is the rate constant ($cm^3\ s^{-1}$). As given by Smoluchowski, the constant rate, k_p can be expressed as

$$k_p = 8\ D\ \pi\ r \qquad (2.11)$$

Substituting the diffusion coefficient D from the equation 2.7 in the equation 2.11, the rate of the reaction becomes

$$-dn/dt = 4\ k_B T\ N^2 / 3\eta \qquad (2.12)$$

and it may be concluded that in monodisperse systems the rate of fast agglomeration is independent on the size of the particles. In practice, the right hand side of the equation is multiplied by a factor, $\alpha_{p,}$ which is the fraction of collisions leading to permanent agglomeration. The extended Smoluchowski theory for polydisperse systems shows that the rate of coagulation of particle with different size is much greater than the rate of coagulation of particles of same size. The smaller particles disappear more quickly than the larger ones.

2.2 Natural aquatic colloids in laboratory

Colloids are present in all natural waters to some extent, their amount and nature depending on the associated geological structure. Accordingly, a wide variation appears in their chemical composition, size distribution and number density. Aquatic colloids may be of inorganic nature, like: clays, silica, aluminum oxide minerals, as well as hydroxides of metal, e.g. iron, or, organic polyelectrolytes, like humic acid, with incorporation of inorganic elements, depending on how the waterborne trace inorganics and organics are dispersed from the given geochemical composition [6, 30].

2.2.1 Aluminosilicate colloids

Aluminosilicate colloids in nature

Aluminosilicates constitute the large majority of rock and soil forming minerals in nature, comprising clays, micas, feldspars. Clay minerals are essentially hydrous layer aluminosilicates (phyllosilicates), which carry a permanent negative charge due to the substitution of cations with variable valence in the phyllosilicates sheets structure, (e.g. Al for Si and Mg, Fe for Al), charge which is balanced by the cations in the interlayer. In the aluminosilicates structure, an additional, pH-dependent charge originates from protonation/deprotonation of the –OH groups at the edges of the planes. Due to their high capacity for retaining water and their cation exchange capacity, clay minerals like smectites have been proposed as backfill material at nuclear waste disposal sites [33]. A special type of highly hydrated, secondary aluminosilicates, are protoimogolite and imogolite,

with a Si/Al ratio of 0.5-1, with spherical or ring shaped morphology and particles diameter of 3.5-5.0 nm (Fig. 2.5). Their structure has Si in tetrahedral coordination and Al in octahedral coordination, though not in sheets as in the case of phyllosilicates. The AlOH (aluminol) outer surface is connected to the SiOH (silanol) inner surface through O bridges [34]**.** Their structure is limited to the range of very small particles (short-range order), which is in contrast to the other clay minerals. Poor-crystalline aluminosilicates, like imogolite and allophane are essential transient phases in geochemical processes such as soil weathering and adsorption phenomena. Although the occurrence of these minerals is commonly reported for soils with accumulated volcanic ash like andisols and spodsols, they have been also identified in stream sediments, coatings of primary particles and soils derived from igneous and sedimentary rock sandstones in different geographical regions [35]. Much attention has been recently paid to the aqueous hydroxyaluminosilicates (HAS) of the imogolite type in diverse contexts [22-24, 36]. Besides their geochemical relevance, HAS appear to be involved in biochemical reactions related to the toxicity of Al for plants and animals. A review article [24] has summarized the present knowledge on silicate complexes of Al(III) in aqueous systems. It has been concluded from kinetic studies on Al(III)-Si(IV) interactions at high pH, that simple hydroxyaluminosilicates (HAS) probably form and dissociate quickly even at low to neutral pH, so that their physiological behavior is thermodynamically controlled. However, the results from Taylor et al. [37],

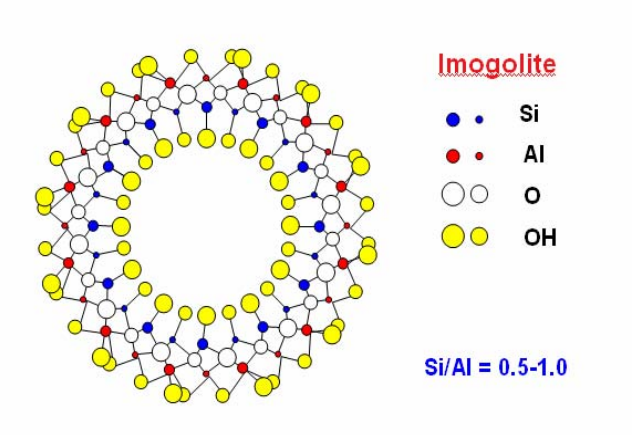

Fig. 2.5 Structure of imogolite (hydroxyaluminosilicate or HAS) [34].

show that Al(III) may be sequestered by the oligomeric Si(IV), process which may yield kinetically inert HAS species –indeed, their high apparent stability may reflect the slow dissociation kinetics. This process may be physiologically more important, as the kinetic inertness of cage or ring HAS structures, once formed, may retain Al(III) for long periods. The inert cage aluminosilicate solutes may act merely as reservoirs for the slow hydrolytic release of the small, active, acyclic species. The conclusions of the authors reflect not only the very high probability that very stable aqueous aluminosilicate colloids may form even under natural conditions but at the same time, they indicate that the current knowledge regarding the mechanisms of colloid generation and stability is limited and there is need for research. It is therefore meaningful to choose the aluminosilicates as representative examples for answering questions regarding the formation of natural aquatic colloids as well as about their interaction with actinides.

Aluminosilicate colloids in laboratory [25-28]

As we have already seen from the theoretical considerations presented in the previous sections, inorganic aquatic colloids may form either by condensation reactions or by dispersion from minerals. We have also seen that colloid formation and stabilization is a very complex process depending on energy barriers and therefore not only thermodynamics but also kinetic factors are involved. The most common condensation process occurring in the hydrosphere is the hydrolysis of polyvalent cations (e.g. Si^{4+} and Al^{3+}), the formation of sparingly soluble hydroxides and hydrous oxides and the neoformation of clay minerals at coprecipitation.

The key information for attaining supersaturation and thus coprecipitation of Si and Al is derived from the thermodynamic solubility data for $SiO_{2(am)}$, $Al(OH)_{3(am)}$ and several aluminosilicates, illustrated in Fig. 2.6. In a previous study [25, 26], the above mentioned solubilities were calculated from literature data at constant room temperature, atmospheric pressure and 0.03 M NaCl (background electrolyte). As can be seen in Fig. 2.6, amorphous $Al(OH)_3$, silimanite and kaolinite show similar pH dependency, with minimum solubility in the neutral pH region. Amorphous silica (SiO_2) shows constant solubility (about $2x10^{-3}$ M) up to pH 9, which then increases sharply through formation of polysilicic acids. The pH range of interest, 4-9, in which colloids can form during the coprecipitation is selected according to the low solubility region of the different aluminosili-

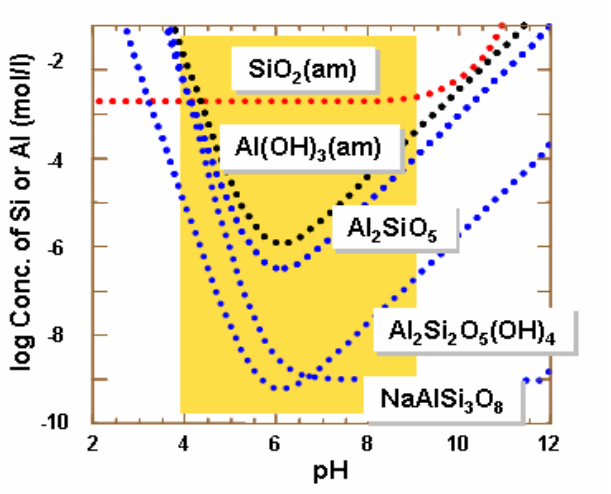

Fig. 2.6 Thermodynamic solubility of amorphous SiO_2, $Al(OH)_3$ and of several aluminosilicates calculated based on the available data for sillimanite (Al_2SiO_5), kaolinite ($Al_2Si_2O_5(OH)_4$) and low albite ($NaAlSi_3O_8$); the selected pH range for aluminosilicate colloids formation is indicated as highlighted zone. Selection is made for the highest and lowest solubility of aluminosilicates [25, 26].

cate compounds, and also falls within the pH limits encountered in natural waters [30]. Selection of the Si concentration range for the experiment is based on the following considerations. In natural aquifer systems the concentration of water borne Si may reach above millimoles at over-saturation via formation of polysilicic acid [38], but is normally below one millimole [28] and Si is present as monosilicic acid. However, polysilicic acid may enter the water also directly, through dispersion from minerals [39]. The conditions for the formation of monosilicic and polysilicic acid are especially important since polysilicic acid has been shown to have a 10^6 times higher affinity for Al as compared with monosilicic acid [37]. This fact implies that the formation process of aluminosilicate colloids and hence their interaction with the actinides may also be different, depending on whether monosilicic or polysilicic acid is involved as initial reactant. Therefore, in a previous screening experiment [26], three initial concentrations of Si, namely 10^{-4}, 10^{-3}, and 10^{-2} M, below and above the Si saturation concentration ($2x10^{-3}$ M), have been combined with varying Al concentrations from 10^{-7} to 10^{-3} M, in the pH range 4-9. The radiometric experiment, using ^{241}Am as contestant in the coprecipitation of Al and Si have evidenced that optimum formation of HAS-colloid-borne Am occurs at a concentration ratio Si/Al in the mother solution of 100 and for the following concentration combinations:

I: [Si]: 10^{-3} M (0.7 x saturation) + [Al]: 10^{-5} M ([Si]/[Al] = 100)

II: [Si]: 10^{-2} M (6.4 x saturation) + [Al]: 10^{-4} M ([Si]/[Al] = 100)

The synthetic hydroxy-aluminosilicate colloids, generated by coprecipitation in the neutral pH range as described above, have been characterized for particle number density and morphology by several techniques: LIBD (Laser induced break-down detection) AFM (Atomic force microscopy) and SEM-EDX (Scanning electron microscopy coupled with X-ray energy dispersive spectrometry). The HAS colloids prepared out of mother solutions with Si/Al atomic ratio of about 100 appear to be similar to the natural aquatic colloids of protoimogolite/allophane type (precursors of imogolite) in respect with the particle size, shape and Si/Al atomic ratio. The characteristics of the synthetic HAS colloids [26] are summarized below.

	Present system	Natural system
Particle size	10-50 nm(LIBD) 5-10 nm height (AFM) 10-50 nm length (AFM)	very often < 50 nm
Number density	10^{11} - 10^{14} particles/L (LIBD)	10^{8} – 10^{14} particles/L
Si/Al ratio (AFM, SEM-EDX)	0.7 – 1.2	imogolite 0.5-1

Taking into account the atomic Si/Al ratio of the HAS colloids of approximately one, their formation from polysilicic acid has been presumed as:

$$n\ Al(OH)_{3-y}^{y} + Si_nO_{n-1}(OH)_{2n+2} \leftrightarrow Al_nSi_nO_{4n+2-x}(OH)_x^{x-n-4} + (7-ny-x)H^+ + (2n-y-1)H_2O$$

In the equation , the y-values varies from -1 to +3 following the degree of Al hydrolysis in the present experimental pH range (4-9) and the x-value determines the anionic charge of the HAS colloids. The predominant silicic acid species appears to be H_4SiO_4, unless Si concentration is oversaturated and therefore a neutral polysilicic acid species has been proposed as reactant for the above formulated reaction. As the precise structure analysis of the HAS colloids is not possible due to the very low mass concentration the n-value re-

mains unknown. The surface characterization of the HAS colloids has been performed by determining of the zero point of charge (pH_{pzc}). The colloids prepared from a mixture of 10^{-3} M Si and 10^{-4} M Al show a pH_{pzc} of 3.53 ± 0.5 [27], which means that the HAS colloids have a negatively charged surface in the pH range of interest (4-9) and therefore high potential to migrate with the water flow with little interaction with the geomatrix.

2.2.2 Humate Colloids

Humic acid as colloids in nature

Beside the inorganic colloids, humic acids (HA) are always present to some extent in aquatic environments [1, 3, 6,] and have been shown to play an important role in the sequestration and mobilization of trace metals [11, 40, 41]. Humic acids are operationally defined from the extraction procedure of humic substances (HS) as the insoluble fraction at acidic pH (pH < 2) [42]. Humic substances are thought to be produced by a combination of degradation and condensation reactions of plant breakdown products, with an important role of bacteria [43-45]. HS are composed of heterogeneous components with a wide range of molecular weights, size and different chemical moieties. The humic skeleton, consisting in mainly aromatic cycles covalently linked with aliphatic moieties, is highly substituted with oxygen containing functional groups: carboxylic and phenolic as most important together with ketonic, enolic and amino groups. In the pH range of natural waters (pH 4-9), humic acids are negatively charged and present mainly as colloidal species, with particle diameter of 4-400 nm [7, 45-47], while their distribution of molecular weights is reported to vary between 500 to 100000 Da [44, 45, 48]. In surface waters the humic acid concentration varies between 1-10 mg/L [49], but in natural groundwater concentrations of 80-100 mg/L may be reached [7, 46]. Apart from their colloidal size, the influence of humic acid on the migration of actinides in the aquatic environment arises from its ability to bind all metals with charge $z \geq +2$, and to modify the surface properties and reactivity of minerals [29, 41, 49]. The reactive nature of humic acid is mainly the consequence of the acidic functional groups of the humic macromolecule, giving rise to multiple binding possibilities (electrostatic and specific, including chelate formation) as compared with the simple ligands [10, 20]. For metal complexation, the functional groups

involved are primary carboxylic, as pointed out by spectroscopic measurements (EXAFS) [50], phenolic groups being expected to have contribution at pH above neutral [51, 52].

The colloidal stability of the clay minerals surfaces may increase in the presence of sorbed natural organic matter [29, 53] due to electrostatic or steric effects [54]. Several reactions have been proposed to describe the interaction reactions between the humic acids and minerals**:** electrostatic to cationic sites of the mineral surface, hydrogen bonds, polyvalent cation bridging and ligand exchange [20, 53-56]**.** Fig. 2.7 depicts a potential structure of humic macromolecule binding to a clay mineral surface. In the aquatic environment, humic colloids are usually composed of humic acid loaded with inorganic elements, either by complexation or by peptizing small inorganic composite particles [57].

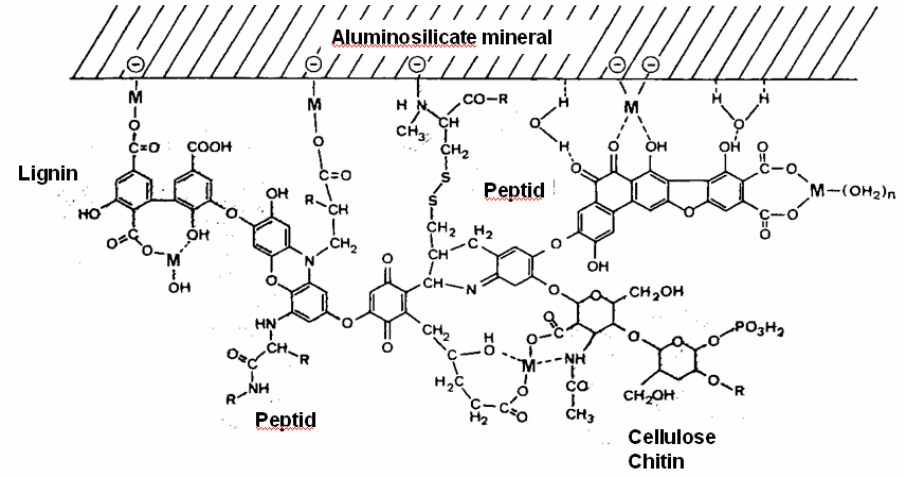

Fig. 2.7 Hypothetic structure of humic acid macromolecule binding to a clay mineral surface; (M = metal cation) [58].

Purified [^{14}C]-humic acid for experiments

Natural humic acid, originating from the groundwater of the bore hole Gohy-573 in the Gorleben aquifer (Germany) is used for the experiments. The humic acid was isolated, purified and characterized by Buckau et al. [42], following the procedure by NaF treatment, repeated precipitation with $HClO_4$/dissolution with NaOH and freeze drying.

The proton exchange capacity, measured by potentiometric pH titration is of 4.82±0.05 meq/g. In order to trace the behavior of the humic acid, we use ^{14}C-labelled humic acid. The radiolabelling was performed by A. Mansel [59] at the Institut für Isotopen Forschung (IIF-Leipzig), via diazotization and azo coupling reactions (covalent binding at the carbon skeleton of the humic acid). The reaction is illustrated schematically in Fig. 2.8. The [^{14}C]-aniline hydrochloride (Amersham) is converted with sodium nitrite to diazonium ion in a hydrochloride solution at 0 ^{o}C. The diazonium ions react with the activated aromatic residues of the humic acid at pH~9 and 0-5 ^{o}C. The resulting product is again purified and characterized by size exclusion chromatography. The specific activity of the [^{14}C]-humic acid (solution of pH 6.5) is 1.76 x10^{8} Bq/g. The labelling procedure will be published elsewhere [59].

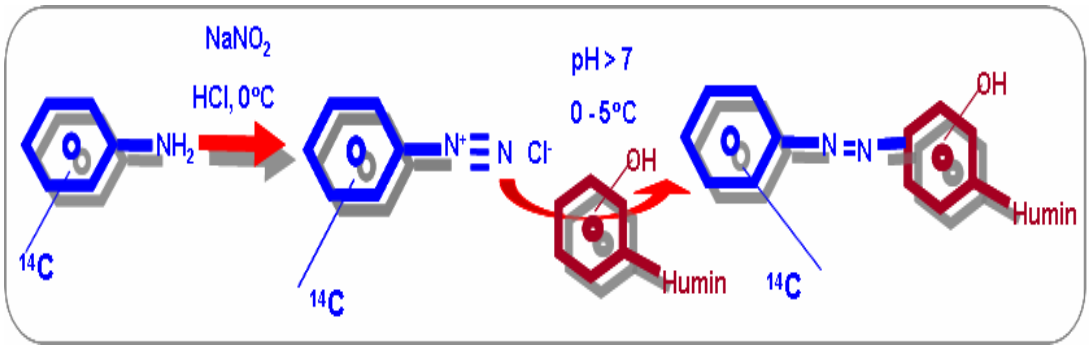

Fig. 2.8 Schematic illustration of the main steps in the labelling process of the humic acid [59].

2.3 Actinide colloids in natural aquatic systems [31, 60, 61]

Actinides may become aquatic colloids by two processes leading to the formation of either actinide "real" colloids or of the so-called actinides "pseudocolloids". These processes are described in the followings.

Real colloids of actinides

The behaviour of actinides (An) in aquatic systems is primarily defined by their oxidation state; An solubility and tendency towards chemical reactions differ significantly from one oxidation state to another. Characteristic for An is that multiple oxidation states are possible, (Fig. 2.9), however, the water redox chemistry (Eh, pH) set limits on the

oxidation states that An can have in aqueous solutions.

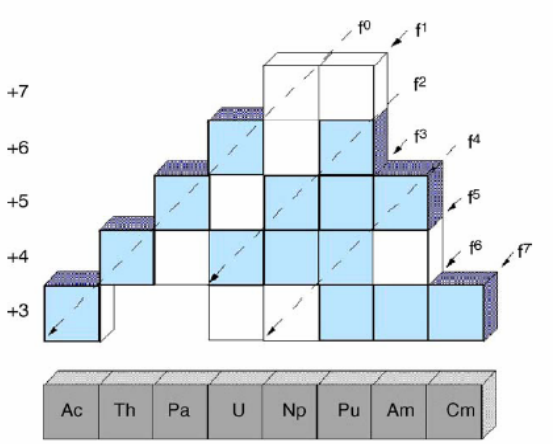

Fig. 2.9 Known oxidation states for actinide elements Ac to Cm (indicated at left). The oxidation states stable in natural environments are highlighted [60].

The aspect of variable oxidation states is particularly important in case of Pu, as redox and disproportionation reactions permit the coexistence in solution under appropriate conditions of the oxidation state III, IV, V and VI. In case of Th the tetravalent state is common and stable. Am(III) is stable in solution, however, Am(V) has been identified in brines at pH > 8. In natural oxic waters, the penta- and hexavalent oxidation state is stable for Np and U, respectively. In reducing environments, which may be encountered at large depths in some granite waters, U and Np may be stabilized in the tetravalent state.

An tendency toward hydrolysis, complexation, sorption and colloid formation correlates generally with the charge density (i.e. the ratio between the effective charge and the ionic radius), which is decreasing in the series $An^{4+} > AnO_2^{2+} > An^{3+} > AnO_2^{+}$ [61]. Once released into solution the actinides undergo several interrelated geochemical reactions (Fig. 2.10), leading to their immobilization or mobilization in the aquatic system. Such reactions are directly related to the physicochemical characteristics of the aquifer (redox potential (Eh), pH, CO_2 partial pressure, ionic strength, the presence of complexing ligands) and to the properties of the geomatrix. Actinides can be stabilized in the liquid phase as solution species, i.e. aquo ion, hydrolyzed species, complexes with organic or inorganic ligands and as colloidal species. The process of actinide hydrolysis, polynucleation and further aggregation to colloidal size particles under over-saturation leads to the

formation of "real" colloids of actinides as generally described in literature [30]. However, stabilization of the colloidal state requires polarization in order to prevent agglomeration of particles to a precipitate phase. A recent publication [62] has referred to the conditions for the formation of stable colloids of tri and tetravalent actinides. As ascertained in the study, the generation of stable colloids is due to the mutual aggregation of species with different oxidation states, which are likely to hydrolyze: either actinides or the actinide and trace metal ions present as impurities in solution. Thus, the enhanced colloidal stability observed under near-neutral pH conditions arises from the surface polarization introduced by the difference in the oxidation states. Individual tetra- and trivalent actinide ions in their pure state are expected to form colloids only as transitional state for precipitation, under conditions of near-neutral pH and concentration close to the oversaturation.

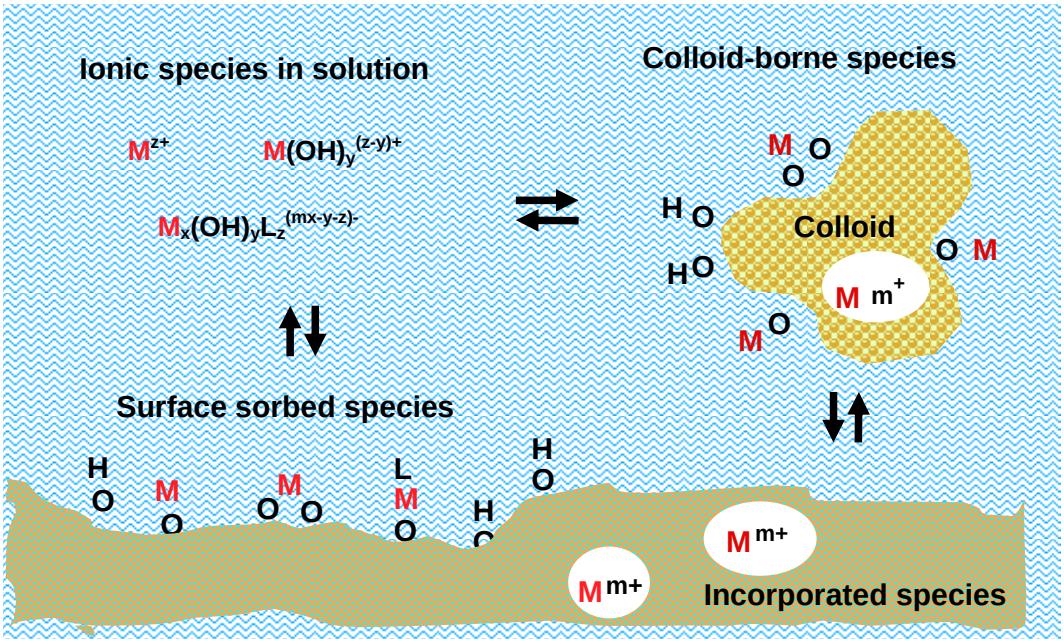

Fig. 2.10 Solid-water interactions of metal ions (M) including actinides in a natural aquifer system. Distribution of M species: in solution, colloidal (mobile species, with migration potential) and solid (immobile) phases.

Pseudocolloids of actinides

Formation of actinide pseudocolloids is considered as an association of actinide with the

aquatic colloids, either of inorganic or organic nature. The process includes co-nucleation, ion exchange, complexation or isomorphic substitution of a lattice component by actinide. Numerous studies have focused on the interaction of actinides with inorganic [15, 16, 64, 65] and humic colloids [7, 49, 65-74] under various conditions (pH, I, component concentration), and on the stability [21, 71] and migration of such actinide pseudocolloids [18, 19, 64]. Other studies have concentrated on ternary systems, investigating the influence of humic acid on the actinide interaction with mineral colloids, [49, 55, 68, 75, 76]. Despite the extensive investigations, the underlying mechanisms for the generation of aquatic colloids and of the colloid-borne actinides have not been yet well understood.

Colloid-facilitated migration has been shown to be particularly important for contaminant species with high charge density, e.g. M^{4+} [13]. As such species have low solubility in absence of complexation ligands, and strong sorption properties towards mineral surfaces like rocks, they have been initially considered to be easily immobilized in environment. Providing the colloids are mobile since in natural waters solid surfaces are generally negatively charged, and the interaction of An with the colloids is strong, the An will have high susceptibility to be transported along with the water flow with little retardation.

2.4 Methods for the analysis of actinide colloids

Analysis of actinide aquatic colloids requires information regarding the conditions of formation of colloids themselves, colloid concentration and morphology and, on the nature of the actinide-colloid binding. Investigations of the geochemical behavior of sparingly soluble actinides (usually below 10^{-6} M) in the presence of low concentrations (ppb range or less) of small aquatic colloids (< 50 nm) require sophisticated methods which have been developed in the last decades [8, **77**]. Due to the complex chemical and physical characteristics of the actinide-colloidal systems and of the limitations of the analytical methods, the combination of several (complementary) methods is necessary in order to have more complete information about both physical and chemical speciation.

2.4.1 Detection and chemical speciation of colloid-borne actinides

We present in the followings a brief description of the methods that have been used to characterize the HAS colloidal system and of colloid-borne-actinide species.

Filtration / ultrafiltration and radiometry

Filtration and ultrafiltration are classical size fractionation techniques. These are non-destructive methods, which enable the separation of particulate matter (usually with diameter >1000 nm) from the colloidal particles (diameter between 1-1000 nm) and from the dissolved species. The combination of filtration using a variety of nominal filter pore sizes with the radiometric detection of actinides is a primary tool for the investigation of natural aquatic colloids.

Liquid Scintillation Counting (LSC) is a suitable technique for the analysis of alpha and beta emitters, allowing much higher detection efficiency as compared to α- or γ-spectrometry using semiconductor detectors. Alpha emitters can be detected with almost 100% efficiency, whereas for the beta emitters having the maximum decay energy, E_{max} >156 keV (C-14), the detection efficiency is higher than 96 %. Another advantage is that LSC enables the simultaneous measurement of an alpha and beta emitting radionuclide in the sample. The partial overlap between the beta tailing of high energy beta emitters and the alpha spectrum can be separated manually, by choosing appropriate counting windows, or electronically, by taking the advantage of the Pulse Decay Analysis which separates the alpha and beta counts based on their different decay time [78]. The principle of the liquid scintillation counting is based on the conversion of the decay energy of the emitting radionuclide to light photons, by the means of a scintillation cocktail, which is mixed with the liquid sample. The intensity of the scintillation is a function of the energy deposited in the scintillator. A photomultiplier converts the light photons to photoelectrons which are further amplified and the electrical pulses are registered as counts. The counts accumulated during this process are sorted into separate channels, with the amplitude of the signal determining the energy channel into which the counts are sorted.

Spectroscopic speciation

Several spectroscopic techniques have been developed for investigations of actinides speciation at molecular level, information which is necessary for macroscopic predictions. Due to the difference in physical and chemical properties among the actinides, no single spectroscopic method can adequately probe all actinides [8]. Among the con-

ventional techniques, the absorption spectroscopy (UV-VIS-NIR) on the transitions within the 5 f electron shell has been used to characterize the oxidation states and complexation of actinides. The spectroscopic resolution of actinides transition bands is high, but the intensity is very weak. Special methods, making use of the high intensities of laser radiation sources have been developed for speciation of trace level actinides, which are expected in natural waters. The enhancement of sensitivity is attained by detection of different relaxation processes of the photon excited states (Thermal lensing spectroscopy, Photoacoustic spectroscopy, Time-resolved laser induced fluorescence), instead of transmission as in the case of conventional absorption spectroscopy. Another powerful technique providing information at molecular level on actinide speciation is the synchrotron-based X-ray absorption spectroscopy.

Time-resolved laser florescence spectroscopy and X-ray absorption spectroscopy are used in the present study in order to investigate the bonding state of the actinide in aluminosilicate solutions. A description of the principle is given in the following.

Time-resolved laser florescence spectroscopy (TRLFS) [33, 79-81] is most sensitive for the chemical speciation of actinides. The method is based on the selective excitation combined with selective time-resolved measurements of the florescence emission. However, the method is limited to the elements with fluorescence emission, to which belong only Cm(III), Am(III), Pa(IV) and U(VI) from the actinides. Speciation of Cm (III) in aquatic environment is possible in the nanomolar concentration range. The fluorescence emission spectrum of the aqueous uranyl ion is complex [82] and several ligands like humic acids cause strong quenching of the uranyl florescence limiting somehow the applicability to natural systems.

The actinide of interest is excited at prominent absorption wavelength. Following the absorption of light, the electron is promoted to a higher energy level. The relaxation process, in which the electron returns to the ground state, may take place by both non-radiative emission (energy is dissipated as heat) and emission of light. In aqueous solution, the dominating non-radiative decay occurs via energy transfer to excited vibrational states of the surrounding ligands, like OH vibrations of the coordinated H_2O or OH^-.

Spectroscopic information is derived from the excitation and emission spectra and from the fluorescence life time (reciprocal of the fluorescence decay rate). An empirical relationship correlates the fluorescence decay rate with the number of water molecules in the coordination sphere of Cm(III)): $n(H_2O) = 0.65*k_{obs}-0.88$, where k_{obs} is the decay rate

of the fluorescence (ms^{-1}) and $n(H_2O)$ is the number of coordinated water molecules [33, 79, 80]. Based on this correlation structural information is gained from experimentally determined life times of various Cm species. The spectral shifts (changes in the position of the emission peak) and eventually splitting of the emissions band are indications about changes in the ligand field. TRLFS has been extensively used to investigate the complexation of Cm or Am with various ligands, including humic acids as well as its interaction with minerals [16, 33, 67, 83]. Formation of inner-sphere complexes is accompanied by a red-shift in the fluorescence emission of Cm and an increase in the florescence emission life time. Sensitized TRLFS, that has been previously applied for studying the complexation of Cm(III) with humic acids [66, 67, 79], is based on the energy transfer from the photon excited organic chromophores to the complexed f-element ion, which is then able to emit its characteristic luminescence. Using two excitation wave lengths, the fluorescence of the Cm(III)-humate complex is generated either by direct excitation of the Cm ion, or indirectly, by intramolecular energy transfer from the humic ligand, when the non-complexed Cm can not be excited (Fig. 2.11). An indicator of the energy transfer is peak area ratio of the emission peaks at direct and indirect excitation. The emission life time of Cm, in order of 10^{-4} s, allows the efficient suppression of the short lived fluorescence of the humic acid by the time-resolved detection.

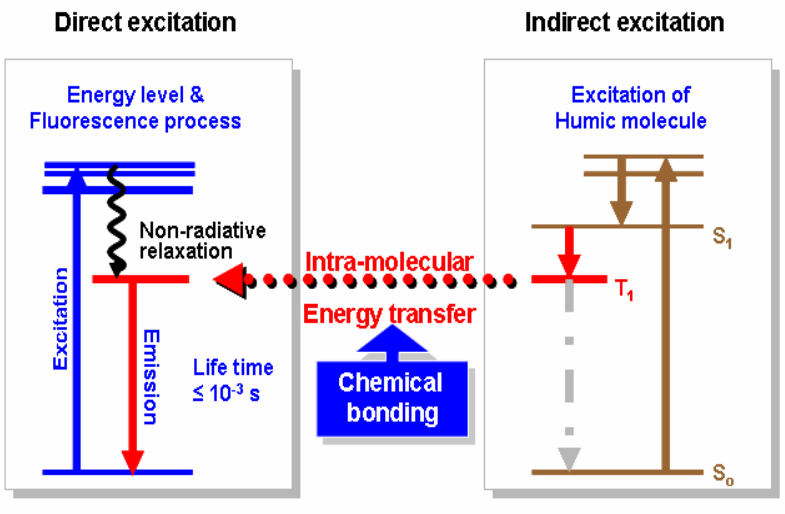

Fig. 2.11 Schematic illustration of ground and excited state energy levels of Cm(III) (left) and humic acid (right). After indirect excitation of Cm via intra-molecular energy transfer from HA, the complexed Cm follows its own emission.

Synchrotron-based X-ray absorption spectroscopy (XAS) [83, 84, 85] is a non-destructive technique, providing average information at a molecular level about the oxidation state, local structure, and the identity of neighbors in the first few coordination spheres (up to 5-6 Å) surrounding a specific absorbing element. Since XAS does not require long-range order or crystalline structures, it is particularly useful for the investigation of the actinide speciation in solution, amorphous precipitates or colloidal compounds, which cannot be characterized with X-ray diffraction. By means of XAS technique, actinides can be investigated at concentrations down to tenths of a mili molar level. The neighbor type can be determined within Z ± 1, and the interatomic distances can be obtained within ± 0.02 Å. Coordination numbers are determined with less precision, within 20-25 %.

In an XAS experiment one measures the absorption of the X-ray in a sample as a function of the incident energy E = hν. The absorption for a given sample length x, is given by the Lambert-Beer law: $\mu(E) = \ln(I)/dx = \ln[I_0(E)/I_1(E)]$, where I_0 and I_1 represent the intensity of the incident and the transmitted photon, respectively. The absorption coefficient, μ, generally varies smoothly with energy but also shows several regions where it sharply increases. These regions are known as absorption edges. Absorption edges are element specific and correspond to the transition of a core electron to higher energy valence and continuum states via the photoelectric effect. The exact position of an absorption edge depends on the oxidation state of the absorbing element and its shape on the specific coordination. The L_{III} absorption edges for actinides arise from the dipole allowed 2p→6d electron transitions. The X-ray absorption spectrum is divided into two regions: the X-ray absorption near-edge structure (XANES), the region usually within about 40 eV of the main absorption edge, and the extended X-ray absorption fine structure (EXAFS), which is the oscillating part of the spectra ranging from about 30 eV to about 1000 eV above the absorption edge (Fig. 2.12, lower part graph)**.** XANES spectroscopy gives information about the oxidation state and coordination geometry of the absorbing element. EXAFS spectroscopy gives information on the type, numbers and distances to near neighbors. Photon absorption generates a photoelectron with a wave number, $k = 2\pi/\lambda$, which propagates away from the atom. The oscillatory structure of μ above the absorption edge results from the constructive and destructive interference of outgoing photoelectron waves with the waves backscattered on the neighboring atoms (Fig**.** 2.12, upper right part).

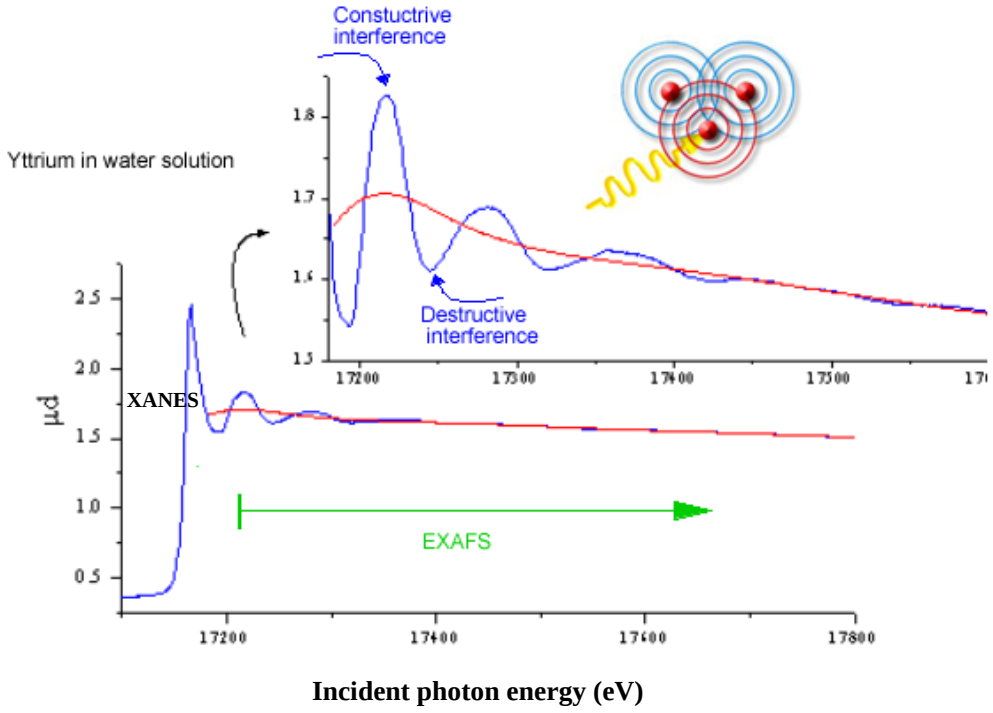

Fig. 2.12 The yttrium K-edge X-ray absorption spectrum including the XANES and EXAFS regions (lower part). Illustration of destructive and constructive interference of an outgoing photoelectron wave with the backscattered wave (upper part), leading to minima and maxima of the oscillations in the absorption coefficient, (here μd), observed in the EXAFS regime (middle part graph) [86].

The EXAFS function (χ(k)) is defined as the normalized oscillatory part of the absorbtion coefficient above the absorption edge as a function of k:

$$\chi(k) = \frac{\mu - \mu_0}{\mu_0} \qquad (2.13)$$

where the μ_0 is the atomic absorption coefficient in the absence of neighbor atoms and μ(E) is the experimental absorption coefficient. μ_0 is generally unknown and modeled by fitting the smooth atomic background of a spectrum with a number of spline or polynomial functions (see red line in the middle graph of Fig. 2.12). To extract the EXAFS oscil-

lations first the energy axis is converted to the photoelectron wave number k,

$$k = \sqrt{\frac{2m_e(E - E_0)}{\hbar^2}} \tag{2.14}$$

where m_e is the electron mass, ħ is Plank's constant divided by 2π. The kinetic energy of the photoelectron is given by the difference between the energy of the incident X-ray (E) and the ionization energy (E_0). The isolated χ(k) is often weighted with k^n, with n=1-3. This accents the oscillations at higher k, where they are considerably dampened (particularly of low Z elements). After the EXAFS data are converted to k space, the fine structure is related directly to the sum of dampened sinusoidal oscillations from n coordination shells. Under the assumption that the photoelectron can be approximated by a plane wave and the sample has a minimum of disorder, the analytical expression for the EXAFS signal, χ(k), is given by the equation (2.15):

$$\chi(k) = \frac{S_0^{\ 2}}{k} l^{-1} \sum_{i=1}^{n} N_i \left| f_i(k,\pi) \right| \frac{e^{-2R_i/\lambda(k)}}{R^2{}_i} e^{-2k^2\sigma^2} \sin(2kR_i + \phi_i(k,R)) \tag{2.15}$$

where the sum is from a contribution of each spherical shell, i of N_i equivalent neighboring atoms at a distance Ri from the absorbing atom. $f_i(k, \pi)$ is the backscattering amplitude function for the neighboring atom type**.** $\phi(k, R)$ is the total phase shift of the photoelectron. $S^2{}_0$, the amplitude reduction factor, is introduced to describe effects of multielectron excitations. l (the angular momentum quantum number), λ(k) (the mean free path length of the photoelectron), and σ^2 (Debye-Waller factor) is the average mean square displacement from the mean bond length. The functions $f_i(k)$ and $\phi(k, R)$ are dependent on the backscatterer type. This dependency allows identification of the type of elements comprising a coordination shell. These functions are unknown and must be extracted empirically from EXAFS data of reference compounds with known structure or theoretically calculated. The EXAFS oscillations are Fourier transformed in order to separate the contribution of each individual shell from k-space into R space. In order to obtain quantitative information on the structure environment of the absorbing atom, either χ(k) or the Fourier transformed data are fitted to the EXAFS equation (2.15).

EXAFS spectroscopy requires an intense polychromatic X-ray radiation and the most suitable light source is a synchrotron radiation from an electron or positron storage ring. The synchrotron radiation has a continuous band of wavelengths and therefore, to record a spectrum, an appropriate double-crystal monochromator, using Bragg diffraction is used to select and vary the wavelength around the E_0 of the element of interest. An experimental set-up for the XAS is illustrated schematically in Fig**.** 8.1 (Appendix). To record a spectrum, measurements can be carried-out using the transmission detection, by measuring the photon intensity in front of the sample (I_0) and behind the samples (I_1) at specified energies. Another possibility is detection of proportional secondary processes which occur when atoms relax following inner-shell excitation such as fluorescence photon emission. Fluorescence detection is required for dilute samples, i.e., where the actinide concentration is less than around 1% and for samples which are totally absorbing or impermeable for X-rays.

2.4.2 Quantification and characterization of colloids [7, 8, 87]

Colloidal systems show broad size and concentration distributions and one single method can generally not cover the whole range with adequate sensitivity. Due to the susceptibility of the colloidal systems to disturbance, the non-invasive investigation methods are desirable. Direct methods for the quantification of aquatic colloids are based on the dynamic or static light scattering using laser sources like Photon Correlation Spectroscopy (PCS) or Single Particle Counting (SPC). Intensity of the scattered light decreases with the sixth power of the inverse particle diameter and restricts the sensitive detection of ultra-trace levels to particles larger than 100 nm diameter.

LIBD (Laser induced break-down detection)

LIBD has been developed for the quantification of groundwater colloids, with low number density and very small average size. The sensitivity of the method shows a less pronounced colloid size dependency. Colloidal particles with a diameter down to about 10 nm, and at a concentration as low as 10^7 particles/L can be detected. The method is based on the plasma generation of colloidal particles by intense laser light absorption. The breakdown effect results from the ionization of matter in the electric field generated in the focus area of a pulsed laser beam. The critical energy density energy to produce plasma

(the breakdown threshold) is much lower for solids than for liquids. By adjusting the laser pulse energy density just below the breakdown threshold of the solvent, the plasma is generated exclusively by colloidal particles present in the focus volume. The breakdown event can be detected by measuring the plasma light emission with a charge coupled device or by detecting the photo-acoustic signal with a piezoelectric detector. Since every event corresponds to one single colloid, the particle number density can be evaluated from the breakdown probability, which is the number of breakdown events relative to a predefined number of laser shots. Size information is gained from the determination of the breakdown probability at different laser energy densities; the breakdown threshold decreases with increasing particle size and this dependency is used as a calibration curve for particle sizing. By calibration of LIBD with reference polystyrene colloids, a mean particle diameter and a number density can be derived.

Electron Microscopy (Scanning Electron Microscopy-SEM and Transmission Electron Microscopy-TEM) is largely applied for the investigations of the colloidal systems, including elemental composition and internal structure, but the original state of the colloids is disturbed. The method requires high vacuum and time consuming sample preparation. In case of TEM, the electrons passing through the sample produce a "direct image", whereas in case of SEM an "indirect" image of the sample is created. In the latter case, secondary products (secondary electrons, backscattered electrons, and X-ray photons) are generated and detected, serving as a measure of the interaction strength. Particle counting and sizing is performed by deposition of colloids onto a grid and evaluating the pictures. The detection of the specific X-rays energy resolved by energy dispersive spectrometry (EDX) gives information on the elemental composition of the sample from the characteristic spectral lines. The intensities are proportional to the mass concentration within the interaction volume, allowing quantitative determination of the element abundance.

Atomic Force Microscopy (AFM) is a non-destructive method of atomic resolution, mapping the surface of colloids. The method requires concentrated colloidal suspensions and sample condensation might be necessary. Imaging is obtained by scanning the repulsive and attractive forces between atoms of an ultra thin SiN_3-tip used as a sensor and the surface atoms of the sample at a separation distance of few Å. Moving the tip relative to the sample the surface topography is scanned. The interaction leads to elastic oscillation proportional to the interaction between the cantilever tip and the sample surface.

Detection of the corresponding movements of the cantilever-tip is performed by sending a laser light to the back of the tip and registering the reflected light by a 4-quadrant photo-detector. The attained resolution is 0.1 Å and the sample surface is $1nm^2$ up to $1\mu m^2$. The advantage over electron microscopy is that it can be operated in situ and can be used for studying the colloid morphology even in aqueous conditions.

3. Experimental section

Ultra-high purity, double deionized water, provided by a MiliQplus® system ($18.2x10^{-6}$ Ω cm^{-1}) is used in the experiments.

3.1 Preparation of inactive and radioactive stock solutions

MOPS buffer stock solutions

0.05 M MOPS (3(N-morpholino) propanesulfonic acid) buffer solutions are prepared by dissolving the free acid in deionized water and neutralizing with 1M NaOH to pH 6.6, 7.2 and 7.8.

EDTA stock solutions

0.1 M EDTA stock solutions of pH 5, 7 and 9 are prepared by dissolving the disodium salt of the ethylenediamine tetraacetic acid (Merck) in deionized water followed by pH adjustment with micro volumes of HCl or NaOH.

Al stock solutions

Al stock solutions of**:** $2x10^{-5}$, $2x10^{-4}$, $4x10^{-3}$ M Al in 0.03 M HCl and of $2x10^{-2}$ M Al in 0.04 M HCl are prepared by appropriate dilution of an Al solution (ICP standard, Aldrich) containing 0.37 M Al in 1.23 M HCl, with HCl 0.1 M and deionized water.

Si stock solutions

Two sets of stock solutions are prepared for the present experiments, starting from sodium-waterglass solution and following two approaches as illustrated in Fig.3.1:
(1) Solutions of $2x10^{-3}$, $2x10^{-2}$ M Si in 0.03 M NaOH, and of $2x10^{-1}$ M Si in 0.2 M NaOH. These solutions are prepared starting from an initial Si solution (ICP standard, Aldrich) containing 0.3489 M Si in 0.83 M NaOH, which is diluted and adjusted for pH with HCl or NaOH, to a final pH of approximately 12. The solutions remain under-saturated relative to the solubility concentration of amorphous silica (see Fig. 2.6) and thus Si is present as monosilicic acid in the stock s olution. This preparation mode follows approach A in Fig. 3.1.

Fig.3.1.

(2) Solutions of $4.2x10^{-2}$ M Si in 0.01 M MOPS buffer solution at pH 6.6, 7.2 and 7.8.

The solutions are obtained by neutralization in MOPS buffer of a solution containing 7.0 M Si in 4.0 M NaOH (Aldrich). The initial alkaline Si solution, in which monosilicic acid prevails, is diluted directly to the neutral pH range. Thus, the solution becomes oversaturated ($4.2x10^{-2}$ M Si corresponds to 21 times the solubility concentration of amorphous silica) leading to instantaneously polymerization of the monosilicic acid [27]. This preparation mode of the Si stock solutions follows the approach B in Fig. 3.1.

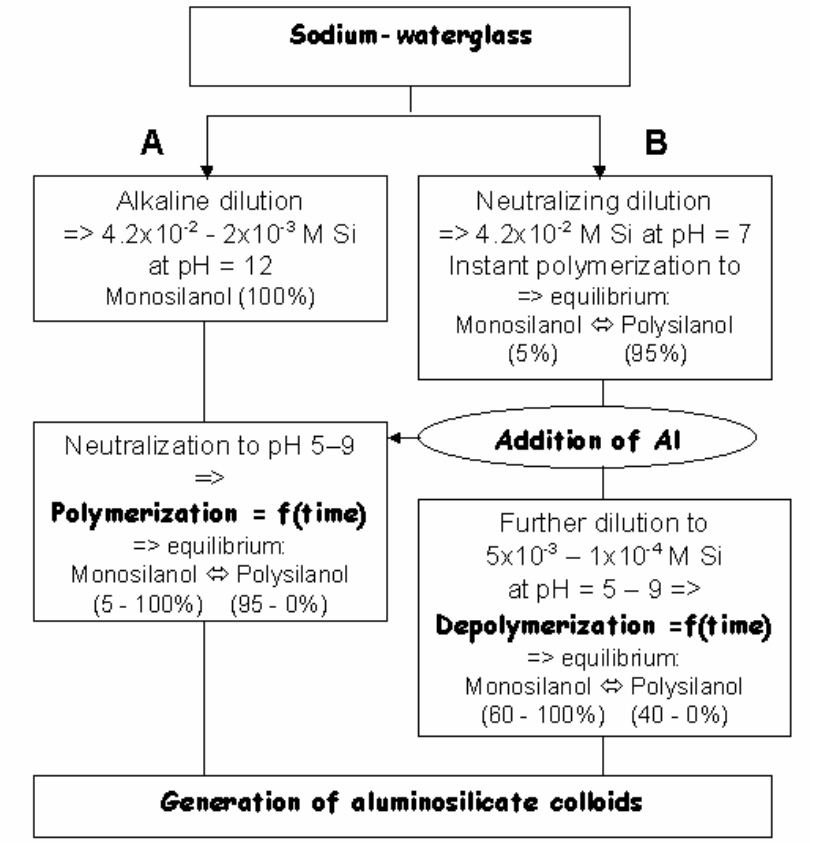

Fig. 3.1 Two experimental pathways for the preparation of Si stock solutions and generation of hydroxy aluminosilicate (HAS) colloids from sodium water glass by (A): alkaline dilution and neutralization or (B): neutralization and dilution [27].

Eu, ^{232}Th and ^{238}U stock solutions

Several actinide (or lanthanide as analogue) stock solutions are prepared from either europium nitrate, thorium (^{232}Th) nitrate AAS standard solutions (Aldrich Chemical), or uranyl (^{238}U) nitrate salt (p.a. Merck). Suprapure HCl/HNO_3 is used for dilutions. The following stock solutions are prepared:
(a): 0.02 M Eu in 0.04 M HCL, 0.02 M Th in 0.8 M HNO_3 and 0.02 M U in 0.04 M HCl
(b): 4.0 x10^{-3} M Th in 0.9 M HNO_3 and 9.4x10^{-3} M U in 0.5 M HNO_3.

^{241}Am, ^{234}Th, ^{237}Np and ^{233}U stock solutions

Radioactive solutions of ^{241}Am, ^{237}Np and ^{233}U are provided by the INE Karlsruhe as well as by the Institute of Radiochemisty (RCM) Munich and are used without further purification. Stock solutions of 8.0x10^{-5} M ^{241}Am in 0.1 M HCl, 2.4x10^{-3} M ^{237}Np in 0.1 M HCl and 5.0x10^{-4} M ^{233}U in 0.1 M HCl are prepared by acidic dilutions of the original solutions.

^{234}Th is prepared in laboratory by milking from natural uranium, as can be seen from the ^{238}U decay scheme in Fig. 3.2.

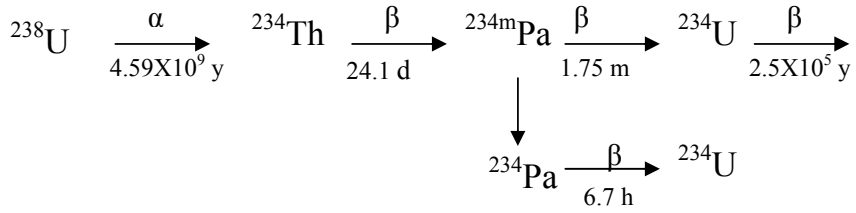

Fig. 3.2 Principal pathway of the ^{238}U decay scheme [25].

Th separation is performed in two consecutive steps [25]:
(1) 25 g $UO_2(NO_3)_2$*6 H_2O (p.a. Merck) is brought to the chloride form, UO_2Cl_2, by addition of conc. HCl, evaporation to dryness, dissolution in 8 M HCl and applied to a column (4.4 cm diameter, 72 cm length) filled with 750 mL of the anion exchange resin Dowex 1X8 (100-200 mesh). Th(IV), unlike U(VI) and Pa(V), does not form chloro-complexes and is eluted with 8 M HCl. The eluate is evaporated, dissolved in concentrated HNO_3 and H_2O_2 and evaporated three times until all organics are destroyed. The residue is di-

solved in 8 M HNO_3 for the second purification step. (2): The hexanitrato complex of Th is sorbed onto a small column filled with 80 µl anion exchange resin Dowex 1X8. The remaining U and Pa impurities are washed out with 8 M HNO_3. Th is eluted with 8 M HCl. The eluate is evaporated several times with conc. HNO_3 to dryness and re-dissolved in approximately 0.8 M HNO_3 resulting in approximately 1.5 x10^4 Bq ^{234}Th.

Humic acid stock solution

A stock solution of 200 mg/L humic acid is prepared by dissolving 0.0042 g purified Gohy-573 humic acid provided by INE Karlsruhe [42] in 5 mL 1 M NaOH. After 1 h reaction time, the solution pH is adjusted to pH of ~ 12 by addition of 4.5 mL 1 M HCl followed by further pH adjustment to pH ~ 7 with 0.1 M HCl/0.1 M NaOH.

The ^{14}C-labelled humic acid (purified Gohy-573) stock solution of 4.8 mg/L is provided by the IIIF Leipzig [59] and is used without further dilution.

3.2 Mother solutions for actinide/colloids interaction

HAS colloids

A typical 40 ml coprecipitation sample is prepared by titrating 20 ml Al stock solution containing an aliquot of the acidic stock solution of the radionuclide under investigation and eventually the actinide or lanthanide carrier, with a 20 ml Si solution (stock solutions 1 as described in section 3.1). The actinide participates in the co-nucleation of Al and Si, i.e. the actinide interacts with HAS in 'statu nascendi'. The coprecipitation is carried out to a preset pH with the aid of an automatic titrator (736 GP Titrino, Tinet 2.4 software, Metrohm). By the coprecipitation procedure, different combinations of Al/Si concentration ratios are prepared at the initially preset pH values of 4.0, 5.0, 6.0, 7.0, 8.0, 9.0. Al concentration is varied between 0, 10^{-5} and 10^{-4} M, that of Si between 0, 10^{-3} and 10^{-2} M. At 10^{-3} M Si, the solution remains under-saturated and monosilicic acid prevails. At 10^{-2} M Si, the initial alkaline solution (containing monosilicic acid) becomes oversaturated by neutralization during the coprecipitation experiment which leads to the formation of polysilicic acid. HAS mother solutions of 10^{-5} M Al/ 10^{-3} M Si generate the HAS-monosilicic acid colloids, those of 10^{-4} M Al/ 10^{-2} M Si generate the HAS-polysili-

cic acid colloids.

The Eu, ^{232}Th and ^{238}U solutions are used with trace amounts of actinides (^{241}Am, ^{234}Th and ^{233}U) in the experiments involving higher actinide concentrations. Eu is added for final Am+Eu concentration above $5x10^{-8}$ M; ^{232}Th, for final Th concentration above $2x10^{-12}$ M, and ^{238}U for final concentration of U above $8x10^{-6}$ M.

A similar coprecipitation procedure of Si and Al but without actinide addition, is carried out for the preparation of HAS mother solutions which are then conditioned for variable time periods (3h to 35 d). Aliquots of actinide (lanthanide) stock solutions (either ^{241}Am+Eu, ^{234}Th + ^{232}Th, or ^{233}U) are added to the aged HAS mother solutions.

HA colloids

Samples of 40 mL mother solutions containing adequate amounts of the actinide and Al stock solutions and variable amount of [^{14}C]-HA, are prepared in MOPS buffer at pH 6.6, 7.2 and 7.8. In some experiments the Al solution is replaced by solutions of either: Eu, ^{232}Th or ^{238}U. For the experiments regarding Th, two sets of samples are in each case prepared: either with ^{234}Th (and ^{232}Th) and unlabelled humic acid to monitor Th behaviour, or ^{232}Th and [^{14}C]-humic acid for monitoring the humic acid. A high number of mother solutions for parameter screening experiments are generated from different combinations of several parameters: the final concentration of Al lies between 0 and $1x10^{-5}$ M, Eu concentration is $1x10^{-5}$ M, Th concentration varies between $5x10^{-12}$ M and $1x10^{-5}$ M and that of U between $3x10^{-7}$ M and $1x10^{-5}$ M. Humic acid concentration is adjusted between 0 and 8 mg/L. Variable HA/Al or HA/An concentration ratios are generated. This is achieved either by maintaining the Al or An concentration constant and increasing HA concentration, or by decreasing the Al or An concentration while maintaining a constant HA concentration.

HAS + HA colloids

Samples of 40 mL mother solutions are prepared in MOPS buffer, by neutralizing the acidic solution containing variable aliquots of the actinide (^{241}Am / ^{234}Th +^{232}Th / ^{233}U stock solution and Al stock solutions, with the Si solution. The Si stock solutions used here (stock solutions 2 described in section 3.1) are especially important for the case that

the aluminosilicate colloids are generated from polysilicic acid, in order to overcome the polymerization kinetics the neutralization of alkaline monosilicic acid especially at pH ≤ 7 [27]. Thus, introduction of such Si solution maintains the polysilicic acid transiently (ca 1 h) to react at once with Al and actinides. After one hour sample conditioning time, an aliquot of the [^{14}C]-HA solution is added. As mentioned in case of humate colloids, for the experiments regarding Th, parallel experiments are carried out. In the present experiment the pH varies from 6.6 to 7.8, Al concentration lies between 0 and $1x10^{-3}$ M and Si concentration ranges from 0 to 10^{-2} M. HA concentration is kept constant at 6.5 mg/L.

All coprecipitation experiments are carried out at room temperature (20 ± 2 °C) and atmospheric presssure. Calibration of the pH-meter is performed using buffer solution standards and the accuracy of pH measurements is of ± 0.03 pH units. Magnetic stirring is applied during the coprecipitation reaction. All coprecipitated samples are stored in tightly closed polyethylene bottles and conditioned for time period from 3 h to 35 d. The reproducibility of the coprecipitation experiments is found within 10% (1σ).

3.3 Activity partition in solution, colloids and precipitate

Consecutive filtration and ultra-filtration are performed on the coprecipitated sample for a sequential separation of the precipitate and colloids. The first filtration is made by a membrane filter of nominal pore size of 450 nm (Sartorius) to separate the precipitate fraction. The second filtration is carried out on this filtrate to separate the colloids at a pore size of 10 kDa (approximately 1.5 nm nominal pore size) (Centricon YM-10, Milipore) by centrifugation in the Biofuge primo Heradeus-Kendro for 1h at 5000 x g. Activity of the radionuclide: ^{241}Am / ^{234}Th /^{237}Np/ ^{233}U, and/or of ^{14}C is determined in the filtrates by liquid scintillation counting (LSC) as will be described below. The first filtrate at 450 nm contains both the colloidal and ionic species of the element under investigation. Thus, the difference in the activity of the initial solution and the first filtrate represents the activity of the precipitate. The activity difference between the first and the second filtrate is then ascribed to the colloid-borne species, since the second filtrate from the 10 kDa pore size contains only the ionic species.

Determination of activity of ^{241}Am, ^{234}Th, ^{237}Np, ^{233}U and ^{14}C by LSC

Activity in the samples is measured using a Tri-Carb 29000 CA (Canberra Packard) Scintillator Analyzer. The measurements are performed in antistatic–polyethylene vials of 18 mL. 1 mL filtrate sample is mixed with 10 mL Hionic Fluor (Perkin Elmer) cocktail and measured to a preset statistic precision (2σ) of 0.5 %. Information about the radionuclides used in the present radiometric experiments, including their half-life and decay mode is summarized in Table 3.1**.**

Table 3.1 Radionuclides used in the experiments, life-time, decay mode and energy [30]

Nuclide	Half-life	Decay mode	Energie (MeV)
^{241}Am	433 y	α (γ)	5.49/5.44
^{234}Th	24.1 d	β^- (γ)	0.2
(^{234m}Pa)	1.17 m	β^- (γ)	2.3
^{237}Np	$2.14x10^6$ y	α (γ)	4.79/4.77
(^{233}Pa)	27 d	β^- (γ)	0.3/0.6
^{233}U	$1.59x10^5$ y	α (γ)	4.82/4.78
^{14}C	5730 y	β^- (γ)	0.156

In case of ^{241}Am the alpha counting window is 150-400 keV. A fraction of about 99% of the ^{241}Am total counting rate (in the 0-2000 keV) is found in the above mentioned alpha counting windows. ^{234}Th is measured together with its daughter, ^{234m}Pa, whose short life-time allows the secular radioactive equilibrium to be reached in about 5 minutes. The energy window of 0-1000 keV is used for counting.^{234}Th counting rate is always corrected for decay relative to the beginning of the experiment. In case of ^{237}Np, the contribution of the beta tailing activity of the daughter ^{233}Pa into the alpha-energy region of ^{237}Np is separated using the pulse decay analysis option of the scintillator analyzer according to the procedure described by the Packard manufacturer [78]. The discriminator setting is estab-

lished using ^{241}Am and ^{45}Ca standard solutions with composition and geometry similar to that of the samples. A Pulse decay discriminator (PDD) of 120 is chosen as discriminator setting in order to minimize the spillover of beta events into the alpha counting window. The beta counting window is set as 0-2000 keV and the alpha window as 140-350 keV. For these counting windows and the chosen PDD the beta spillover into the alpha window is below 0.1 %. ^{233}U is measured in the 120-400 keV energy window, where approximately 98% of the ^{233}U total counting rate is recorded.

For the dual-labelled samples (i.e. actinide-[^{14}C]-humic acid samples), the degree of overlap between the ^{14}C low maximum energy (156 keV) and the alpha energy region of ^{241}Am or ^{233}U can be resolved manually, by choosing appropriate energy windows. Selection of the windows is achieved by measuring reference solutions containing only the radionuclide of interest, i.e. either ^{241}Am, ^{233}U or ^{14}C and calculating the degree of spectral interference in the counting windows. The ^{14}C counting window is set as 0-120 keV. The alpha counting windows are 150-400 keV for ^{241}Am and 120-400 keV for ^{233}U. In the beta counting window (0-120 keV), ^{241}Am is found to contribute with about 0.5% of its counting rate in the alpha window, whereas the ^{233}U contribution is found to be of approximately 1%. In all cases the counting rate in the beta window is corrected. Due to the interference of the low energetic beta emitters ^{234}Th and ^{14}C the simultaneous measurement of the two radionuclides is not possible by LSC. Therefore, parallel samples are prepared labelled either with ^{234}Th or ^{14}C. Typical LSC spectra of samples containing ^{234}Th, both [^{14}C]-humic acid and ^{241}Am (or ^{233}U), and ^{237}Np are presented in Fig.3.3.

Aliquots of the radioactive solution used for spiking are measured along with each set of samples and are considered as reference input activity. Blanks consisting of 1 mL 0.1 M HCl and 10 mL scintillation cocktail are also measured and the sample counting rate is corrected accordingly.

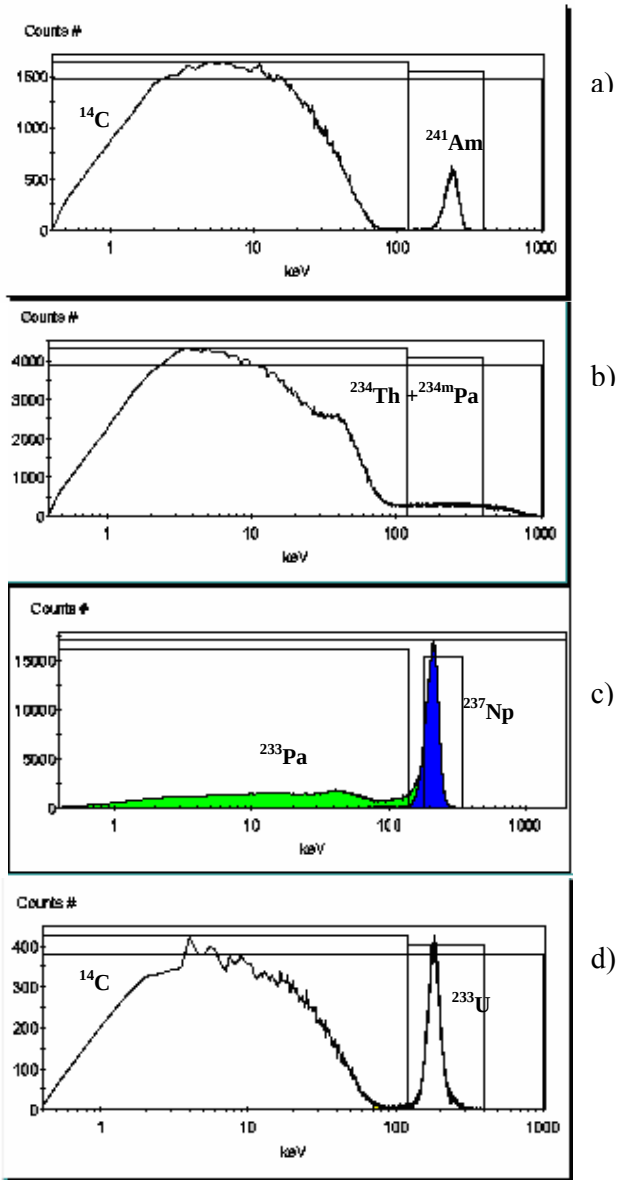

Fig. 3.3 LSC spectra of samples containing: a) both ^{14}C and ^{241}Am, b) ^{234}Th in equilibrium with ^{234m}Pa; c) ^{237}Np in equilibrium with ^{233}Pa, with separation of ^{237}Np alpha contributions (blue region) from the low energy beta tailing (green) of the daughter ^{233}Pa; d) both ^{14}C and ^{233}U. Energy counting windows set as for the experiments.

3.4 Colorimetric quantification of Si and Al

Monomeric silicic acid

Monomeric silicic acid is quantified by the molybdenum test (Spectroquant® 1.14794 Silicon, Merck) [25, 27]. The colorimetric method is based on the selective detection of monomeric /dimeric silicic acid species, the so-called soluble silica, reacting fast with the molybdic acid as compared to the oligomeric (colloidal) species. The method uses the reaction between silicate ions and ammonium molybdate forming a silico-molybdic complex which is further partially reduced to the silico-molybdenum blue form. The latter complex shows maximum absorbance at 820 nm. Measurements are performed in 10 mm plastic cuvettes using a Cary 5000 spectrophotometer assisted by the Cary WinUV 3.0 Software. The precision of the method is within 1% (1σ) in the concentration range 0.1 to 5 mg/L Si.

Soluble Al

In the present work the soluble Al is defined as the Al in a solution passing a 10 kDa pore size filter (after removal of precipitate and colloids) and that can be measured by colorimetry using Chromazurol S as complexation agent (Merck Standard Procedure, Spectroquant 1.14825-Al). The Al-Chromazurol complex has maximum absorbance at 548 nm. In case that Al is present in solution complexed with EDTA, an additional preparation step is required in order to destroy the Al-EDTA complex [88]. Thus, prior the Chromazurol addition the samples are mixed with an acidic solution of 1.5 M $Pb(NO_3)_2$ in 0.1 M HCl for a final Pb concentration in the sample ten fold in excess relative to EDTA. The exchange reaction between the EDTA complexed-Al and Pb^{2+} ion is found to be complete within 1 h at pH 1 and ambient temperature. Details on the optimization of this experimental procedure will be published elsewhere [88]. Measurements are carried out in 10 mm quartz cuvettes using a Cary 5000 spectrophotometer assisted by the Cary WinUV 3.0 Software. Al determination is possible in the linear range of $7x10^{-6}$ M up to $1x10^{-4}$ M. The precision of the method is approximately 2% (1σ).

3.5 Spectroscopic characterization of the actinide/colloid binding

TRLFS for the speciation of colloid borne Cm

The measurements are performed by using an excimer-pumped dye laser system (Lambda Physics, EMG 201 and FL 3002). Cm is excited directly at 375 or 383 nm and alternately, indirect at 370 nm via excitation of humic acid [135]. Cm fluorescence emission is measured in the spectral range of 580-620 nm, using a delay time of 1.2 µs at a gate width of 1.3 ms. An optical multichannel analyzer is used for detection, which consist of a polychromator (Jobin Yvon, HR 320) with a 1200 lines/mm grating and a time-gateable intensified photodiode array (Spectroscopy instruments, ST 180, IRY 700 G). For the fluorescence life-time measurements, the delay time is stepwise shifted at 5-25 µs within the time interval of 1.2-1000 µs [28, 97].

EXAFS spectroscopy for the speciation of Th(IV), Np(V) and U(VI) in aluminosilicate solutions

The coprecipitated samples for X-ray absorption spectroscopy are prepared by titration. We use aliquots of actinide stock solutions of 4 $x10^{-3}$ M Th(IV) in 0.9 M HNO_3 and $9.4x10^{-3}$ M U(VI) in 0.5 M HNO_3 (cf. section 3.1, b) and $7.56x10^{-2}$ M Np(V) (^{237}Np) in 0.1 M $NaClO_4$. An acidic solution containing a mixture of the actinide solution and Al solution of $4.0x10^{-3}$ M Al^{3+} in 0.03 M HCl is titrated with an alkaline Si solution of 0.2 M $Si(OH)_4$ in 0.2 M NaOH (stock solution of set (1) in 3.1). Titration is conducted to the preset pH of 8.5 for Th and U and to pH 12 for Np. For Th and U blank solutions are prepared by titration of only the actinide solution without Al, with the alkaline Si solution. One Th-containing sample is also prepared by titration of an acidic solution containing both Th^{4+} and Al^{3+} with a NaOH solution, without Si addition. The coprecipitated samples are measured without any filtration step.

From the final sample volume of about 20 mL obtained after coprecipitation, aliquots of 2.5 mL (in case of Np aliquot of 0.5 mL of 1.5 mL total) are transferred to Eppendorf centrifuge tubes and sealed for the measurements. The sample containing only Th and Al is measured as a wet paste separated from the liquid phase by centrifugation (15

min. at 3000 g) and placed in a 0.5 mL Eppendorf tube. None of the other samples contains visible precipitate. Prior the measurement, the samples are aged for three to four days. Sample preparation and measurement are performed at ambient temperature and atmosphere, but without controlling the equilibration with the atmospheric CO_2.

Th -L_{III} (16.3 keV), Np-L_{III} (17.608 keV) and U-L_{III} (17.155 keV), X-ray absorption spectra are collected at the INE-Beamline at ANKA [89], using a Ge(422) double-crystal monochromator, detuned to 70% of maximum flux. The measurements are performed in both transmission mode, using Ar gas–filled ionization chambers for monitoring the intensities of the incident and transmitted light, and, in the fluorescence mode, using a 5-element solid state Ge fluorescence detector (Canberra). Energy calibration is performed relative to the first inflection point in the XANES of a Zr reference foil (Zr-K edge at 17998 eV). Up to seven scans are collected, interpolated and averaged.

The data from the florescence detection mode are analyzed in case of Th-aluminosilicate and Th-silicate samples, and from the transmission detection for the Th/Al, U and Np containing samples. The isolation of the EXAFS oscillations from the raw absorption spectrum via spline fitting and the least-squares EXAFS curve-fitting are performed using both the WINXAS 2.3 and UWXAFS programme packages. Theoretical backscattering amplitude and phase functions used in the fits are calculated with FEFF8.2 [85] code using simple single scattering (SS) paths for each pair of atoms.

Only single scattering paths are included in the fits of the data to the EXAFS equation (eq. 2.15). Multiple scattering (MS) paths along the Np(V)-O_{axial} and U(VI)-O_{axial} bonds have been reported [90] to contribute to the EXAFS with an effective distance twice the An-O_{axial} distance. Preliminary calculations of the 4 legged (MS) path O_{axial}↔An↔O_{axial} using the difference method [90] show that the MS feature does not change significantly the remaining fit parameters. During the fits, the amplitude reduction factor (S_0) is held constant at 1. The shift in the ionization energy, ΔE_0, is constrained to be the same value for each shell (i.e. one global parameter for both O shells, another one for the Si(Al) shell, and one for the Th shell when necessary. In case of U(VI) the number of the axial O atoms is held constant at 2 during the final fit since preliminary fits result in a coordination number of about 1.7.

3.6 Desorption of activity with chelating agents

The desorption experiments are conducted by addition of the 0.1 M EDTA stock solution (see 3.1) to the actinide-aluminosilicate solutions or aluminosilicate solutions without actinide. After EDTA addition, the pH of the sample is readjusted by slow addition of small volumes of 0.1 M NaOH solution. The EDTA concentration in the sample is ten folds higher than that of Al. Following varied contact time period from 3 h to 35 d, the solutions are filtered through 0.45 μm pore size to eliminate the precipitate, followed by filtration at 10 kDa pore size combined with centrifugation (5000 g) for separation of the colloids. Activity in the colloids is further determined as described in section 3.3. The soluble Al is measured in the filtrate passing the 10 kDa filtrate as described in section 3.4. By difference with the Al concentration introduced initially in the sample we obtain the Al that is not desorbed by EDTA, or what we call the EDTA resistant Al.

4. Interaction of actinide(III-VI) with aluminosilicate colloids

The investigations aim at giving a better insight into the process of the interaction of actinides with aluminosilicate colloids in the course of their generation by conucleation. The present work is an extension of the former investigations of actinides(III, IV) to actinides of higher oxidation states (Np(V), U(VI)), and also to the characterization of the actinide-HAS colloid binding. Accordingly, the study concerns the following issues: identification of the conditions for the formation of stable actinide-HAS pseudocolloids including kinetic aspects of the incorporation process, determination of the colloids capacity to incorporate increasing amounts of actinide, characterization of the An binding state within the HAS bulk and investigation of the stability of HAS-colloid-borne actinides.

4.1 Co-nucleation of Si, Al and actinide(III)/(IV)/(V)/(VI)

4.1.1 Formation of colloid-borne actinides: parameter screening

A radiometric screening experiment is performed in order to ascertain the conditions favorable for the formation of stable actinide-HAS colloids in respect with pH, Si and Al concentration and their concentration ratio. Following the previous experiments regarding Am(III) and Th(IV) [25, 26], a tracer amount of either ^{237}Np(V) or ^{233}U(VI) is allowed to participate in the co-nucleation process of Al and Si. The chosen Np and U concentrations are of $7x10^{-6}$ M and $8x10^{-7}$ M, respectively. The actinides concentration level is chosen in order to avoid the colloid formation in the actinide pure solution without Si and Al. Thus, as can be seen in Fig. 4.1, in samples without Si and Al, most activity of Am, Th, U is present in the precipitate at the current concentration, indicated by the dashed line. The minimum U and Np concentration is however limited by the necessity to achieve a good enough counting statistic of ^{233}U and ^{237}Np, respectively. The final concentration of Si and Al and their ratio are of $1x10^{-3}$ M Si, $1x10^{-5}$ M Al and $1x10^{-2}$ M Si, $1x10^{-4}$ M Al. They correspond to the optimal conditions (cf. section 2.2.1) previously determined [27] for the formation of the HAS colloids from monosilicic and polysilicic acid, respectively. For $1x10^{-2}$ M Si (6.4 times the over-saturation concentration) the fraction of polysilicic acid formed during co-nucleation is expected to reach a maximum level of 85 %, cf. Fig. 3.1 (approach A), corresponding to the equilibrium dictated by the solubility of amorphous silica. Blank mother solutions containing the actinide only, without Si and Al, and the actinide with only Al or Si are also analyzed in order to compare the actinide be-

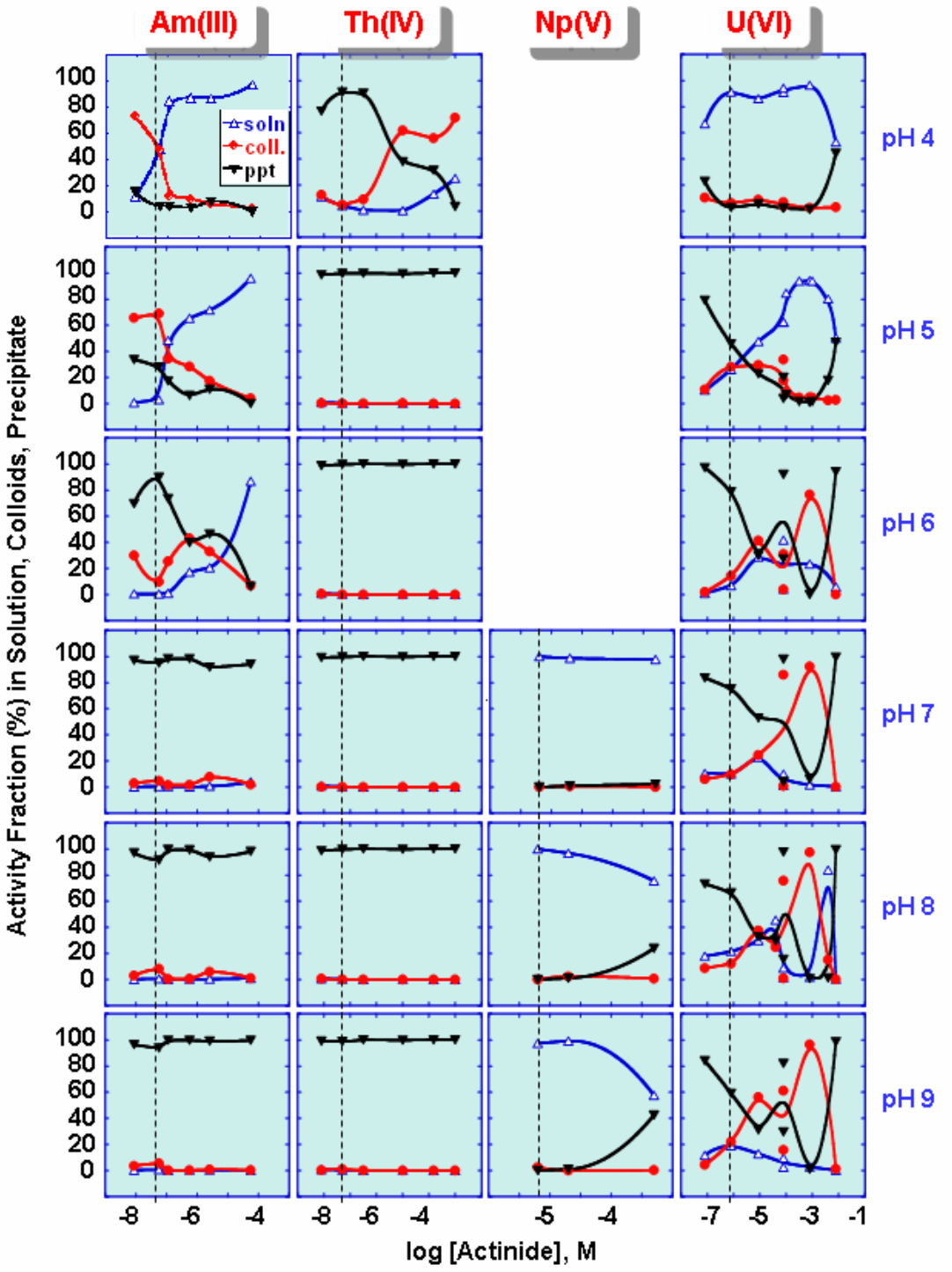

Fig. 4.1 Distribution of actinide activity fraction (%) between solution, colloids and precipitate as a function of initial actinide concentration, for samples at different pH after 35 d conditioning time, containing only the actinide. Dashed lines mark the actinide activity used in the parameter screening experiment (section 4.1.1) of: $5x10^{-8}$ M Am / $5x10^{-8}$ M Th / $7x10^{-6}$ M Np / $8x10^{-7}$M U. Results for Am(III) and Th(IV) are taken from [25].

behaviour with and without the HAS colloid formation. Fig**.** 4.2 depicts an overview of the actinides incorporation pattern into the colloidal phase in the pH range 4-9. Results are shown for blanks, HAS-monosilicic and polysilicic acid after 35 days sample conditioning time. The present results for U(VI) and Np(V) as well as the previous results for Am(III) and Th(IV) are included for the purpose of comparison. As can be observed from the diagram, there is an enhanced activity fraction of Am, Th and U in the colloidal phase in the presence of Si and Al as compared to the blank samples. The activity transfer from precipitate (in blank samples) to colloids observed in the presence of the aluminosilicates is an indication of actinides binding to the HAS colloids. As one can further observe in Fig. 4.2, the actinides incorporation patterns into the HAS colloids are different, depending on whether the HAS colloids are generated on the basis of monosilicic or polysilicic acid. This suggests different incorporation mechanisms depending on the conditions of colloid formation. The actinides show also different incorporation behaviour. Thus, Am(III) colloid-borne fraction exhibits several maxima: at pH 5 and 8-9 for the HAS colloids generated from monosilicic acid and in the pH range 8-9 for HAS–polysilicic acid based colloids. In contrast, generation of colloid-borne Th(IV) and U(VI) is poor for HAS colloids generated from monosilicic acid. Maximum colloid-borne fraction is found for Th(IV) and U(VI) for HAS colloids formed from polysilicic acid. In this case, the actinide activity fraction in the colloidal phase increases with increasing pH and more than 90% activity fraction appears to be associated with the colloidal phase in the pH range 6-9. Another distinct feature of Th(IV) and U(VI) is their incorporation into the colloidal phase in the pH range 8-9 in presence of polysilicic acid without addition of Al. The observed fact suggests the co-nucleation of the two actinides with the polysilicic acid, however, in the pH range 5-7 the presence of both Si and Al is necessary in order to generate stable colloid-borne Th(IV)/U(VI). This behaviour indicates a distinct incorporation mechanism for the tetra- and hexavalent actinides as compared to the trivalent actinides. Np(V) appears not to interact with the HAS colloids in the investigated pH range 7-9. Only a small Np fraction of 13.5 %, is found in the colloidal phase in case of the HAS colloids formed from polysilicic acid at pH 9. Most of the Np activity remains in solution as found also in the blank sample (Fig. 4.1) for which such behaviour could be expected from the thermodynamic solubility data [91]. It is evident from the results presented so far, that the conditions for maximum An incorporation into the HAS-polysilicic acid colloids correspond to

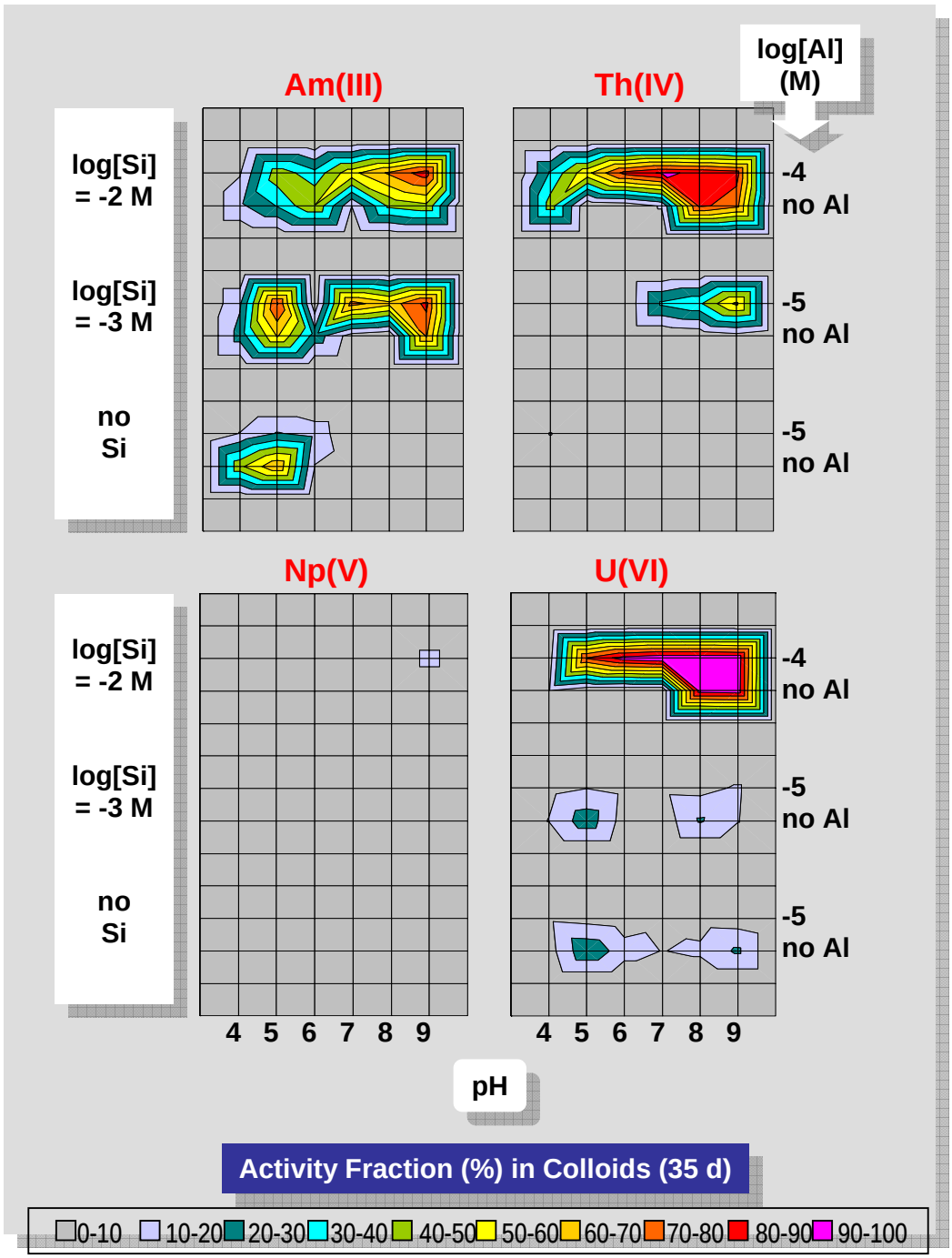

Fig. 4.2 Colloid-borne activity actinide fraction (%) normalized to the input activity as a function of pH after 35 d sample conditioning time. Input activity is $5x10^{-8}$ M Am / $5x10^{-8}$ M Th / $6x10^{-6}$M Np / $8x10^{-7}$ M U. Si and Al concentrations are indicated on the left and respectively right side of the diagram. Mother solutions with 10^{-5} M Al, 10^{-3} M Si generate HAS-monosilicic acid colloids whereas those with 10^{-2} M Si, 10^{-4} M Al generate HAS-polysilicic acid colloids. Results for Am(III) and Th(IV) are taken from [25, 27].

the conditions of advanced hydrolysis, i.e. depend on the actinide and pH and as can be seen from the speciation diagrams in Figs. 4.3 and 4.4.

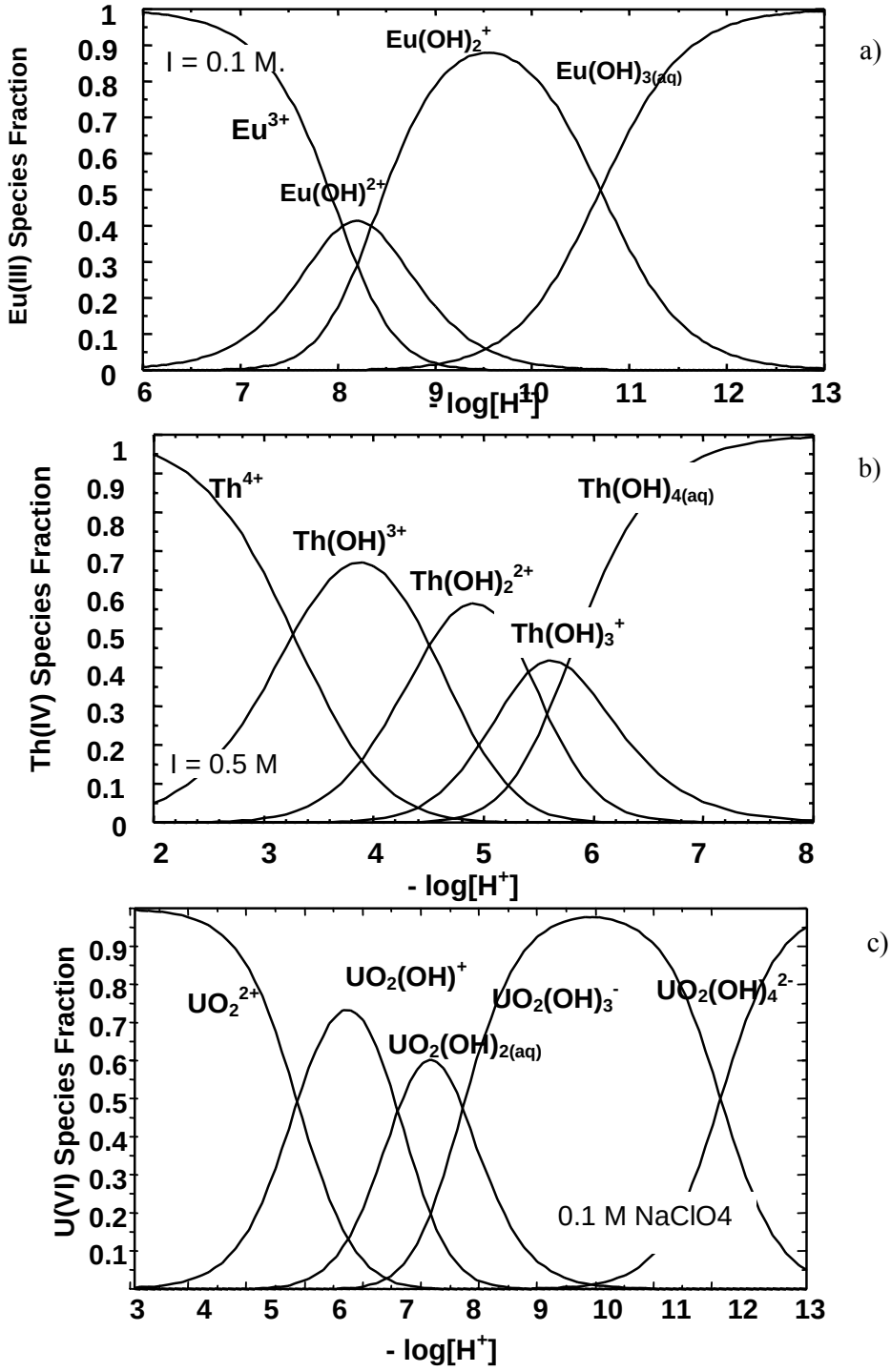

Fig. 4.3 Distribution of solution species as a function of pH in carbonate–free solutions of 0.1 M $NaClO_4$ or 0.5 M $NaClO_4$ at 25^0 C for: a): Eu(III), b): Th(IV) at $[Th]_{total}<10^{-9}$ M and c): U(VI) at $[U]_{total} < 10^{-9}$ M [92].

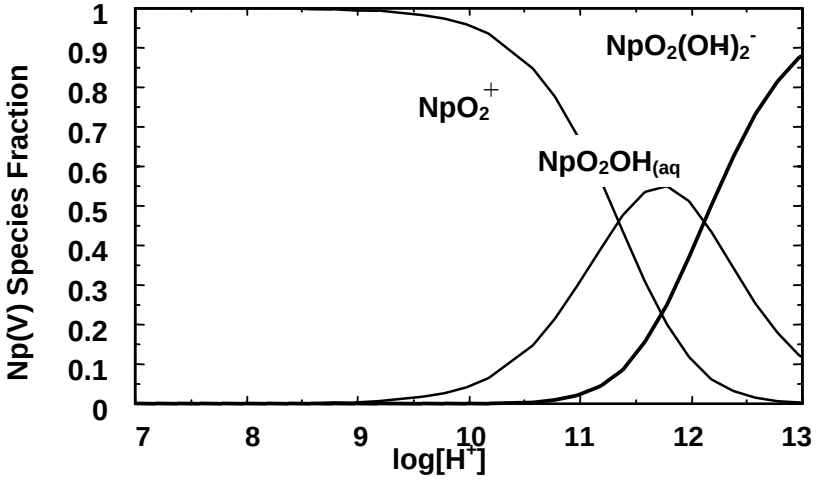

Fig. 4.4 Distribution of solution phase Np(V) hydrolysis species, $NpO_2(OH)_n^{1-n}$, as a function of pH, in a carbonate-free solution of 0.1 M $NaClO_4$ at total dissolved [Np]< 10^{-6} M [91].

We attribute the very low interaction between Np and the HAS colloids to the reduced tendency of Np(V) towards hydrolysis, starting only at pH 10 as appears from Fig. 4.4.

4.1.2 Kinetics of actinide incorporation into colloids

In order to get more information about different mechanisms of interaction, the kinetics of actinide incorporation into the colloidal phase at different conditioning times of the mother solution, from 3 h to 35 days, is analyzed. Np(V) behavior is analyzed under the pH conditions favoring its hydrolysis, namely in the pH range 10 to 12. Fig. 4.5 illustrates comparatively the actinide activity fraction in the colloidal phase for HAS colloids generated from both monosilicic and polysilicic acid. Selected results for Am, Th and U are shown for the pH range 6-9.

In case of Am, Th and U in presence of the HAS colloids generated from monosilicic acid (Fig. 4.5 a), the activity fraction in the colloids decreases in time in the pH range from 7 - 8 or remains constant at pH 9. Although the U colloid-borne fraction is very poor at pH 9, this trend is observed for all the three actinides. Therefore, the increased colloidal stability observed in at pH 9 might be due to the increased negative charge of the functional groups of the aluminosilicate colloids.

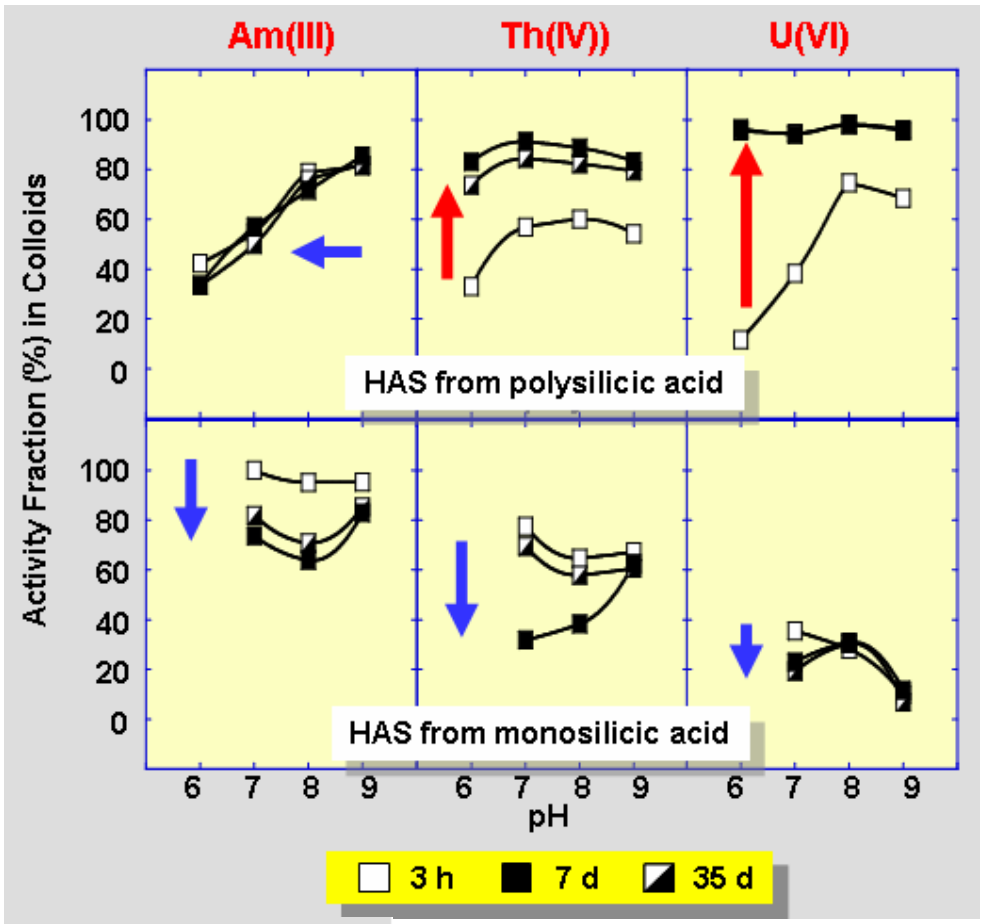

a)

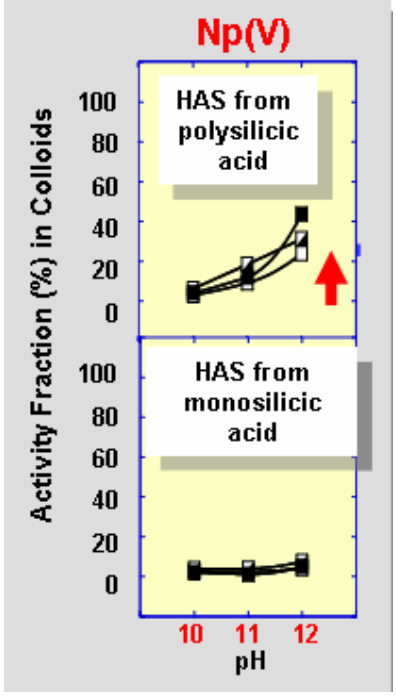

b)

Fig. 4.5 Colloid-borne actinide activity fraction (%) normalized to the input activity as a function of pH after different conditioning times of the sample, from 3 h to 35 d. Samples contain: $5x10^{-8}$ M Am, $5x10^{-8}$ M Th, $8x10^{-7}$ M U(VI) and $6x10^{-6}$ M Np in HAS colloids solution generated from monosilicic acid (10^{-5} M Al/10^{-3} M Si) and polysilicic acid (10^{-4} M Al/10^{-2} M Si). The results for Am and Th are taken from [25].

For the HAS colloids generated from polysilicic acid, Am(III) activity fraction in the colloidal phase remains constant in time in the pH range between 6-9. On the contrary, the colloid-borne fraction of Th(IV) and U(VI) increases with time, the effect being more pronounced at lower pH values. For example, at pH 6, the initial amount of colloidal U of approximately 60%, increases to 95% within 35 days conditioning time of the mother solution. The time dependent incorporation of Th(IV) and U(VI) into the colloids follows the polymerization behavior of the monosilicic acid, which has been shown to occur rather slowly at low pH and low Si concentration, as illustrated in Fig. 4.6. As can be seen, for a Si solution with concentration corresponding to the experimental conditions for the formation of HAS–polysilicic acid colloids (6.4 times the saturation concentration), approximately 10 days are needed for the polysilicic acid to attain the equilibrium level in solutions of pH 5-7. The fact that Th(IV) and U(VI) follow the behavior of the silica might further suggest that, the hydroxo-complexes of U(VI) and Th(IV) copolymerize with silicic acid prior formation of Th/U-HAS pseudocolloids (i.e., binding to the to Al sites). This aspect shall be discussed later in section 4.2.2.

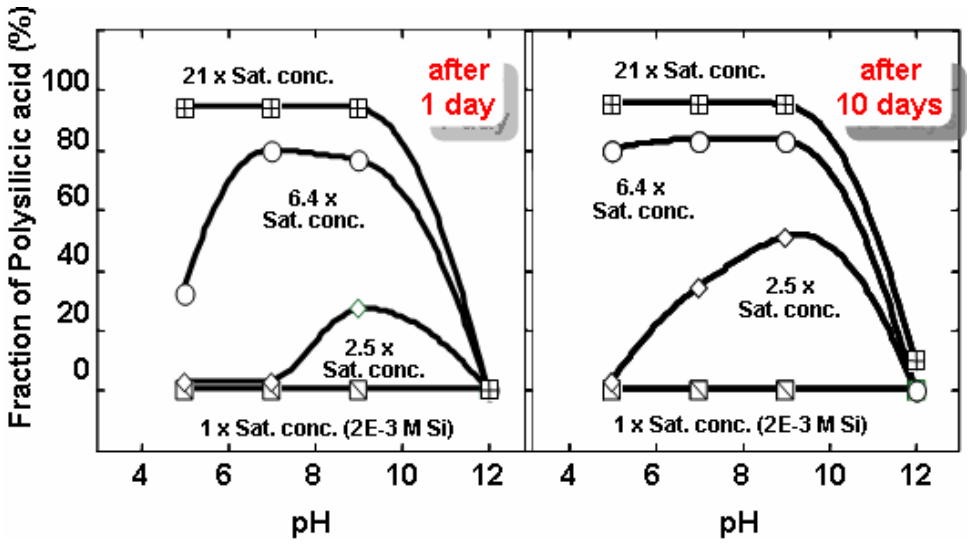

Fig. 4.6 The pH dependent polymerization of monosilicic acid. Fraction of polysilicic acid formed in solutions with different initial Si concentrations after 1 d (left) and 10 d (right) after pH adjustment of the original Si solution of pH 12 [27].

In case of Np in HAS-monosilicic acid solutions (Fig. 4.5 b), no colloid formation is observed during the 35 d observation time, Np activity fraction remains mainly in solution. The same observation is valid for the HAS -polysilicic acid colloids at pH 10-11. However, for HAS colloids formed from polysilicic acid at pH 12, corresponding to the pH region where the Np(V) hydrolysis is already advanced according to thermodynamic data (Fig. 4.4), we observe an increase of the fraction of colloid-borne Np with time. Hence, 20% of Np activity appears to be associated with the colloidal phase at the first moment of the experiment, increases to 40% with aging of the mother solution to 35 d and is found to remain stable up to 60 days. The interaction kinetics resembles, as in case of Th and U the polymerization behavior of the monosilicic acid.

The differences in the interaction kinetics between Am(III) and Th(IV)/U(VI) support the idea of distinct incorporation mechanisms suggested earlier from the incorporation patterns.

4.1.3 Capacity of colloids to incorporate actinides

The results presented in this section refer to the maximum concentration of actinide possible to be incorporated into the HAS colloids generated from either monosilicic or polysilicic acid. For this purpose, increasing amounts of actinide (up to $8x10^{-3}$ M U, $1x10^{-3}$ M Th and $5x\ 10^{-4}$ M Eu, as chemical homologue of Am, are separately included in the generation process of the HAS colloids, in addition to a constant tracer amount of the actinide of interest. Figure 4.7 illustrates selected results for the actinide fraction incorporated into the colloidal phase as a function of actinide concentration for coprecipitation samples after 35 days conditioning time in the pH range 7-9. The results refer to the actinide behaviour in presence of HAS colloids from monosilicic and polysilicic acid and also to blank samples containing only the actinide.

Regarding the results on Am(III) and Th(IV) [25], several remarks can be made as described in the followings. In the selected pH range 7-9, the maximum concentration of the incorporated Am(Eu) is found to be of approximately $4.5x10^{-5}$ M for HAS colloids formed from polysilicic acid out of a solution of $1.3x10^{-2}$ M Si and $1.5x10^{-4}$ M Al. Taking into account the Si/Al atomic ratio in the HAS colloids of approximately 1 (as discussed in section 2.2.1), the incorporated Am(Eu) has been found to correspond in this case to about 50 % of Al or Si concentration in the HAS. Similarly, the maximum colloid-borne

Th is found at pH 9 for HAS colloids formed from polysilicic acid, with the maximum amount corresponding in this case to 1.3 x10^{-4} M Th and equivalent to 80% of Si or Al concentration in the HAS colloids. At actinide concentration above approximately 10^{-4} M, the HAS-colloid-borne actinides are destabilized and the actinides are transferred to the precipitate.

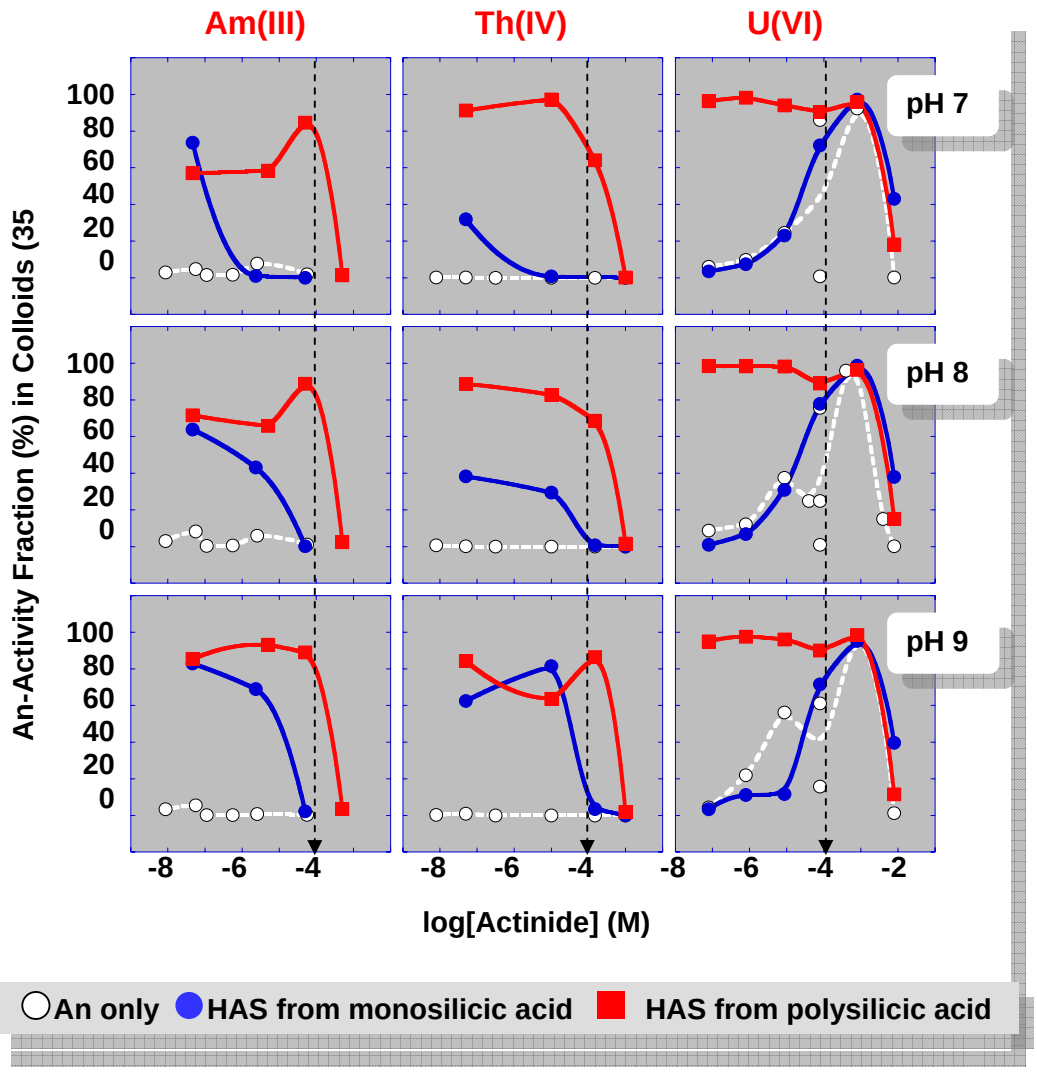

Fig. 4.7 Colloid-borne actinide activity fraction (%) as a function of actinide concentration at different pH values after 35 days sample conditioning time. The three different samples series contain: only the actinide, 1x10^{-3} M Si/1x10^{-5} M Al corresponding to HAS–monosilicic acid colloids and 1x10^{-2} M Si/1x10^{-4} M Al, forming HAS-polysilicic acid colloids. The vertical lines mark the maximum actinide concentration above which the actinide-HAS pseudocolloids are destabilized. Results for Am(III) and Th(IV) taken from [25].

HAS colloids generated from monosilicic acid appear to have lower capacity to hold Am(Eu) and even much lower for Th, in the latter case a 100 times less as compared to the HAS generated from polysilicic acid. For both HAS-monosilicic or polysilicic acid colloids the capacity of incorporating Am and Th increases generally with increasing pH.

As can be observed in Fig. 4.7, the HAS colloids generated from polysilicic acid in the pH range 7-9 appear to have also high capacity to incorporate U. We can unambiguously differentiate at pH 7-8 a maximum concentration of incorporated U of $6x10^{-6}$ M (corresponding to approximately 78% of $8x10^{-6}$ M U migrating from the mother solution to the HAS). The capacity of the HAS colloids formed from monosilicic acid appears to be very low irrespective of the pH. Similar to the case of Am and Th, the maximum amount of U migrating from solution to the HAS colloids seems to be limited by the concentration of Si or Al in the HAS colloids (10^{-4} M). Unfortunately at U concentration around 10^{-4} M the generation of U real colloids becomes abundant and the fraction of colloid-borne U in presence of Si and Al is similar to that in blank solutions, preventing us to draw a clear conclusion. Generation of a marginal amount of colloidal U can be observed in the blank samples already at U concentration of approximately $8x10^{-6}$ M, which is above the equilibrium concentration corresponding to the solubility limit of U(VI) oxides/hydroxides [61]. Formation of U(VI) real colloids is documented in the literature [5]. Polynuclear complexes like $(UO_2)_2(OH)^{2+}_2$ and $(UO_2)_3(OH)^{+}_5$ are reported to form at U concentration above 10^{-6} M in the neutral pH range [31, 93-95] and further condensation of such compounds via oxo-bridging may lead to the colloids generation. The large oscillations observed in the blank curve at U concentration around $8x10^{-5}$ M U indicate the region of low stability at the onset of U colloid formation. We observe that at concentration above 10^{-3} M U the colloidal phase is destabilized and U is transferred to the precipitate.

To summarize, the general observed trend is that the amount of actinide incorporable into the HAS colloids increases with pH and Si concentration and is correlated with the presence of polysilicic acid species. Affinity of HAS colloids generated from monosilicic acid for actinides decreases in the order Am(III) > Th(IV) ≥ U(VI).

4.2 Spectroscopic speciation of aluminosilicate colloid-borne actinides

The results presented in the previous section have evidenced the conditions (pH, concentration of Si and Al) required for the optimum formation of An-HAS pseudocol-

loids. In the followings TRLFS and EXAFS spectroscopy are applied in order to describe the chemical binding of the actinides to the aluminosilicate colloids. Both methods have limitations. Thus, TRLFS cannot be applied in the case of Th(IV) and Np(V) [96] and its application is more difficult in case of U(VI) as does not provide information about the number of water molecules remaining in the U coordination sphere. EXAFS sensitivity is limited to the tenths of millimolar An concentration that is beyond the level that ensures stability of the colloidal phase. An binding state within the aluminosilicate bulk can be investigated, but one should be aware of the fact that the type of binding may change with concentration. EXAFS measurements are performed in order to investigate the coordination environment of An(III-VI) coprecipitating with the aluminosilicates. The questions to be answer are: what types of bonds occur at the interaction of actinides with the aluminosilicates? How many atoms of Si/Al are coordinated via oxo-bridges? In other words, how strong is the interaction between the actinide and the aluminosilicate ligand? The comparison of the results for Eu(III) with those obtained for Cm(III) by TRLFS is also aimed. The essence of the previous work based on TRLFS is summarized in the next section.

4.2.1 Cm(III): Time resolved laser florescence spectroscopy (TRLFS)

TRLFS is the method dedicated to characterize the binding state of trace amounts of Cm(III), the chemical analogue of Am(III). This method has been applied by Panak et al. for studying the speciation of colloid-borne Cm(III) in the HAS solutions generated from both monosilicic and polysilicic acid and the results have been reported in [25-28, 97].

Selected speciation results are illustrated in Fig. 4.8 for Cm in HAS solution generated from polysilicic acid, which have been shown to favor formation of maximum colloid-borne Am(III) (Fig. 4.8 a). The graph in the upper part of Fig. 4.8 b depicts the deconvoluted fluorescence spectra of different Cm species present in solution with increasing pH, whereas the graph in the lower part illustrates the species fractions as a function of pH. The shift of the emission peak towards higher wavelength with increasing pH is attributed to the formation of inner-sphere complexes by an exchange of water molecules with the complexing ligand, either aluminosilicate or silicate. In addition to the Cm aquo ion with its characteristic emission at 593.8 nm and a life time of about 65 µs, three

Cm-HAS species are identified upon increasing pH in the aluminosilicate solutions generated from polysilicic acid: Cm-HAS(I) with the emission peak at 593.8 nm with a life time of 83.5 ± 3.7 µs, Cm-HAS(II) emerging at 601.8 nm with life time of 88.3 ± 5.2 µs, and Cm-HAS(III) which appears at 606.8 nm with much longer life time, of 518 ± 25 µs. The increasing fluorescence life time with increasing pH proves the gradual loss of the water molecules from the coordination sphere of Cm. The speciation results (Fig. 4.8 b lower part) evidence besides the Cm aquo cation with 9 coordination water molecules the Cm-HAS (I) species, found to have 7 remaining coordination water molecules, has its maximum contribution at pH 4-5, while the second species, Cm-HAS (II), with 6 water molecules left in the coordination sphere of Cm, reach a maximum contribution around pH 6.5. Cm-HAS (III) species has one or no water molecule in the coordination sphere and prevails at pH > 6. These three Cm species are confirmed to be colloidal by spectroscopy with the aid of ultrafiltration.

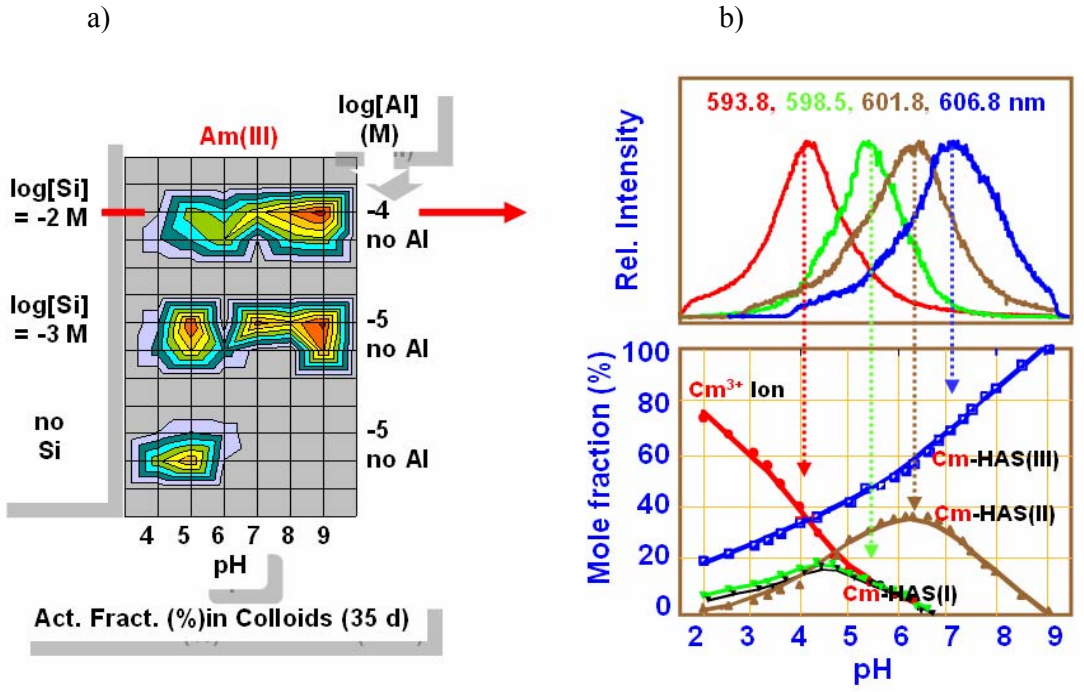

Fig. 4.8 a) Contour diagram showing the formation of colloid-borne Am ($5x10^{-8}$ M) as a function of pH for different mother solutions with Si and Al concentration as indicated on the axes and after 35 d conditioning time. Mother solution of 10^{-2} M Si/10^{-4} M Al generating HAS-polysilicic acid colloids is analyzed by TRLFS. b) Upper part: Emission spectra of the different Cm(III) species after deconvolution of the composite spectra of Cm ($4.9x10^{-8}$ M) in the mixed solution of 10^{-2} M Si and 10^{-4} M Al when increasing the pH from 2 to 9; Lower part: Relative Cm species distribution as a function of pH [from 27].

The authors also report similar spectroscopic characteristics and species distribution pattern for Cm in solution containing only polysilicic acid and those for Cm in HAS generated from polysilicic acid. On this basis, the authors suggest a similar kind of chemical binding of Cm within the HAS and the Cm-HPSi, rather with the silanol (Si-OH) moieties, than with the aluminol (Al-OH) groups. This assumption appears to be supported by the spectroscopic characteristics observed at the interaction of Cm with a suspension of Al hydroxide, showed to be significantly different from those observed in the experiment for the Cm-HAS formation. Based on the number of the water molecules remaining in the coordination sphere of Cm upon the complexation with the silicate ligand, the oxo-bridging binding state of Cm in aluminosilicate/silicate colloids is characterized as bi-dentate for Cm-HAS (I) and tri-dentate for Cm-HAS (II), respectively. Since in case of Cm-HAS (III) species there is virtually no coordination water molecule left in the coordination sphere of Cm, this species corresponds to the complete incorporation of Cm via multidentate oxo-bridging into the colloidal bulk. The results for the speciation of Cm in aluminosilicate solution generated from monosilicic acid (not shown here) have evidenced the formation of two colloid-borne species with spectroscopic characteristics similar to those of Cm-HAS(I) and Cm-HAS(II) for HAS generated from polysilicic acid. However, the Cm-HAS (III) species is not observed at the speciation of Cm in HAS solutions from monosilicic acid and therefore, its formation appears to be conditioned by the presence of the polysilicic acid at pH > 6. The formation of this complete incorporated Cm species is ascribed to the catalytic effect of the polysilicic acid in reducing the energy barrier of the conucleation. Moreover, the authors observe the formation of the Cm-HAS(III) when heating at 90° C for about 90 days the colloids generated in aluminosilicate solutions prepared at pH 7.5 from monosilicic acid [25]. It appears that Cm incorporation into HAS increases with pH, Si concentration and temperature. These are thermodynamic but also kinetic parameters enhancing the polymerization rate of Si. As suggested by the Arrehnius equation: $\ln (k_2/k_1) = E_a/R(1/T_1-1/T_2)$, where k_1, k_2 are the rate constants at temperatures T_1 and T_2, E_a is the activation energy and R is the gas constant, the temperature effect might be achieved by increasing the aging time of the mother solution. In relation to this aspect, we shall refer in section 4.3.2 to the possible influence of the aging time on the binding strength. Fig. 4.9 gives an overview on the Cm- HAS species identified in aluminosilicate solutions under different experimental conditions.

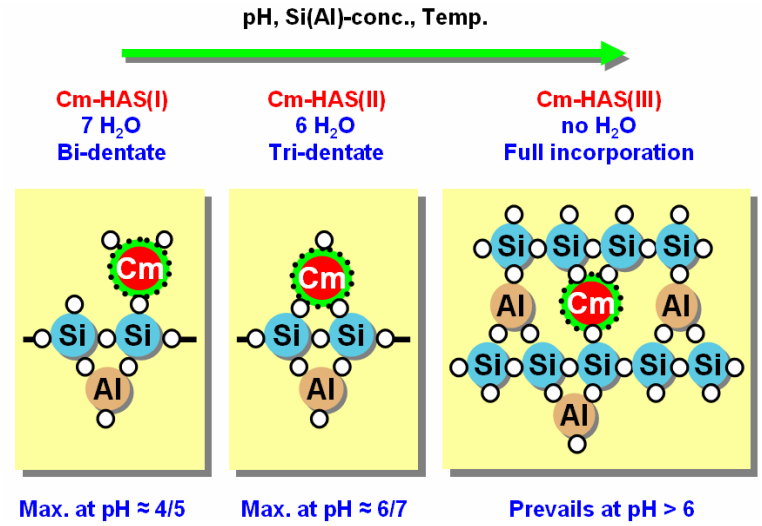

Fig. 4.9 Illustration of the three colloid-borne Cm species which form in the pH range 4 to 9 in a solution of 10^{-2}M Si / 10^{-4} M Al or in a solution of 10^{-3} M Si/10^{-5} M Al by heating 5 days at 90^{0} C.

4.2.2 Actinide(III)/(IV)/(V)/(VI): X-ray absorption spectroscopy

The selected experimental conditions for the EXAFS investigations, namely high pH values and high concentration of Si, correspond to those where the parameter screening experiments indicate maximum interaction of actinides with the aluminosilicate colloids, as discussed in section 4.1.1. Due to limited EXAFS sensitivity the actual actinides concentration is higher than in the radiometric experiment (section 4.1). Si and Al concentrations are approximately tenfold higher than their concentration used in the synthesis of HAS colloids. For the purpose of comparison, the speciation of U(VI) and Th(IV) is investigated also in pure silicic acid solution, without addition of Al. For Th(IV) in aluminosilicate solution, the experiments are carried out at two different Th concentrations in order to observe potential changes in Th(IV) speciation induced by the increased concentration. The final composition of the samples analyzed in the present work is described in Table 4.1. The metrical parameters obtained in the best fits, coordination number (N), bond distance (R), the relative mean squared difference in the interatomic distances or Debye–Waller factor (σ^{2}), and relative shifts in the ionization energy (ΔE_{0}) are summarized in Table 4.2. Figs. 4.10 and 4.11 show the k^{3}-weighted Th L_{III} EXAFS function, $\chi(k)$, and their corresponding Fourier transforms (FTs) together with the theoretical fits for the Th(IV) containing samples. Fig. 4.12 depicts the Np L_{III} data for Np(V) sample and Fig. 4.13 the U L_{III} data.

Table 4.1 Composition of samples analyzed by EXAFS.

	Sample	log[An] (M)	log[Si] (M)	log[Al] (M)	pH	[Si]/[Al]	[An]/[Al]	[An]/[Si]
Eu(III)*	Eu/HAS	-2.86	-1.00	-2.86	8.6	72	1.00	0.014
	Eu/Si(ref.)	-2.85	-1.00	-	8.6	-	-	0.014
Th(IV)	Th/HAS(1)	-3.00	-1.05	-2.70	8.6	45	0.50	0.011
	Th/HAS(2)	-2.66	-1.08	-2.70	8.6	39	1.10	0.026
	Th/Si(ref.)	-2.64	-1.14	-	8.6	-	-	0.032
	Th/Al(ref.)	-2.72	-	-2.72	8.6	-	1.00	-
Np(V)	Np/HAS	-2.30	-1.05	-2.74	12.0	49	2.78	0.056
U(VI)	U/HAS	-2.31	-1.09	-2.92	8.6	68	4.07	0.06
	U/Si(ref.)	-2.28	-1.09	-	8.6	-	-	0.064

*taken from [98]

for the U(VI) containing samples. The FTs are not corrected for the EXAFS phase shift causing peaks to appear at shorter distances relative to the real near-neighbour distances (R-Δ).

Th/HAS(1) ~1% Th (relative to the total concentration of Si and Al) in the sample solution

The FT main peak of the EXAFS spectra for Th/HAS(1) sample (Fig. 4.10, top) is attributed to an O shell, while the second shell is ascribed to the Si or Al atoms. The differentiation between Si and Al in the second coordination shell is not possible in EXAFS, as they are Z+1 elements; their backscattering amplitude and phase shift functions are too similar. Approximately 6 O atoms at an average distance of 2.41 Å are obtained in the fit results. The large asymmetry of the O coordination shell, reflected by a σ^2 value of 0.013 $Å^2$, indicates large variation in Th-O bonds. The relative low coordination number of the O atoms is comparable to that of 6-8 O atoms found for Th incorporated in silicate glasses [99] or Th sorbed onto amorphous silica [100]. In the second Th(IV) coordination shell 3-4 Si or Al atoms are located at an average distance of 3.79 Å. Similar bond lengths have been observed for Th(IV) sorbed onto amorphous silica and montmorillonite and for

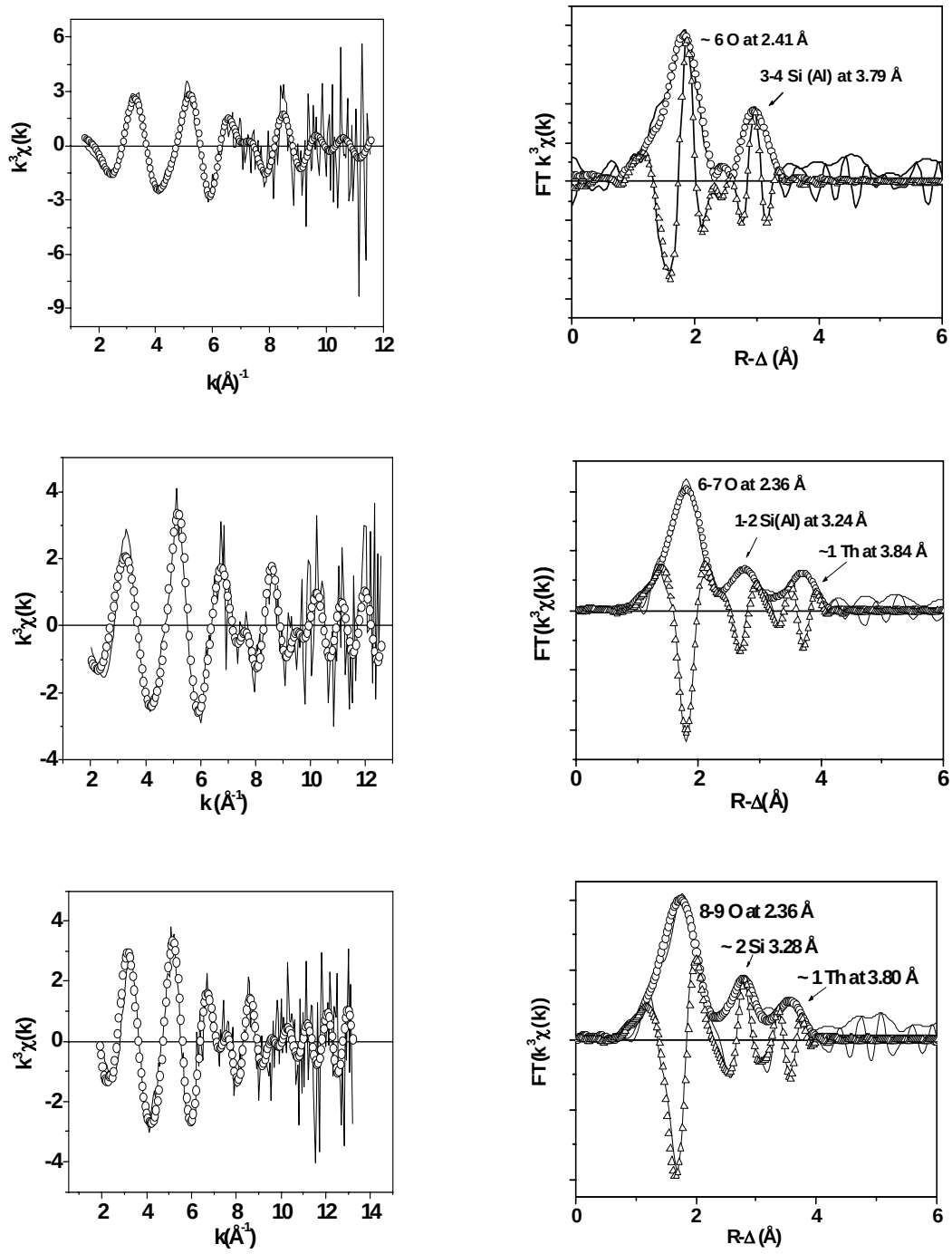

Fig. 4.10 Th L_{III} edge k^3-weighted EXAFS spectra (left) and the corresponding FTs (right), solid lines: the experimental data, symbols: the theoretical fits for the following samples. Top: Th/HAS(1) (~1% Th in sample). Transform k range 1.5-11.6 $Å^{-1}$, fit range 1-3.3 Å; Middle: Th/HAS(2) and bottom: Th/Si(ref) (~3% Th in sample). Transform k range 2-13 $Å^{-1}$, fit range 1.5-4 Å. Both FT amplitude (circles) and imaginary parts (triangles) are shown.

the Th(IV) coordinated to the SiO_4 tetrahedral edges in huttonite (3.69-3.78 Å) [100, 101]. For An(IV) dissolved in silicate glasses prepared at 500-1000° C, the second neighbour environment is described as 3-4 Si(Al) atoms at 3.50-3.85 Å [12]. For the similar system, Farges [99] reports the presence of Th(IV)-Si/Al contributions at two distances 3.25-3.50 Å and 3.80-3.90 Å. We do not detect any splitting in the Th-Si interatomic distances. We do find however the Th-Si(Al) distribution to be asymmetric, reflecting a variation in the distances.

Binding of Th to the Si/Al polyhedron may occur via one O atom, coordination known as corner-sharing link. Such type of coordination leads to a maximum Th-Si/Al distance, equal to the sum of Th-O and Si/Al-O distances, in case of a simple linear monodentate interaction between Th and the silanol/aluminol groups (the bond angle Th-O-Si of 180°). Such kind of configuration is illustrated below (not scaled).

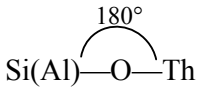

Bond angle smaller than 180° gives shorter Th-Si(Al) distances. The shortest Th-Si(Al) distance is obtained in case of a bindentate link when Th shares two oxygen atoms with one Si/Al polyhedron (edge-sharing link), as can be seen below:

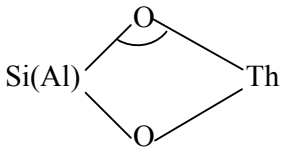

The Th-O-Si/Al bond angle, can be calculated according to the following equation:

$$\Theta = \cos^{-1}\left(\frac{R(Th-Si/Al)^2 - R(Th-O)^2 - R(Si/Al-O)^2}{-2\cdot R(Th-O)\cdot R(Si/Al-O)}\right) \qquad (4.1)$$

where R(Th-Si/Al) and R(Th-O) represents the EXAFS derived bond lengths and R(Si/Al-O) the bond lengths in the Si(Al) polyhedrons taken from literature data. We take into account the experimental Th-O and Th-Si(Al) bond lengths and the average Si-O and Al-O bond lengths for tetrahedral coordination reported for natural aluminosilicates and glasses [35, 103] of 1.64 Å and 1.75 Å, respectively. Calculations according to eq. 4.1 lead to Si(Al)-O-Th bond angles in the range 130-140°, which indicate a corner-sharing link of Th. As in our HAS samples of allophone /protoimogolite type Al could have both tetrahedral as well as octahedral coordination [22], it would be possible that Th(IV) binds to the aluminol groups in the AlO_6-octahedron. In this case, considering the average Al-O distance of 1.9 Å [104], our experimentally determined Th-Si(Al) bond length, 3.79 Å, leads to calculated Al-O-Th bond angle of about 120^0. Based on the comparison between our experimental Th-O/Th-Si distances and those described for the silicate glass and huttonite systems, we conclude that Th binding to SiO_4 (AlO_4) tetrahedra and/or AlO_6 octahedra is a corner-sharing link, where the Th(IV) coordination polyhedron is connected to the Si(Al) polyhedron by one O atom. Edge-sharing link to SiO_4 tetrahedron or AlO_6 octahedron is unlikely because it would lead to significantly shorter Th-Si(Al) distances, calculated as approximately 3.1 and 3.4 Å, respectively.

The Si(Al) coordination number (3-4 atoms) is larger for our coprecipitated aluminosilicates than observed for Th(IV) species sorbed onto amorphous silica and montmorillonite (1-2 atoms) [100, 101]. This indicates the presence of multiple links of Th(IV) units to the Si(Al) polyhedra. No contribution of any Th-Th distance is detected and thus there is no evidence for the formation of polynuclear-Th complexes or surface precipitate. This fact combined with the large Si/Al coordination number, proves the incorporation of Th(IV) into the polymerized aluminosilicate bulk. We cannot exclude some minor Th-Th contribution undetectable by EXAFS, however. Nevertheless, we can conclude that, under these conditions, the polymerization reaction between hydrolyzed aqueous Th complexes and the aluminosilicate units is favoured over the self-condensation reaction of hydrolyzed Th complexes.

Th/HAS(2) and Th/Si (ref): ~3 % Th in the sample solution

The coordination environment of Th(IV) in samples Th/HAS(2) and Th/Si(ref) appear to be quite similar, as one can see from the FTs of the spectra shown in Fig. 4.10

(middle and bottom). Furthermore, the corresponding structural parameters are different from those observed for sample Th/HAS(1), containing only 1 % Th. This fact indicates changes in Th speciation associated with the increase of the Th concentration in the sample. Hence, the Th-O interatomic distances for Th/HAS(2) and Th/Si(ref.), at an average distance of 2.36 Å, are 0.05 Å shorter compared to the sample with lower Th concentration. We also observe that for the samples with higher Th content, the second neighbour (Si/Al) has a lower N (Si/Al) of about 2 and appears at much shorter distances: 3.24 Å in the aluminosilicate samples and 3.28 Å in the silicate sample. These bond lengths are significantly shorter than the Th-Si/Al distances for Th(IV) sorption onto amorphous silica [100] or montmorillonite [101] discussed above and close to those found for Th(IV) dissolved in silicate glasses [99] and leachates [105]. Another distinct feature of the spectra for the samples with higher Th concentration as compared to Th/HAS(1) is the presence of a Th-Th distance. About 1 Th atom is observed at 3.84 Å and 3.80 Å in the Th/HAS(2) and Th/Si(ref), respectively. This suggests polynuclear Th species and/or a surface precipitate formation. At this level of Th concentration the interaction between the Th(IV) hydrolysis species becomes important. A similar Th-Th interaction (0.7 Th atoms at 3.77 Å) is described in [101] for Th(IV) sorbed onto montmorillonite at pH 5. The Th-Th distances in samples Th/HAS(2) and Th/Si(ref.) are however different from those observed in $Th(OH)_4$(am) or Th (IV) colloids (3.96 Å and 3.99 Å, respectively [106]).

Applying eq. 4.1 to the EXAFS derived Th-O and Th-Si(Al) distances, the calculated Th-O-Si(Al) bond angle is of approximately 110° in case of Th(IV) coordination to SiO_4 tetrahedron and of approximately 100° for Th(IV) coordinated to the AlO_6 octahedron. The very small bond angle of 100° indicates the edge sharing link of Th(IV) to the AlO_6 octahedron as a potential candidate for bidentate binding of Th(IV) to the aluminosilicates. In this case, taking into account an average Al-O bond length of 1.90 Å and our experimental Th-O of 2.36 Å, the calculated Th-Al distance (3.29 Å) would be only 0.05 Å shorter than the experimental one (3.24 Å). Although the calculated bond angle of 110° corresponding to Th coordination to SiO_4 tetrahedron is also small, the edge-sharing link to SiO_4 tetrahedron is unlikely because would lead to significantly shorter bond lengths, calculated as approximately 2.9 Å. The small angle and the observation of 2 Si(Al) atoms in the second coordination shell indicate rather a double corner sharing link, where Th binds to the silanol/aluminol groups of two neighbouring polyhedra. These polyhedra should have a certain orientation to accommodate Th in the given coordination,

i.e., with the distance between the two neighbouring Si or Si/Al calculated as approximately 3.2 Å. Such type of binding (double corner sharing) was proposed for Th sorbed onto amorphous silica [100] and for Hf(IV) onto mica [107].

Th/Al(ref) 50 % Th in sample (relative to the total concentration of Th and Al in solution)

As can be seen from Fig.4.11, the Th L_{III} EXAFS spectra and corresponding FT for Th(Al) sample differs completely from the previous cases. The O atoms shell is split into two distances. The majority of O atoms are located at average distance of 2.41 Å (O_1) and a smaller O contribution of about 1 atom (O_2) is found at about 3.03 Å. Such O coordination environment of Th (with respect to the split of the O shell at the corresponding distances) resembles that encountered in amorphous $Th(OH)_4$ and in amorphous Th colloid samples, as described by Rothe et al. [106].

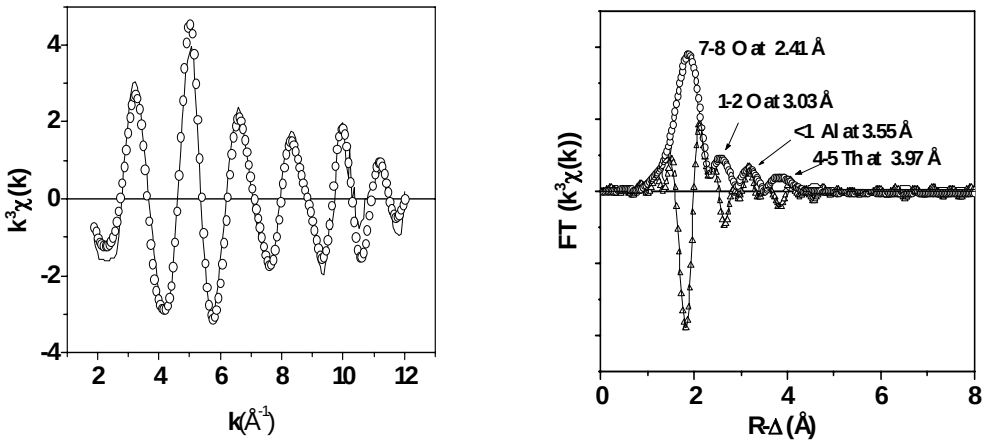

Fig. 4.11 Th L_{III} edge k ^{3}-weighted EXAFS spectra (left) and the corresponding FT (right) for Th/Al(ref) sample. Lines indicate experimental data and symbols the theoretical fit curves. Transform k range 1.8-12.2 $Å^{-1}$, fit range 1.5-4 Å.

The FT peak at R-Δ about 3.5 Å is well modelled using a shell of Al atoms. However, the fit is possible only by constraining the Debye-Waller factor of the O_2 to positive values. The FT peak representing the Th-Th interaction in this sample is pronounced and the fits yield coordination numbers of about 3-4 Th atoms, but with large disorder (σ^2 = 0.021 Å). The presence of Th neighbours at about 3.92-4.0 Å has been reported for amor-

phous $Th(OH)_4$ and microcrystalline ThO_2 [100, 106]. Giaquinta et al. [108] has described the environment of Th(IV) sorbed onto bentonite clay under hydrothermal conditions as a ThO_2-like polynuclear species with observed Th-Th distance at 3.93 Å.

Np/HAS

The FT of the EXAFS spectrum for the Np/HAS (Fig. 4.12) exhibits two peaks, ascribed to the axial O atoms (O_{ax}) and to the equatorial O atoms (O_{eq}). EXAFS analysis (Table 4.2) yields approximately two O atoms at about 1.85 Å, characteristic for the pentavalent neptunyl cation with Np-O_{ax} distances reported to vary in the range 1.83 to 1.85 Å [109-111]. The second shell consists of approximately five O_{eq} atoms at an average distance of 2.40 Å. The Np-O_{eq} distance is significantly shorter than expected for the aquo cation (2.49-2.53 Å) [109-112].

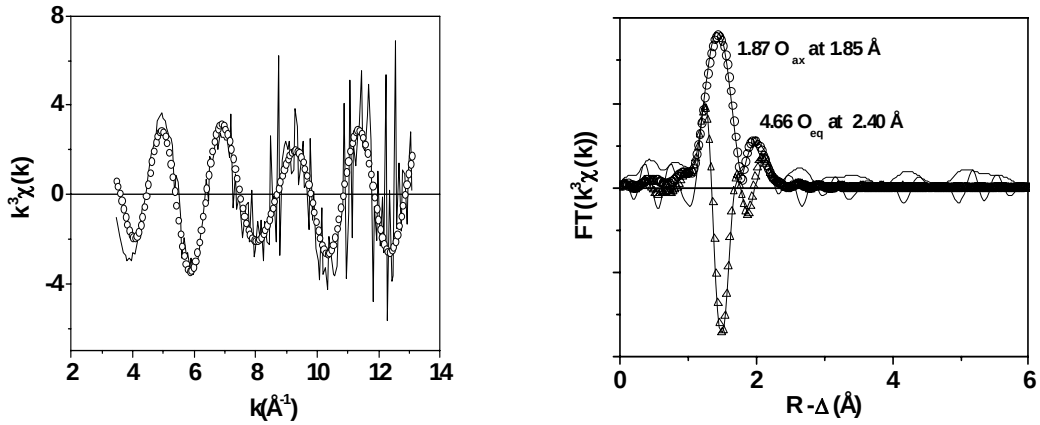

Fig. 4.12 Np L_{III} edge k^3-weighted EXAFS spectra (left) and the corresponding FT (right) for Np/HAS sample. Lines: the experimental data, symbols: the theoretical fit curves. Both FT amplitude (circles) and imaginary parts (triangles) are shown. Transform k range 3.4-14 $Å^{-1}$ and fit range 1-2.5 Å.

The Np(V) coordination sphere appears to be highly asymmetric, as indicated by the relatively large Debye-Waller factor of about 0.014 $Å^2$. The large asymmetry is likely a result of the contribution of different ligands, such as coordinating water molecules, OH

Table 4.2**:** EXAFS structural parameters obtained by fitting the An L_{III}-edge EXAFS of the samples with the composition described in Table 4.1. Uncertainty in the coordination numbers and in the interatomic distances are within 20% and 0.02 Å, respectively.

Sample	Shell	N	R [Å]	σ^2 [Å^2]	ΔE_0 (eV)	Residual[a]
Eu/HAS*	O	7.8	2.40	0.0039		
	Si/Al	4.8	3.70	0.0024		
Eu/Si(ref)*	O	5.7	2.39	0.0140		
	Si/Al	3.4	3.65	0.0150		
Th/HAS (1)	O	5.8	2.41	0.013[b]	2.6	0.7
	Si/Al	3.3	3.79	0.006[b]	-4.0	
Th/HAS (2)	O	6.5	2.36	0.0126	-1.82	7.6
	Si/Al	1.8	3.24	0.0085	-1.6	
	Th	0.8	3.84	0.0024	4.6	
Th/Si(ref.)	O	8.5	2.36	0.0172	-1.8	8.9
	Si	1.7	3.28	0.0060	3.1	
	Th	0.6	3.80	0.0014	-2.0	
Th/Al(ref.)	O_1	7.2	2.41	0.0095	-0.61	4.9
	O_2	1.2	3.03	0.0001[c]	-0.61	
	Al	0.7	3.55	0.0026	13.0	
	Th	4.2	3.97	0.0219	2.0	
Np(V)/HAS	O_{ax}	1.9	1.85	0.0003	2.1	8.8
	O_{eq}	4.7	2.40	0.0130	2.1	
U/HAS	O_{ax}	2[d]	1.73	0.0040	-6.27	4.0
	O_{eq}	5.4	2.25	0.0077	-6.27	
k range 2.8-12	$Si_{(1)}$/Al	1.1	3.20	0.0098	9.24	
Winxas	$Si_{(2)}$/Al	2.1	3.40	0.0121	9.24	
U/Si(ref)	O_{ax}	2[d]	1.78	0.0040	-4.96	1.0
	O_{eq}	6.7	2.25	0.0131	-4.96	
k range 2.1-10.6	Si	3.7	3.38	0.0260	8.96	
Fefffit						

*Results taken from [98].

[a]- residual (R) (%) is an indicator of the fit quality and represents the relative difference between experimental and theoretical data, [b]-includes the 3rd cumulant correction; [c]– constrained to positive values during the final fit; [d] –fixed during the final fit.

groups and the aluminosilicate ligand. We do not detect any Si(Al) coordination shell as for the other samples that would have been a direct proof of inner sphere complexation with the aluminosilicate ligand. Also, in the absence of Np-Np interactions there is no evidence for the formation of a surface precipitate in the sample.

However, that no Np-Si(Al) shell is observed in the FT spectrum does not necessarily exclude the presence of electrostatic and/or inner-sphere interaction between the Np(V) and the aluminosilicates. Loss in overall EXAFS oscillatory amplitude can result through destructive interference of a number of oscillations having small differences in their frequencies due to their small variations in bond length [33, 113]. The literature data regarding Np(V) in inorganic matrices are rare. The result for the coordination environment of Np(V) in aluminosilicate solution is similar to that reported for Np(V) embedded in borosilicate glasses [102]. In the glass matrix the authors observed about 4 O_{eq} atoms at mean distance of 2.35 Å. Here, too, no further neighbour distances are detected. The coordination environment of Np(V) sorbed onto kaolinite at pH 9 has been investigated by Reich et al. [110]. The authors found no evidence of inner-sphere complexation of Np(V) with the functional groups of the mineral but reported the formation of Np carbonato species at the mineral surface. Although under the present experimental conditions of pH 12, the carbonate concentration should be also quite high [114], the presence of the carbonate ligand can be excluded since from the EXAFS spectrum there is no evidence of Np-C interactions which have been observed in the above mentioned study at distance of 2.94 Å [110].

At the moment one cannot draw a clear conclusion about the nature of Np(V) interaction with the aluminosilicates from the EXAFS results. Np(V) association with the aluminosilicate colloids observed in the radiometric experiments (section 4.1.1) might have been the result of Np(V) surface complex. A polynuclear complex or surface precipitate formation may be excluded due to the lack of any Np-Np distance in the FT of the EXAFS spectrum.

U/HAS and U/Si(ref)

The U L_{III} EXAFS spectra and FT for samples U/HAS and U/Si(ref.) shown in Fig. 4.13

have similar characteristics, both displaying two significant FT peaks. The major FT peak results from contributions from the axial and equatorial O atoms. The second, smaller peak, which appears at longer distance, is attributed to Si(Al) backscatters in the third U(VI) coordination sphere. The results yield O_{ax} at distances of 1.73 and 1.78 Å, respectively. These values compare well with other EXAFS results for U-O_{ax} interatomic distances reported for uranyl species in inorganic compounds, 1.75 to 1.81 Å [103, 112, 115]. Approximately 6 O_{eq} are found at an average distance of 2.25 Å.

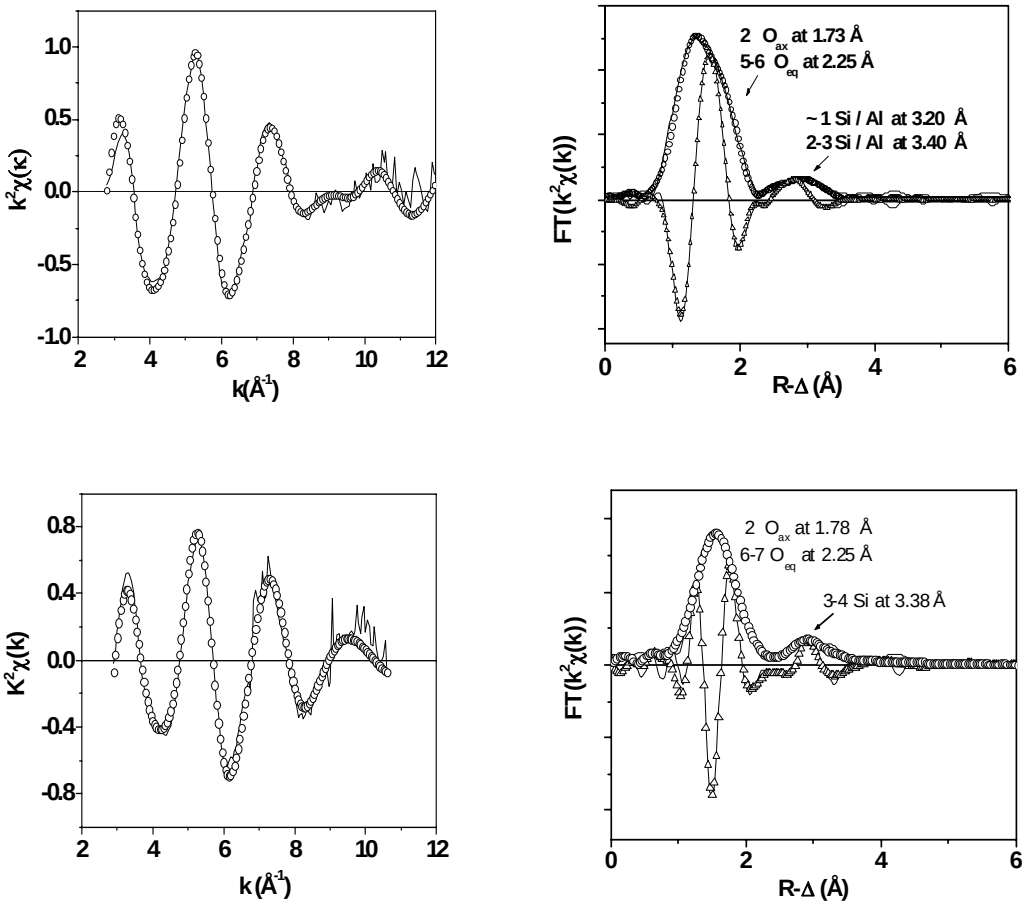

Fig. 4.13 U L_{III} edge k^2-weighted EXAFS spectra (left) and the corresponding FTs for U/HAS (top) and U/Si(ref.) (bottom) samples. Lines indicate experimental data and symbols theoretical fit curves. Transform range k 2.8-12 $Å^{-1}$ and 2.1-10.6 $Å^{-1}$, fit range 1-3.5 Å.

This is significantly shorter than that expected for uranyl aquo-complexes, of 2.41-2.43 Å [104, 116, 117] and indicates a strong inner-sphere complexation of the uranyl cation.

$U\text{-}O_{eq}$ distances near 2.25 Å are 0.09 Å shorter than that reported for the inner-sphere complexes of uranyl in naturally occuring Al-Si gels found in uranium deposits (2.34 Å), 0.06 Å shorter than that in silicate minerals such as soddyte (2.31 Å), and comparable to that in U(VI) oxides precipitates formed at pH values above 7 and in uranyl hydroxides formed under alkaline conditions (2.26 Å) [104, 117-121]. The present results compare best to the oxygen coordination environment reported for the uranyl cation in silicate glasses and melts, where approximately 5 O atoms at distance of 2.23 -2.25 Å are observed [103, 122].

The coordination numbers and the average interatomic distances obtained in the preliminary fit for the second neighbor, Si or Al in the aluminosilicate sample and Si in the silicate sample, suggest that both samples have a similar U(VI) coordination environment. However, a significant better fit of the data for the U/HAS sample is obtained with the third shell split into two distances Si/Al(1) and Si/Al(2). In case of the U/Si(ref) sample, there is not enough resolution in the interatomic distance due to the limited k range in this case. The fits using the split shell model yields interatomic distances of about 3.2 and 3.4 Å. The splitting of the Si(Al) shell into two distances observed in the aluminosilicate sample indicates the possibility that U(VI) exists in different coordination environments. The U-Si distances are comparable to the U-Si distances observed in uranyl silicate minerals: soddyte or uranophane (3.1-3.2 Å) and boltwoodite (3.5-3.6 Å) [116-118, 123]. The uranyl species sorbed onto silica containing compounds and clay minerals, where the complexation is attributed to a bidentate binding to the the silanol sites, show generally shorter U-Si distances, between 2.77-3.16 Å [104, 113, 115, 117, 123]. Crystallographic data on compounds with direct binding of U(VI) to the Al-O sites appear not to be available in the literature; several EXAFS studies have either failed to detect any U-Al interaction, or characterize it as weak [115, 116, 121, 124]. U-Si(Al) distances of 3.3 Å have been found by Henning et al. [104] and Arai et al. [35], for U(VI) sorbed onto montmorillonite at pH 5-7, and onto imogolite, respectively. In both studies, the observed distances have been ascribed to edge-sharing coordination of U(VI) to the alumina octahedron.

Using the $U\text{-}O_{eq}$ and U-Si(Al) bond lengths of 2.25 Å and (3.2-3.4 Å), respectively, determined from EXAFS analysis the Si(Al)-O-U bond angle is calculated in a manner similar to that used for Th(IV) discussed above (eq. 4.1). The short distance of 3.20 Å observed in the U/HAS sample gives a calculated bond angle of 100° and 110° considering U(VI) binding to the AlO_6 octahedron and $Si(Al)O_4$ tetrahedron, respectively.

Such very small angle of approximately 100° and the N (Si/Al) of about 1, suggests an edge-sharing link of U(VI) to the AlO_6 octahedron. This assumption is supported by the fact that the calculated U-Al distance of 3.14 Å is only 0.06 Å shorter than the experimental one. Edge-sharing link to SiO_4 tetrahedron would lead to much shorter U-Si bond lengths (calculated as approximately 2.8 Å) as compared to the experimental values. The longer U-Si(Al) distance, of 3.40 Å, gives U-Si(Al) bond angle in the range 110-120° and indicates a corner sharing of U(VI) with the Si(Al) polyhedrons. The presence of about two and three Si/Al atoms in the aluminosilicate and silicate sample, respectively may indicate in this case also double corner sharing link to neighboring Si(Al) polyhedrons. In order that such coordination to be possible the polyhedrons should be oriented in such way that the Si-Si(Al) distance is about 3.24 Å. The results above support the presence of several coordination environments for U(VI) in our aluminosilicate solution, the EXAFS parameters reflecting the average structure of the species mixture.

A very recent EXAFS study [35] has characterized the speciation of U(VI) sorbed onto synthetic imogolite in the pH range 5-9, in air equilibrated system. At pH 8.8, which is similar to our pH conditions, the authors have reported the presence of two U(VI) species: U(VI) bis-carbonato inner-sphere surface complex and U(VI) tris-carbonato outer-sphere complex. In the present samples the formation of U(VI) carbonate complexes can rule out since trying to consider in the fit this U-C distance at about 2.9 Å, as characteristic for the carbonate coordination of uranyl cation [35, 125] is not successful.

The coordination number determined experimentally for Si(Al) atoms of about 3 suggests a strong interaction (incorporation) of the uranyl into the aluminosilicates/silicates structure**.** Generally, not more than one Si(Al) atom has been found for uranyl surface complexes with silica containing compounds/aluminosilicate minerals [35, 101, 112, 117, 123]. However, the specific experimental conditions of the above mentioned studies differ from those of the present work, as they have been generally carried out using solid phases with different degrees of structural order. In our system, U coprecipitates with aluminosilicates/silicates in solutions rich in polysilicic acid, known to have high affinity for metal cations [37] and the poorly structured aluminosilicates have less lattice constrains and may allow incorporation of the U(VI) into the bulk. In another EXAFS study [115] concerning the structural analysis of U(VI) coprecipitated with zeolites precursors from alkaline solutions and at temperatures of 50-90° C**,** approximately 2

and 3 Si(Al) atoms were detected at 2.93 Å and 3.60 Å respectively, together with about 3 U atoms in the third coordination shell. The results were interpreted by the authors as formation of mixed uranyl phases: U(VI) oxide/hydroxide together and U(VI) silicate. The present EXAFS spectra do not indicate the presence of any significant FT peak, which could be attributed to U-U distances similar to those reported for schoepite, soddyte, or uranyl sorbed onto silica compounds (3.7 to 3.9 Å) [115, 116, 118, 123]. This indicates there is no formation of a uranyl polynuclear complex or surface precipitate, despite the fact that under these conditions of high pH and U(VI) concentration U(VI) colloidal species are detected by radiometry in the blank solutions (without Si and Al), (see discussion in section 4.1.3). It appears that the reaction between the U(VI) hydroxocomplexes and the aluminosilicates is preferred over the polimerization reaction between the U(VI) hydroxocomplexes.

The Debye–Waller factor, σ^2 for both O and Si coordination shell in Table 4.2 is much larger in case of the U/Si(ref.) compared to that for the U/HAS sample, suggesting a more ordered U(VI) coordination environment in the aluminosilicate sample. One explanation might be that the presence of the Al octahedra in the aluminosilicate bulk generate more flexible (i.e., steric available) sites better able to accomodate the uranyl ion. More detailed interpretation of data in view of the identification of the second neighbor of Th(IV)/U(VI) is difficult at the present time. The structure of the aluminosilicate bulk is not known. Given the polymerization of silicic acid that generates a variety of structures including linear and cyclic ones [37] and the possibility that Al changes its coordination number from 6 to 4, various binding sites for the actinide can exist, in principle.

EXAFS has been previously applied to investigate the speciation of Eu(III) in our aluminosilicate /silicate system [98], under conditions of high Si concentration and pH (Table 4.1) where TRLFS evidenced the complete replacement of all Cm(III) coordination water molecules by the polysilicate/aluminosilicate ligand. The Eu L_{III} EXAFS results (Table 4.2) for the Eu/HAS sample showed the Eu(III) first coordination shell to be comprised of 7-8 O atoms and a second shell consisting of 4-5 Si/Al atoms. No further Eu-shell could be evidenced that excludes surface precipitate formation. Calculations according to eq. 4.1, gives Eu-O-Si/Al bond angle between 120° and 130° and indicates that Eu binds to each $SiO_4(AlO_6)$ polyhedron by only one O atom (corner sharing link).

Fig. 4.14 gives an overview of the EXAFS results on the actinide speciation in aluminosilicate solutions.

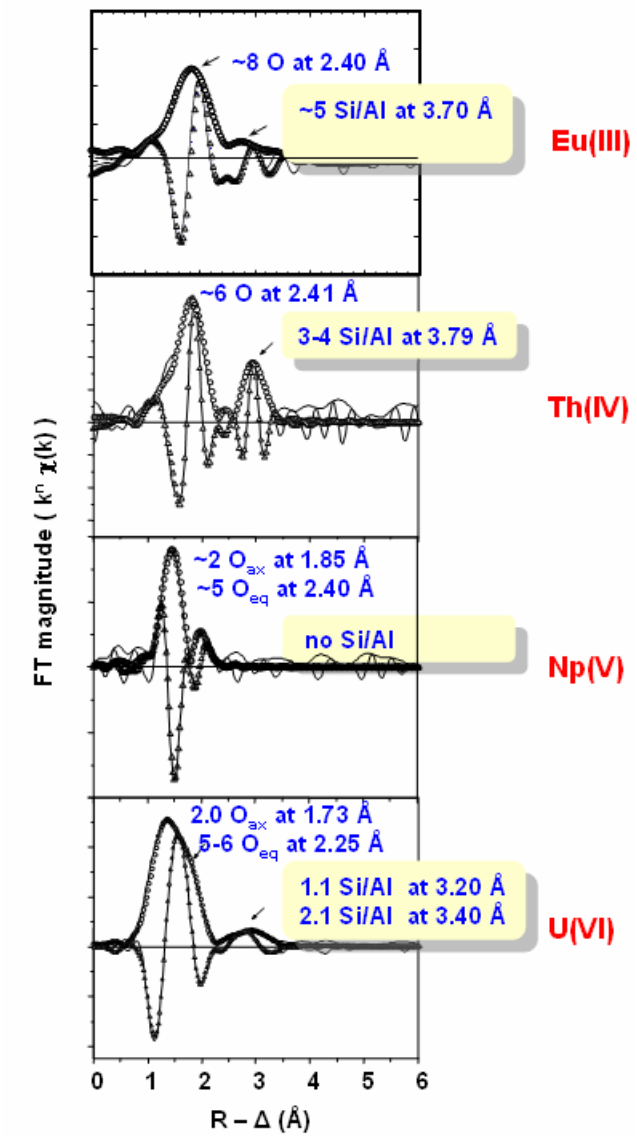

Fig. 4.14 Fourier transforms of the k^n-weighted An L_{III}-edge EXAFS spectra of actinides in HAS solutions (overview). Mother solutions contain approximately 10^{-3} M actinide, 10^{-3} M Al and 10^{-1} M Si. Sample pH is of 8.5 for Am, Th and U and 12 in case of Np. Si/Al neighbors are identified in the actinides coordination sphere except in case of Np. Results for Eu are taken from [98].

Several general observations can be made. EXAFS spectroscopy proves the inner-sphere complexation of An(III, IV, VI) with the aluminosilicates and silicates, as predicted from the radiometric experiments. In case of the HAS samples there is evidence

that the An(III, IV, VI) binding to each SiO_4/AlO_6 polyhedron occur via one O atom (corner-sharing link) and that U(VI) could also bind to an AlO_6 polyhedron via two O atoms (edge-sharing link). If one further considers the number of Si/Al atoms relative to the number of O atoms in the actinide coordination shell, rough calculations indicate approximately 60-70 % of the O atoms to be contributions from the aluminosilicate ligand and support the idea that the actinides are incorporated into the polymerized aluminosilicate bulk. The An-aluminosilicate interaction appears to be preferred over the formation of An(IV,VI) polynuclear complex/surface precipitate. Within the HAS bulk, the An(IV, VI) binding might be directed to both Si and/or Al, at the present limited knowledge of the HAS structure. There is no evidence for the formation of inner-sphere complexes of Np(V) with the aluminosilicates under the pH conditions where radiometric experiments show maximum Np-HAS colloids interaction, but however, formation of Np surface precipitate can be excluded based on the EXAFS measurements.

4.3 Stability of aluminosilicate colloid-borne actinides

The stability of actinide binding to colloids is one of the relevance criteria for the colloidal facilitated migration of actinides. Stable incorporation of actinides into stable aquatic colloids promotes the colloids as carrier for actinide migration with the water flow without substantial geochemical hindrance. Stability of actinide-colloids binding refers to the actinide ability to remain as colloid-borne species upon changes in the environmental conditions. Therefore, the binding stability is operationally defined by the selected conditions like variations in pH, temperature, ionic strength, the presence of anionic ligands, as potential changes that may occur in the natural environment.

The present work considers the stability of the colloid-borne actinides and of the colloid-borne Al (Al-O-Si binding in the HAS) relative to the pH decrease and EDTA as competitive ligand.

4.3.1. pH reversibility of the colloid-borne Al and actinide(III)

The pH reversibility has been previously investigated for Cm-HAS colloid borne species formed in HAS solutions generated from polysilicic acid at pH 9 [27]. As discus-

sed in section 4.2.1, under these conditions the only Cm species present in solution is the Cm-HAS (III) corresponding to the complete incorporation of Cm into the HAS. The spectroscopic speciation is carried out upon decreasing the pH of the solution from 9 to 2 and the results on the distribution of Cm species are illustrated in Fig**.** 4.15 a. As can be seen, lowering the pH induces a gradual conversion of the Cm-HAS(III) species to Cm-HAS(II) and Cm-HAS(I) accompanied by an increasing fraction of the Cm aquo cation. Thus, the completely incorporated Cm species appears to be pH reversible; increasing acidity promotes the breakage of the Cm-O-Si bonds and the gradual dissociation of Cm from the colloids. The authors have also investigated the stability of the Cm-HAS(III) species at each pH value as a function of time. The results are shown in Fig. 4.15 b. We observe that at pH values above 5, the Cm-HAS(III) fraction remains stable in solution up to 63 days. Only after decreasing the pH of the original solution below pH 5 the stability of the Cm-HAS(III) species is significantly lower.

In analogy with Cm(III), the present work considers the pH reversibility of the colloid-borne Al generated under similar conditions, namely in the presence of polysilicic acid at pH 9. The experiments are carried out with HAS solutions freshly prepared (1 h), without actinide addition. Al behavior is observed in separate samples upon acidification to pH values between 4 and 1 and in 2 M HCl. The soluble Al is determined at different time intervals in the solution resulting after elimination of precipitate and colloids as described in section 3.3. The fraction of Al bound within HAS colloids represents the normalized difference between the Al initial concentration in the mother solution and the concentration measured in the filtered solution after lowering the pH.

Fig. 4.15 c illustrates selected results for the fraction of Al bound to the HAS-polysilicic acid colloids as a function of time at different pH values. As can be seen, upon decreasing the initial solution pH to the value of 4, the Al-colloid-borne fraction remains stable within the observation time of 60 days. From pH 3 down, the Al dissolution is evident, but nevertheless, a significant fraction of Al (about 50 %) is still stable in the aluminosilicates up to 60 days. At higher acidity (i.e. pH 1) the Al-O-Si binding is strongly destabilized within few days. Although as in the case of Cm(III) the Al(III)-O-Si bond appears also to be pH reversible, the binding starts to be destabilized from lower pH as compared to the Cm(III)-O-Si, namely 3 instead of 5. This result suggests that, within the HAS, the Cm(III)-O-Si binding is weaker than the Al(III)-O-Si binding.

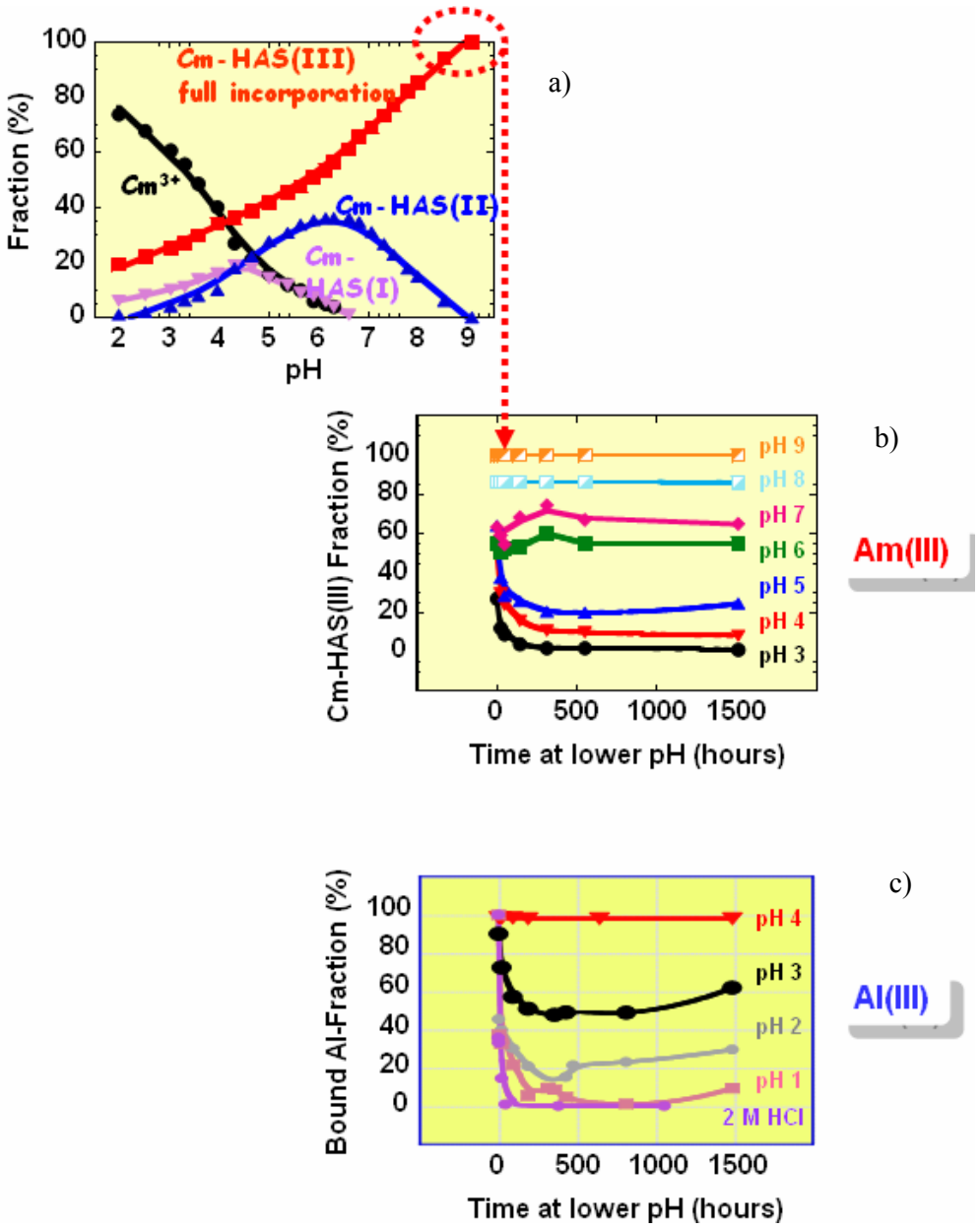

Fig. 4.15 a): Relative Cm(III) species distribution as a function of pH at reverse titration of a solution initially of pH 9 and containing Cm ($5x10^{-8}$ M), Si $1x10^{-2}$ M and Al $1x10^{-4}$ M (forming HAS-polysilicic acid colloids); b) Stability of the colloid-borne Cm-HAS(III) species as a function of time at different pH values (from [27]); c): Stability of the colloid-borne Al as a function of time at different pH values after decreasing the pH of the original solution. The original HAS solutions are prepared with $1x10^{-2}$ M Si and $1x10^{-4}$ M Al at pH 9.

4.3.2 EDTA resistance of colloid-borne Al and actinide(III)/(IV)/(V)/(VI)

In order to get a relative assessment of the actinide-colloid binding strength under the condition of maximum formation of colloid-borne actinides, a ligand competition experiment is we further carried out, with the aid of EDTA as competitor for the HAS. The stability of colloid-borne Al (the Al-O-Si binding within the HAS) is also considered. EDTA is a well known chelating agent which forms in solution very stable complexes with most metal ions. As example, the stability constants of several complexes formed between EDTA and actinides and Al are summarized in Table 8.1 (Appendix). For the experiment, two modes of the generation of actinides pseudocolloids in natural systems are considered: the co-nucleation of actinides with Al and Si, and the interaction of An with aged HAS colloids.

Actinides interacting with HAS colloids in statu nascendi (conucleating Si and Al)

The desorption experiments are carried out on 3 series of samples corresponding to Am(III), Th(IV) and U(VI). Each series of sample consists of 8.6×10^{-7} M actinide and 10^{-2} M Si / 10^{-4} M Al corresponding to the synthesis of HAS from polysilicic acid at pH 7 and 9. The samples are conditioned for 1 day, enough to ensure the formation of maximum colloid-borne fraction of Th(IV) and U(VI) which have been shown to have fast kinetic of incorporation at these pH and Si concentration. In case of trivalent actinides, as outlined in section 4.2.1 the "complete incorporated Cm", (Cm-HAS(III) species), forms during co-nucleation process and prevails under the experimental conditions. After the 1 day conditioning time with actinides, EDTA is added at a final concentration of 1×10^{-3} M. The partition of actinide activity fraction in the three phases is monitored before EDTA addition and at different intervals thereafter.

EDTA competes with the HAS for binding the actinides and promotes their desorption from the HAS colloids by formation of complexes in solution. The experimental EDTA concentration, one order of magnitude higher than that of Al, is in larger excess to the actinide ensuring its complete complexation. The stability constants of such complexes are shown in Table 8.1 but, once in solution, the actinides tend to hydrolyze with formation of hydroxo complexes and hydroxide solid phases, reaction which will compete with the complexation by EDTA. Therefore, blank experiments are performed by adding

EDTA to solutions of pH 5, 7 and 9 containing only the actinide. The results show that the activity fraction is transferred completely to the solution and the precipitation of hydrolysis species is not attained. Selected results are given in Tables 8.2 and 8.3 (Appendix).

Tables 8.4, 8.5 and 8.6 (Appendix) give the results on the actinide partition between the three phases in presence of HAS as a function of EDTA contact time. Fig. 4.16 illustrates comparatively selected results regarding the colloid-borne actinide activity fraction remaining in the colloidal phase at pH 9. As can be seen, Am activity fraction in the colloidal phase decreases rapidly upon contact with EDTA. About 90 % of the initially colloid-borne Am is desorbed from the colloids within 2 days contact time with EDTA**.** It is obvious that under the conditions ensuring the strongest An(III) binding to the HAS (i.e. incorporation of Cm(III) into the HAS colloids), the HAS colloid-borne Am is not EDTA resistant. In contrast, Th(IV) and U(VI) activity fraction in the colloidal phase remain unchanged, the actinides can not be displaced by EDTA within 35 days. The fact that Th and U remain as colloid borne species in presence of EDTA suggests that the HAS colloids (i.e. the Al-O-Si binding) are stable, since as outlined in the section 4.1.1, maximum and stable incorporation of Th/U into the colloidal phase requires the presence of both Si and Al.

Therefore, the EDTA resistance of the Al-O-Si binding is analyzed in the followings, not for only HAS generated from polysilicic acid but also for HAS generated from monosilicic acid. For this purpose HAS solutions are prepared in absence of actinides at pH 5 and 9. After a conditioning time varying between 3 hours and 9 months, the HAS solutions are brought into contact with EDTA at a final concentration of 10^{-4} and 10^{-3} M for the HAS-monosilicic acid and HAS-polysilicic acid, respectively. At different time intervals, the soluble Al is determined in the solution remaining after removal of precipitate and colloids, as described in section 3.3. The EDTA resistant Al is obtained by subtracting the concentration of soluble Al from the Al concentration initially introduced in the sample. A separate experiment is carried out under identical concentration conditions but with changed sequence of component addition, namely: Al solution is first contacted with EDTA followed by addition of Si (either monosilicic or polysilicic acid) after 3 hours conditioning time. Separate experiments show that, in freshly prepared samples containing only Al at pH 5 and 9 in the presence of EDTA, Al is present entirely in solution resulting after elimination of the precipitate and colloids. It means that, in the presence of EDTA the formation of the solid Al hydroxide species is not attained. On this ba-

sis one can say that the EDTA resistance exhibited by Al in the presence of HAS is due to the Al binding to the silicic acid.

Fig. 4.17 illustrates the results for the EDTA-resistant Al fraction as a function of EDTA contact time. For the HAS generated from polysilicic acid at pH 9 (Fig. 4.17 b), meaning under the conditions which ensuring maximum actinide binding to the HAS colloids, the colloid-borne Al appears to be EDTA resistant even for only 3 hours aged aluminosilicate solutions (the blue curve). At pH 5 (Fig. 4.17 a), the colloid-borne Al is less stable. After an initial slightly increase of the stable Al fraction, most Al appears to be complexed by EDTA and transferred to the solution within 5 days. A marginal amount of about 20% colloid-borne Al can be still observed up to 20 days. For the HAS-monosilicic acid samples with 3 hours conditioning time (Fig. 4.17 c, d-blue curve), two step dissolution kinetics of Al is observed. After an initial very fast dissolution step when about 50% of the initially bound Al is brought into the solution within few hours, the dissolution kinetics becomes very slow especially at pH 9. Nevertheless, at similar pH conditions, the Al-O-Si binding is less stable as compared to the HAS formed from polysilicic acid. Another observation, valid for both HAS generated from monosilicic and polysilicic acid, is the increase of the EDTA resistant-Al fraction with increasing the conditioning time of the HAS mother solution from 3 hours to 9 months. The results are indicated in Fig. 4.17 by the red curves. The increased Al stability with sample ageing can be due to the changes in the binding state of Al within the HAS. As discussed in section 4.2.1, and suggested by the Arrehnius equation, during prolonged conditioning time the activation energy of the reaction is overcome. One should also take into account possible changes in the geometry (aggregation) of the solid phase resulting in a smaller surface area in contact with the solution and, consequently lower Al dissolution rates. However, as can be seen from the dissolution kinetics, at a given pH, the stability of the colloid-borne Al remains higher for the HAS generated from polysilicic acid as compared to the HAS-monosilicic acid. In Fig. 4.17 the black curves illustrate the results obtained at the reverse order of reactant addition. After addition of the polysilicic acid to the soluble EDTA complexed-Al (fig. 4.17 a, b), Al is immediately converted to the EDTA resistant form. At pH 5, however, the Al fraction is afterwards rapidly destabilized. This behavior might be explained by an initial rapid sorption process of the Al-EDTA complex onto the surface of the polysilicic acid as at pH 5 the EDTA is not fully deprotonated and retains residual protons which may bind to the polysilicic acid surface. During re-equilibration, desorption of the Al-EDTA com-

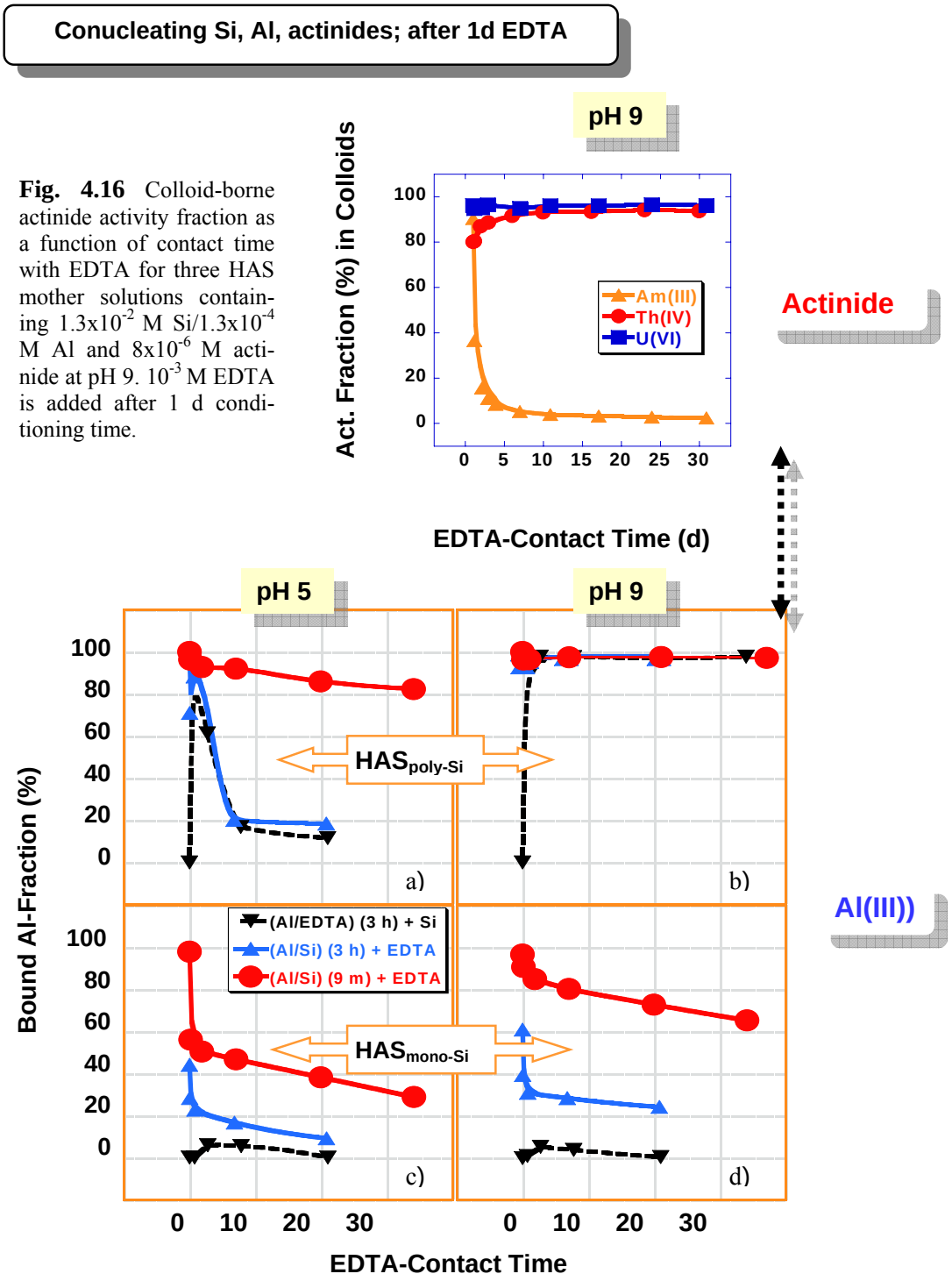

Fig. 4.16 Colloid-borne actinide activity fraction as a function of contact time with EDTA for three HAS mother solutions containing $1.3x10^{-2}$ M Si/$1.3x10^{-4}$ M Al and $8x10^{-6}$ M actinide at pH 9. 10^{-3} M EDTA is added after 1 d conditioning time.

Fig. 4.17 EDTA resistant Al fraction within the HAS colloids normalized to the initial Al concentration in the sample as a function of contact time (days) with EDTA, for different HAS mother solutions. The HAS solutions are generated from polysilicic acid ($HAS_{poly\text{-}Si}$) (a and b) and consist of $1x10^{-2}$ M Si/$1x10^{-4}$ M Al and, from monosilicic acid indicated as $HAS_{mono\text{-}Si}$ (c and d), of $1x10^{-3}$M Si/$1x10^{-5}$ M Al. The order of reactant addition at sample preparation and aging time is indicated in the legend. Time 0 marks the moment of addition of EDTA or silicic acid.

plex occurs and Al is released again into the solution. For the samples prepared at pH 9, the Al fraction remains stable within the observation time. At this pH we expect that EDTA does not interact with polysilicic acid, both molecules being negatively charged [130]. It means that at pH 9 polysilicic acid is a stronger complexing ligand and can displace the EDTA in the Al coordination sphere. This fact is not observed for the aluminosilicate solutions generated from monosilicic acid (Fig. 4.17 c, d) as Al remains in solution complexed with EDTA.

The results confirm the higher affinity towards Al exhibited by the polysilicic acid at pH 9 as compared with the monosilicic acid. On the basis of this result together with those regarding the EDTA stability of the Am-HAS colloids binding, one can conclude that within the HAS formed from polysilicic acid at pH 9, the Si-O- moieties have higher binding affinity for Al as for Am.

The stability constants for the complexation of EDTA with the actinide cations (Table 8.1) indicates much stronger interaction of Th(IV) with EDTA as compared to Am(III) and Al(III). Due to its stereochemistry, U(VI) forms less stable complexes with EDTA as compared to Am(III), Th(IV), Al(III) [129]. The result of the ligand competition experiment showing Th and Al to be EDTA resistant, while Am not, suggests that the desorption kinetics is determined by the actinide lability within the HAS-polysilicic acid.

Actinides interacting with aged HAS colloids

Coprecipitated HAS samples are generated from polysilicic and monosilicic acid at pH 5, 7 and 9 and are conditioned for 7 days. Aging time of the colloids (7 days) is chosen on the basis of previous studies results. As already outlined in section 4.1.2 (Fig. 4.6) in solutions of $1x10^{-2}$ M Si at pH 7 and 9 the polymerization of silicic acid is completed within 7 days, so that formation of the HAS colloids generated under these conditions is expected to be complete. After the 7 days conditioning time of the mother solutions, the actinide is introduced at a final concentration of $8.7\ x10^{-6}$ M. Following another conditioning time of 5 days to ensure that a steady state of actinide sorption is reached, EDTA is added to an end concentration of $1x10^{-4}$ M in case of the HAS prepared from monosilicic acid and $1x10^{-3}$ M in case of the HAS-polysilicic acid. The results for the actinides activity distribution between the precipitate, colloids and solution at different in-

tervals before and after EDTA addition are listed in the Tables 8.7, 8.8 and 8.9 (Appendix) for HAS samples prepared out of polysilicic acid. Figure 4.18 depicts the colloid-borne actinide activity fraction at different pH as a function of time. The time interval up to 5 days corresponds to the sorption of An onto the HAS colloids. The colloid-borne activity fraction at time intervals > 5 days gives the actinide activity fraction remaining in the colloids after EDTA addition.

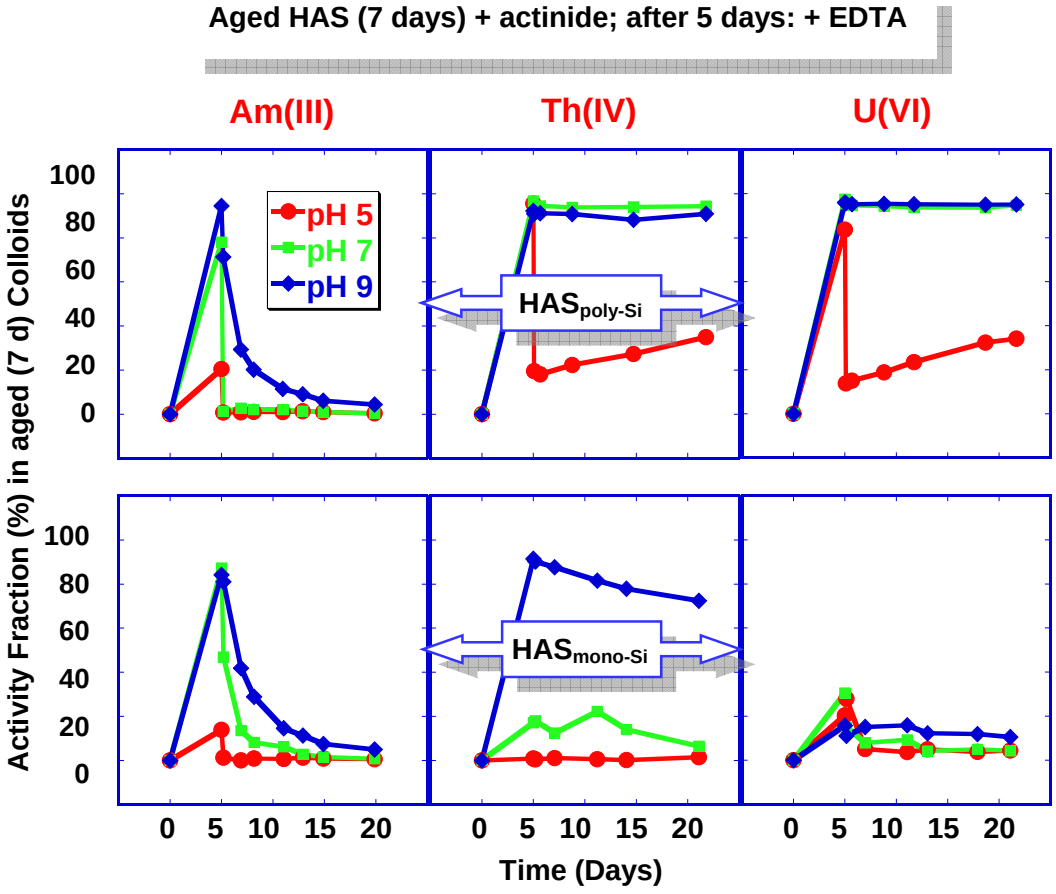

Fig. 4.18 Actinide activity fraction (%) in 7 days aged HAS colloids as a function of time. HAS colloids are formed from mother solutions of pH 5, 7 and 9 and containing: $1.3x10^{-5}$ M Al /$1.3x10^{-3}$ M Si (indicated as $HAS_{mono-Si}$, the lower part graph), and $1.3x10^{-4}$ M Al /$1.3x10^{-2}$ M Si (indicated as $HAS_{poly-Si}$, the upper part graph). In the time interval 0-5 d the curves show the sorption of actinide ($8x10^{-6}$ M) onto the aged HAS colloids; after 5 d: activity fraction remaining in the colloidal phase after addition of $10^{-4}/10^{-3}$ M EDTA.

In case of the HAS colloids generated from monosilicic acid (lower part graph) the fraction of colloid-borne U is very poor as observed also in the co-nucleation experiments (section 4.1). The colloid-borne Am is not EDTA resistant irrespective the pH. In case of Th, only the colloid-borne fraction generated at pH 9 shows higher EDTA resistance: approximately 60 % Th activity fraction remains in the colloidal phase after 20 days contact time with EDTA. For HAS colloids generated from polysilicic acid (upper part graph) we observe the same desorption pattern in case of Am which is readily removed from the HAS colloids, especially at pH 5 and 7 when most activity fraction is transferred to the solution within a few hours. Slower desorption kinetics are observed for Am sorbed onto the HAS colloids generated at pH 9. This pH dependent kinetics might be correlated with the lower stability of the Al-O-Si-binding within the HAS colloids with decreasing the pH, as outlined in the previous paragraph (Fig. 4.17 a, b). Also, as evidenced by TRLFS and discussed in section 4.2.1, different Cm-colloid-borne species with different Cm-HAS affinity form depending on the pH of the solution. It is conceivable that such species show different desorption kinetics. Regarding Th(IV) and U(VI), we observe that at pH 5 the colloid-borne Th(U) fraction is not EDTA resistant. Under these conditions, the desorption kinetics of the two actinides can be divided into two time domains. In the first domain, about 80% of the actinide activity fraction is desorbed very fast (i.e. within few hours), and this may occur in conjunction with the dissolution of the HAS at this pH, as illustrated in Fig. 4.17 a. Only a 20% actinide fraction appears to remain stable within the HAS and increases slowly with time. Different observations can be made at this point as described in the followings. (1) The minor actinide fraction remaining stable corresponds to the residual colloid-borne Al observed to be stable against EDTA in the HAS–polysilicic acid at pH 5, as already discussed. (2) The slow increase in the colloidal activity fraction after prolonged EDTA contact time may be due to an incomplete incorporation of Th and U into the colloidal at the moment of EDTA addition. Initially surface sorbed species, that can be easily desorbed in presence of EDTA, may slowly relocate into the colloidal phase. At pH 7 and 9 no desorption of Th(IV) and U(VI) is observed, the actinides remain as colloid borne species within 30 days observation time. Thus, at high pH, the two actinides appear to have very high affinity also for the aged HAS colloids generated from polysilicic acid. The EDTA resistance of the An(IV, VI) colloidal fraction suggests a fast incorporation mechanism into the colloidal bulk. In presence of polysilicic acid at neutral pH and above (pH 7-9) it is expected that stable HAS colloids form and

Th(IV)/U(VI) remain as HAS-colloid borne species generated either by co-nucleation with Si and Al or by incorporation into preformed HAS colloids.

4.4 Conclusions

Several observations can be outlined based on the results discussed so far. Formation of the HAS colloid-borne An species is favored by increasing pH and concentration of Si and Al. Accordingly, maximum association of An with the HAS colloids is found at neutral or high pH for HAS colloids generated from polysilicic acid. Following the same trend, the stability of the An binding to the HAS colloids and of the Al-O-Si binding within the colloids is higher with increasing pH and Si concentration. The binding stability within the HAS is also increased by increasing temperature or prolonged conditioning time (aging) of the system.

The actinides affinity to co-nucleate with HAS colloids formed from polysilicic acid is higher for the more hydrolyzed actinides in the order An(IV) = An(VI) >An(III), whereas Np(V) does not take part in the process of the HAS colloids formation in its non-hydrolysis pH range. Within the HAS colloids, the binding of Am(III), as that of Al(III) is directed towards the silanol groups, though with lower affinity as for Al(III). Am(III) discrimination at the co-nucleation with polysilicic acid appears to be correlated with its lower tendency towards hydrolysis as compared to that of Al(III). Whereas no kinetic effect is observed in case of Am, the incorporation kinetics of Th and U into the HAS–polysilicic acid colloids, slow at low pH, resembles the polymerization kinetics of the monosilicic acid.

From these observed facts, it appears evident that the essential condition for the co-nucleation is the hydrolysis of the involved elements. The process is controlled by the pH and the characteristics of the element. However, these parameters also influence the self nucleation (polymerization) reaction of individual hydrolyzed species. In order the co-nucleation process to be favorable it is important that the rates of the nucleation reactions of the individual elements are slightly different.

The differences observed in the An incorporation patterns, kinetics, and the different stability characteristics, support the idea of different actinide incorporation mechanisms depending on whether the HAS colloids are generated from monosilicic and polysilicic acid. The proposed mechanisms are described in the followings.

HAS-from monosilicic acid

In this case we lean on the literature data [8, 9], which have recently described the formation of HAS, from acidic solutions undersaturated with respect to amorphous silica, similar to our HAS colloids. We adapt the postulated mechanism to our experimental conditions, namely titration of acidic Al solution with basic $Si(OH)_4$ in the pH range 4-9. The reaction starts with the Al hydrolysis, its dimerization and co-nucleation with $Si(OH)_4$ and the An hydrolyzed species. In this case the formation of a surface takes place by a self-catalyzing mechanism which is a process with slow kinetics. Thus, the HAS colloids are less stable and less efficient to incorporate the actinides.

HAS formed from polysilicic acid

As in this case the silicic acid concentration attains during the reaction an oversaturation level, $Si(OH)_4$ undergoes polymerization generating a surface. This preformed surface catalyzes the co-nucleation reaction with Al and An hydrolyzed species. At this stage we could distinguish different incorporation mechanisms of actinides depending on their oxidation state.

Am(III), just like Al(III) binds to the silanol groups of the polysilicic acid and at pH $\geq$ 8 the well-known high affinity of polysilicic acid towards $Al(OH)_3$ and $Al(OH)_4^-$ species allows the complete incorporation of Am(III) species into the HAS colloids. Th(IV) and U(VI) hydrolyzed species copolymerizes with polysilicic acid, and further binds via oxo-bridiging to the hydrolyzed Al species with the generation of the actinide-HAS pseudocolloids. The non-hydrolyzed Np(V) does not take part in the conucleation process in the pH range $\leq$ 9.

5. Interaction of actinide(III, IV, VI) with humate colloids

Humic acid is omnipresent in natural waters and shows strong affinity to complex Al and actinide as outlined in section 2.2.2, and therefore, its impact on the formation of HAS-colloid-borne actinides is expected to be significant. For a better comprehension of the process, the following investigations focus firstly on the the humic acid itself as far as its colloidal properties are concerned and secondly on the interaction of humic acid either with silicic acid only or with Al and actinides (Am(III), Th(IV) or U(VI)), without silicic acid.

5.1 Humic acid as colloids: influencing parameters

As outlined in section 2.2, humic acids are composed of macromolecules of prevailing size larger than 1 nm and it is also known that the chemical environment influences the aggregation of humic macromolecules [29, 50]. Therefore, the influence of the pH and of the concentration of humic acid itself on its partition between the precipitate, colloids and solution is investigated.

For this purpose, two series of purified ^{14}C-labelled humic acid (Gohy -573) are subject to the sequential filtrations, followed by determination of ^{14}C-activity partition between the solution, colloids and precipitate phase. In one sample series the humic acid concentration is kept constant at 6.5 mg/L and the pH is varied from 4 to 9. In another sample series the pH is kept constant at 6.6 in 0.01 M MOPS buffer and the humic acid concentration is gradually increased from 0.6 to 8.0 mg/L. The concentration range corresponds to the HA level generally encountered in natural waters, however, one should mention that the maximum concentration is used is limited by the strong quenching caused by HA in LSC. The results for the pH dependency are shown in Fig. 5.1. In the neutral pH region, the fraction regarded as humic colloids after sample conditioning time of 35 d is found to reach 80%. A slightly elevated precipitate fraction is observed at pH $\leq$ 5 due to the beginning of the protonation of the humic acid acid functional groups leading to aggregation [55]. However, in the pH range 6-9, (as indicated in the figure and to which we will refer later), the fractions of humic acid distributed in the solution, colloid and precipitate phase remain show very little variation, independent on pH. A similar result is obtained regarding the dependency on the humic acid concentration. Variation of

humic acid concentration at pH 6.6 has been found not to affect the colloid fraction which remains at approximately 80%.

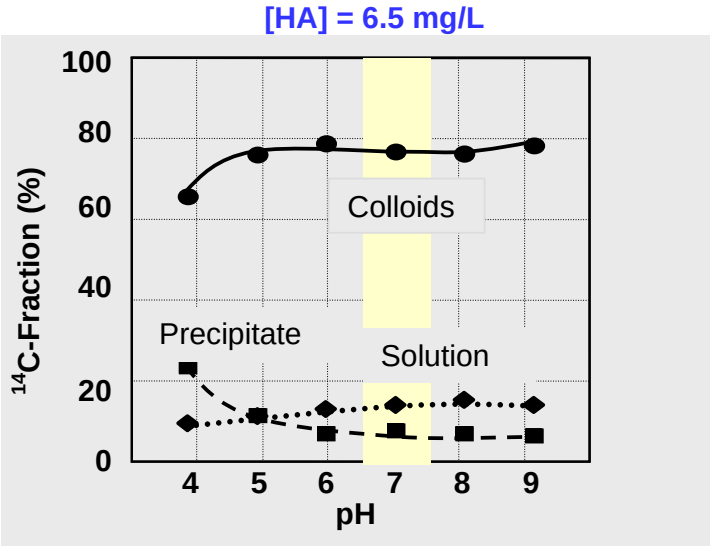

Fig. 5.1 [^{14}C]-humic acid activity fraction (%) normalized to the initial activity in the precipitate, colloids and solution, as a function of pH at contact concentration of 6.5 mg/L HA. Results represent values obtained after 35 d sample conditioning time.

The results indicate that measurements of the ^{14}C-activity facilitate the analysis of humic acid as well as its interaction with water-borne components like actinides, Al and Si.

The effect of Al on the formation of humic colloids is examined by adding $1x10^{-5}$ M Al to gradually increasing amounts of humic acid at pH 6.6 and 7.8. Al is investigated as one of the main component of the HAS and its chosen concentration corresponds to the lowest effective level for the formation of HAS colloids as discussed in section 2.2.1. Selected results for pH 6.6 are illustrated in Fig. 5.2. At low humic acid concentration ($\leq$ 1 mg/L) the effect of Al ions is to destabilize and precipitate the humic colloids completely or partially. This effect depends on the degree of saturation of proton exchange functional groups of humic acid, as it is documented in the literature [51, 57] that by high loading with metal ions, humic acids become hydrophobic and thus precipitate. For humic acid concentration $\geq$ 1.5 mg/L, about 80% appears to be colloidal and comparable to the colloidal fraction of pure humic acid shown in Fig. 5.1.

At pH 7.8 the Al ions introduced at the same concentration have been found to have no effect on the humic colloids stability and the amount of humic colloids remains around 80 % independent on the humic acid concentration. We conclude thus that under the experimental condition, at pH 7.8, the interaction between HA and the prevailing Al species, $Al(OH)_4^-$ [131], is unlikely.

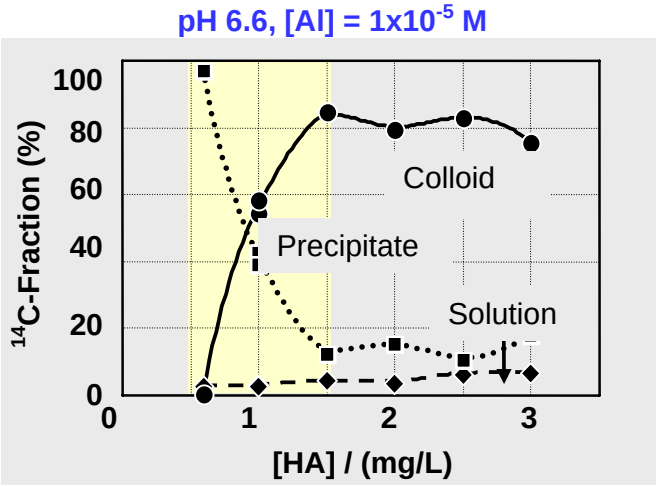

Fig. 5.2 [^{14}C]-humic acid activity fraction in the precipitate, colloids and solution, as a function of humic acid concentration in a solution of pH and Al 10^{-5} M. Results represent values obtained after 35 d sample conditioning time.

The influence of silicic acid, the other component of HAS, is also investigated, by addition of 10^{-2} M Si to solutions of 6.5 mg/L HA at pH 6.6 and 7.8. The results are not shown as no effect of Si is observed: the fractions of humic colloids are similar to those observed for the pure humic acid. Literature data also indicate silicate ions not to be associated with HA in the neutral pH range [74].

In analogy with Al, but this time for tracer amount, the effect of trivalent actinides, i.e. Am on the formation of humic colloids is investigated. The experiment is carried out at pH 6.6 by adding only a trace amount of Am ($5x10^{-8}$ M) without Al to increasing amount of humic acid at pH 6.6. The results are shown in Fig. 5.3. One should mention that Am^{3+} ion is the expected dominating Am species at pH 6.6 at the moment when the actinide is introduced into the solution (cf. Fig. 4.3 a, as Eu has similar hydrolysis tendency as Am). ^{14}C and ^{241}Am activities are measured in the same sample. As can be observed, the colloidal fractions measured by the Am-activity are more elevated than those

measured by the ^{14}C-activity. The ^{14}C-activity measurements specify humic colloids operationally defined by "solution (≤ 1nm) ≤ colloid (≤ 450 nm) ≤ precipitate". The Am-activity measurements distinguish a distribution of Am^{3+} by complexation with humic acid. The preferential distribution of Am in the colloidal phase could be explained by coagulation of humic acid through formation of intermolecular bridges upon complexation with the Am^{3+} ion and thus humic molecules initially in solution, become larger in size. This mode of humic coagulation due to the cross linking ability of the polyvalent cations has been previously ascertained in an atomic force microscopy study [132].

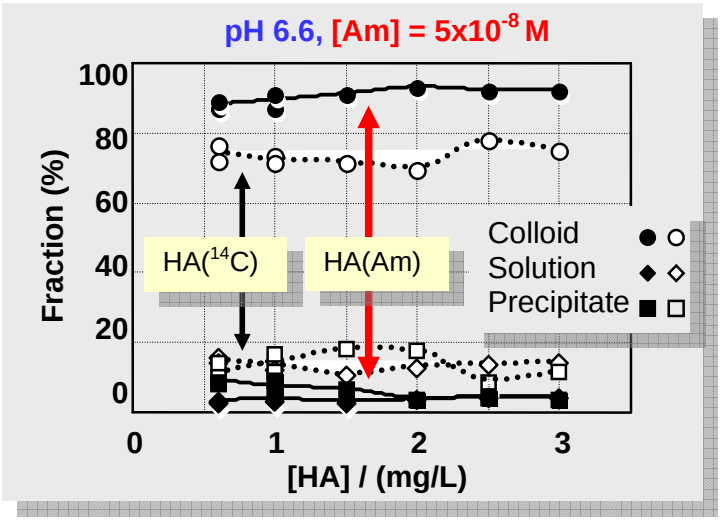

Fig. 5.3 [^{14}C]-humic acid and Am activity fraction (%) in the precipitate, colloids and solution as a function of humic acid concentration in a solution of pH 6.6 containing $5x10^{-8}$ M Am. Results represent values obtained after 35 d sample conditioning time.

The results discussed so far outline that the parameters that appear to have a determining role in the formation of humic colloids are: the concentration of coagulating cation and pH, both in connection with the PEC of humic acid, and in anticipation, the nature of the coagulating cation. Following these observations, the interaction of each actinide/Al with the humic colloids is discussed in the next section turn by turn.

5.2 Complexation of Al and actinide(III)/(IV)/(VI) with humic acid

5.2.1 Formation of colloid-borne actinides: parameter screening

A parameter screening experiment is carried-out in order to assess the general conditions for generation of humate-colloid-borne actinides as a function of pH in presence of variable amounts of Al. Trace amounts of actinide either $5x10^{-8}$ M Am/(Th), or $8x10^{-7}$ M U are added to solutions of pH 6.6, 7.2 and 7.8 containing 6.5 mg/L HA and Al concentration from 0 to 10^{-4} M. The Al concentration range includes the concentrations corresponding to the formation of HAS colloids. The chosen concentration of HA with its PEC ($4.8x10^{-3}$ eq/g) corresponds to the equivalent concentration required for full complexation (neutralization of the functional groups) with a trivalent cation (charge 3+) at concentration of 10^{-5} M. Blank samples, prepared under similar conditions but without HA are also analyzed for comparison. The contour profiles for the formation of colloid-borne An obtained from actinide activity measurements are illustrated in Fig. 5.4**.**

As can be observed in the diagram, in absence of humic acid, Am and Th are entirely present in the precipitate phase. A marginal colloidal fraction is generated in case of U and mainly at pH 6.6 and 7.2 in absence of Al. The increase of Al concentration to over-saturation (cf. Fig. 2.6) causes destabilization of the U colloidal fraction, accompanied by the activity transfer to the precipitate. Upon addition of 6.5 mg/L HA (upper part contours), we observe an enhanced actinide activity fraction in the colloidal phase. The transfer of initially precipitated actinides to the colloidal phase in presence of humic acid proves the actinides complexation with humic acid. Formation of humate-colloid-borne actinides is generally very efficient up to 10^{-5} M Al. Several differences between the actinides incorporation patterns can be distinguished in the diagram. Hence, the generation of humate-colloid-borne actinides appears to be most favorable in case of Am for the investigated pH and Al concentration range. Maximum Am activity fraction in the colloidal phase of approximately 90 % can be observed. Formation of humate-colloid-borne species appears to be less favorable for Th at pH 6.6 and in case of U at pH 7.8, with approximately 70% of actinide activity remaining in the colloidal phase. At Al concentration of $1x10^{-4}$ M, the proton exchange groups of HA are become saturated and the colloidal phase is destabilized and the precipitation of the actinide/Al-humate complexes takes place.

Only in case of Am a colloidal activity fraction of approximately 40 % can be still observed at pH 7.8.

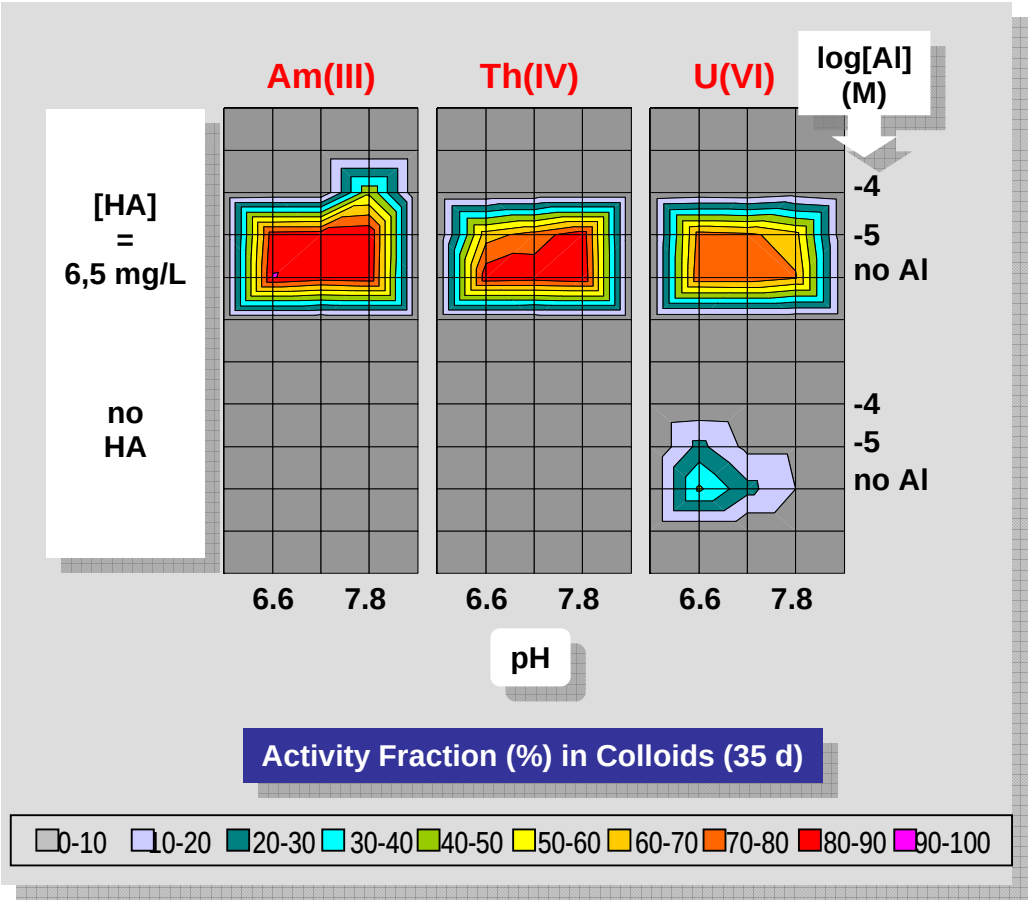

Fig. 5.4 Actinide activity fraction in the colloidal phase (%) normalized to the input activity after 35 days sample conditioning time for samples containing: An/Al (lower contours) and An/Al/HA (upper contours) at pH 6.6, 7.2 and 7.8 and initial An concentration: $5x10^{-8}$ M Am/ $5x10^{-8}$ M Th/$8x10^{-7}$ M U.

In more detail is discussed in the followings the An/Al complexation with humic acid, as a function of its concentration, under the conditions where the formation of colloid-borne species is favored, namely at constant concentration of Al of 10^{-5} M. These conditions are recalled in Fig. 5.5 a. The complexation with humic acid is observed for trace amount of An and 10^{-5} M Al at increasing HA concentration from 0 to 8 mg/L, or decreasing Al concentration while keeping HA concentration constant at 6.5 mg/L.

5.2.2 Complexation behaviour of Al and actinides: comparison

The samples are prepared by adding increasing humic acid concentration up to 8 mg/L, to solutions containing either $5x10^{-8}$ M Am, $5x10^{-8}$ M Th, or $8x10^{-7}$ M U and Al at constant concentration of $1x10^{-5}$ M. The equivalent of further higher HA concentration is obtained by decreasing Al from $1x10^{-5}$ M to $5x10^{-8}$ M (in case of Th) or to $5x10^{-7}$ M (in case of U), while the HA concentration is maintained at 6.5 mg/L. ^{14}C and actinide activities are measured in the same sample and the results are illustrated in Fig**.** 5.5 b.

At pH 6.6, as can be seen in Fig. 5.5 b, in the HA low concentration range (< 1 mg/L), the actinides and HA are precipitated due to the saturation of the HA proton exchange functional group by the Al ions. Upon increasing HA concentration above approximately 1 mg/L, the actinide activity begins to be transferred to the colloidal phase. The complexation of actinides and Al with HA is proved by a similar increase in the colloidal fraction obtained from ^{14}C measurements. We can also observe some differences between the actinides patterns for the formation of humate-colloid-borne species. In case of Am, the colloids appear to be promptly generated with increasing HA concentration and at HA ≥ 1.5 mg/L. 80% of Am activity is found in the colloidal phase. A similar behaviour is observed for U. In case of Th, one needs higher HA concentration (i.e. about 8 mg/L) in order to reach a fraction of about 80 % Th activity in the colloidal phase. That trace amount of actinides species present in solution undergo complexation with HA is evident from the similar pattern of the colloids generation observed from both actinide and ^{14}C-activity measurements. In addition, in the low HA concentration range (≤ 1 mg/L HA) the colloidal fractions from ^{14}C measurements are smaller than those observed at the formation of humic colloids in presence of only Al at concentration of 10^{-5} M at pH 6.6, as discussed for Fig. 5.2.

When increasing pH to 7.8, we observe that in case of Am and Th the conversion of the precipitate to the colloidal phase starts at lower HA concentration (i.e. below 0.6 mg/L), as compared to pH 6.6. With increasing pH deprotonation of humic acid functional groups takes place and more sites become available for complexation. Also, with increasing pH, the element (An/Al) hydrolysis advances as illustrated for example for Al in Fig. 5.6 a. For this reason, the observed shift to lower HA concentration with increasing pH might be correlated to a lower positive charge carried by the ionic species at this pH as for

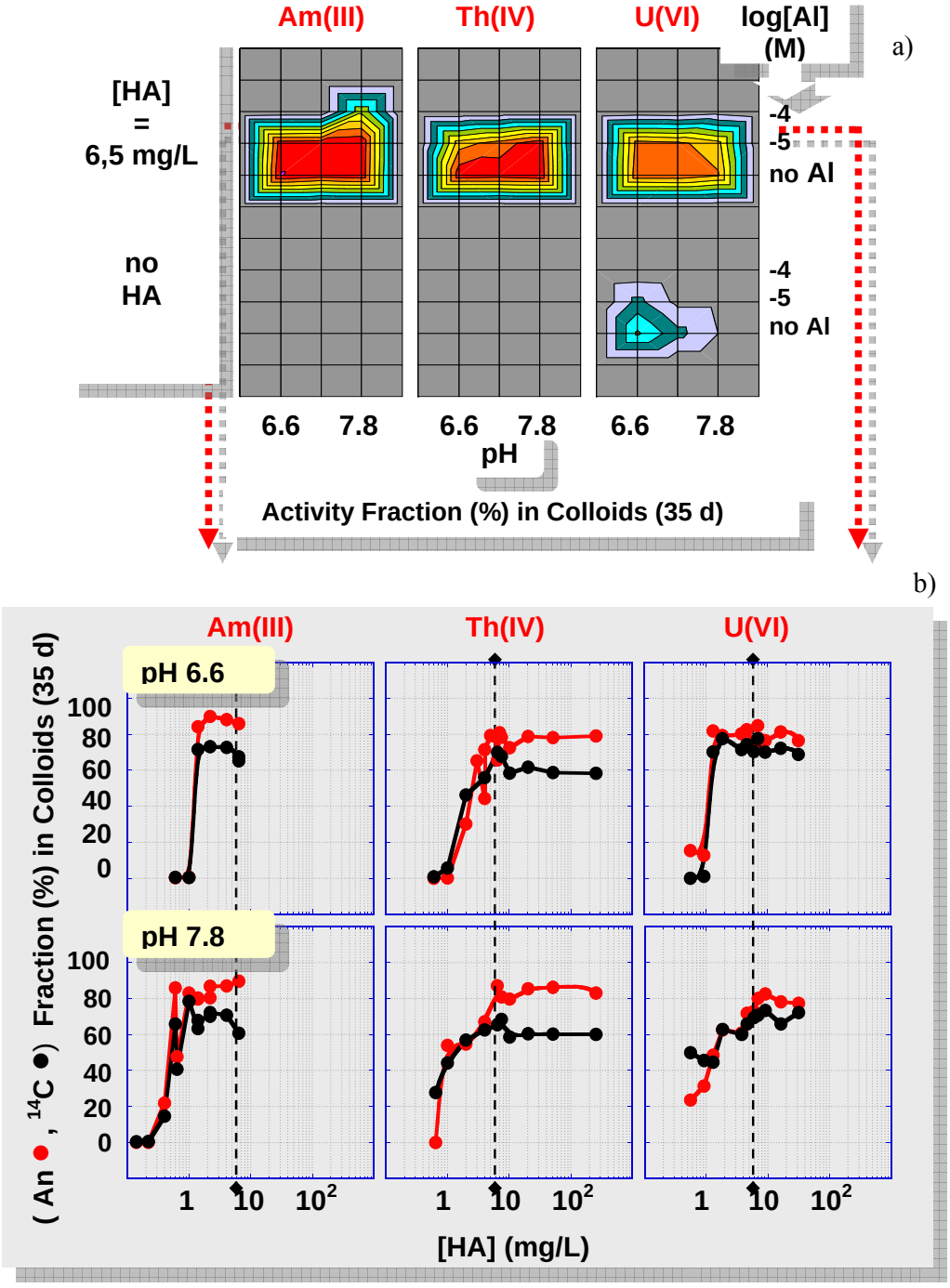

Fig. 5.5 a): Actinide activity fraction in the colloidal phase (%) normalized to the input activity after 35 days sample conditioning time for samples containing: An/Al (lower contours) and An/Al/HA (upper contours) at pH 6.6, 7.2 and 7.8 and initial An concentration: $5x10^{-8}$ M Am/ $5x10^{-8}$ M Th /$8x10^{-7}$ M U; b)**:** Actinide and [^{14}C]-humic acid activity fraction in the colloidal phase as a function of HA concentration up to 8 mg/L and at constant Al concentration of 10^{-5} M and further as a function of Al concentration (decreasing) at constant HA concentration of 6.5 mg/L.

pH 6.6. According to the metal ion charge neutralization [29, 68], describing the metal ion-humate complexation, a lower positive charge requires less amount of HA for complexation, or in other words, there is less positive charge available for neutralization and precipitation of humic acid. As for pH 6.6, the actinide fraction in the colloidal phase increases with HA concentration, but in this case, similar colloidal fractions of approximately 80 % are reached at higher HA concentrations.

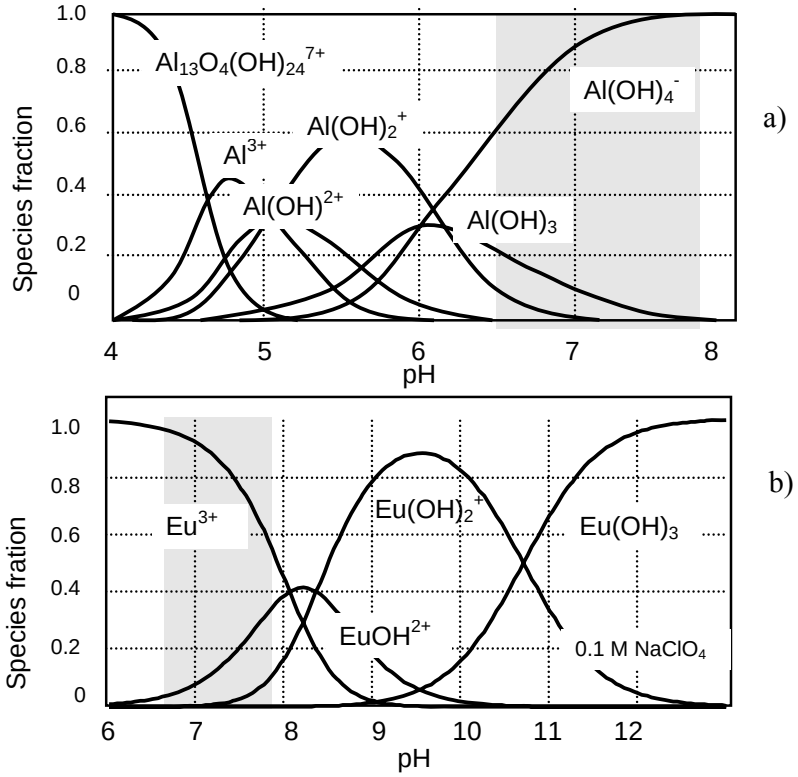

Fig. 5.6 Distribution of solution species at 25°C in carbonate-free solution for: a): Al(III), 10^{-6} M [131] and b): Eu(III) in a 0.1 M $NaClO_4$ solution [133].

Another general remark from Fig 5.5 b, is related to the colloid fractions from ^{14}C and actinide measurements. The following observations can be made: in the region where the colloids generation is observed and in the HA concentration range up to 8 mg/L, the colloid fractions from Am measurements are generally significantly higher than those from ^{14}C measurements.

This behaviour is distinct as compared to that observed for Th and U, for which the colloid fractions from Th/U measurements are lower or equal to that from ^{14}C for the above mentioned HA concentration range. However, Th/U colloid fractions tend to become more elevated than those from ^{14}C measurements with increasing the ratio HA/Al concentration (i.e. decreasing Al concentration). Under the experimental conditions the ^{14}C-activity measurements reflect the distribution of humic colloids at complexation with Al and therefore might be considered as an indicator of the Al effect at the interaction with humic colloids. Providing this assumption is correct, the more elevated colloidal fractions obtained from Am measurements as compared to those from ^{14}C, may reflect a higher affinity of Am for binding to humic colloids as compared to that of Al.

5.3 Identification of humate colloid-borne actinide species

An attempt is made in the followings in order to investigate the underlying reasons for the suggested different quality of Al and Am complexation with humic colloids. Therefore, the effects of Al and Am on the humic colloids formation are examined in more detail in a similar experiment but eliminating the concentration difference between the two elements. Thus, Al is replaced through Eu (as analogue of Am). Maintaining Eu concentration at $1x10^{-5}$ M and adding in each case $5x10^{-8}$ M Am as monitoring tracer, humic acid concentration is gradually increased. Fig. 5.7 illustrates comparatively selected results for the formation of humate-colloid-borne Am monitored as a function of HA concentration, in presence of either Eu or Al, at pH 6.6 (Fig**.** 5.7 a, b) and at pH 7.8 (Fig. 5.7 c, d). Only the colloid fractions obtained from Am activity measurements are shown. The experimental concentration of Eu is at the solubility limit of Eu hydroxide [133] whereas that of Al is above the solubility of its amorphous hydroxide [131] at pH 6.6.

Eu appears to be precipitated in the low humic acid concentration range, where humic acid has been also found to be precipitated upon saturation of functional groups by the Eu^{3+} ion. By further increasing the humic acid concentration, the precipitate is promptly transferred to the colloidal phase beginning with 6.5 mg/L humic acid as can be seen in Fig. 5.7 a. Al is also coprecipitated with humic acid in the very low humic acid concentration range as shown in Fig. 5.7 b. The conversion of the precipitate to the colloidal phase starts at approximately 1.0 mg/L humic acid**.** The humic acid concentration re-

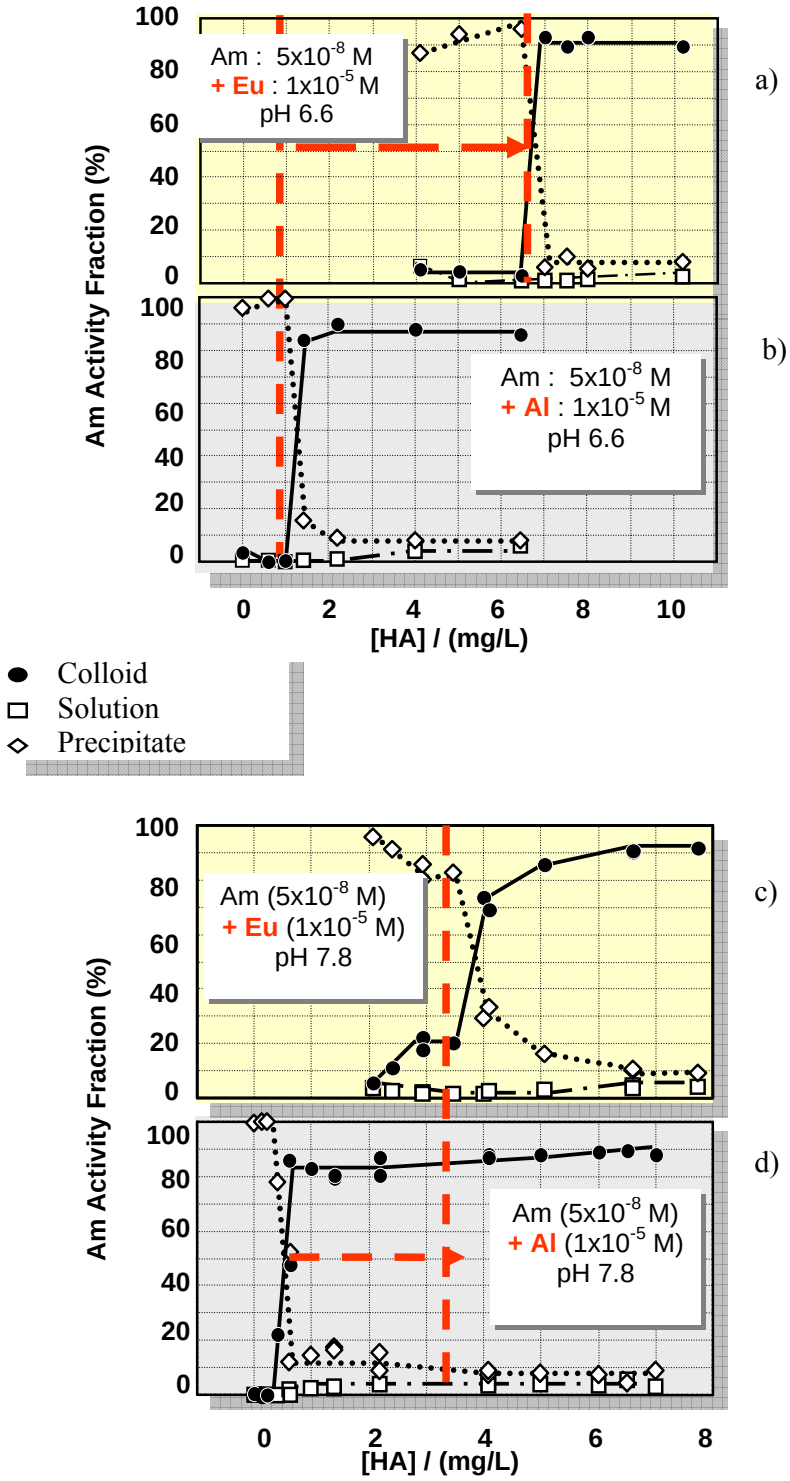

Fig. 5.7 Am activity fraction (%) in the precipitate, colloids and solution as a function of HA concentration. Samples are prepared with $5x10^{-8}$ M Am and either Eu or Al ($1x\ 10^{-5}$ M) at pH 6.6 (a and b) and at pH 7.8 (c and d). Results represent values obtained after 35 d sample conditioning time. The red arrow marks the shift to higher HA concentration required for generation of humic colloids with increasing the effective positive charge of the metal ion.

quired for the conversion of precipitate to colloids is much lower for Al than for Eu, although the same concentration is maintained for both elements. The differences can be correlated to the speciation of both elements given in Figs**.** 5.6 a and 5.6 b and explained by a numerical comparison of equivalent concentrations of the given reactants.

At pH 6.6, the equivalent concentration of 6.5 mg/L humic acid with proton exchange capacity of 4.8×10^{-3} eq/g and 1×10^{-5} M Eu are calculated to be

Humic acid: 4.8×10^{-3} (eq/g) x 6.5 x 10^{-3}(g/L) = 3.1×10^{-5} (eq/L)

Eu^{3+} ion: 1×10^{-5} (mol/L) x 3 = 3.0×10^{-5} (eq/L)

The data show that once Eu^{3+} loads completely the functional groups of humic acid the precipitation prevails as is apparent from Fig. 5.7 a. Thus, for the given Eu^{3+} concentration (1×10^{-5} M) at pH 6.6, the precipitate becomes colloidal with increasing the humic acid concentration above 6.5 mg/L. The process can be regarded as a complexation of the Eu^{3+} ion with humic acid, leading either to precipitate at saturation or to colloids at undersaturation of functional groups.

A similar calculation can be made for Al in accordance to its speciation and the 1.0 mg/L HA required.

Humic acid: 4.8×10^{-3} (eq/g) x 1.0×10^{-3}(g/L) = 4.8×10^{-6} (eq/L)

If we take into consideration the speciation in absence of humic acid given in Fig. 5.6 b, i.e., 10% for $Al(OH)_2^+$, and 20 %$Al(OH)_3$, the concentration of the reactive Al species is estimated to be:

$Al(OH)_2^+ + Al(OH)_3$: 1×10^{-5} (mol/L) x 0.3 = 3.0×10^{-6} (eq/L)

This value is somewhat lower than the humic acid concentration at which the humic colloids begins to be generated as shown in Fig. 5.7 b. The reason might be that the fraction of the $Al(OH)_2^+$ species reacting with humic acid is slightly higher than predicted by the thermodynamic speciation data for Al in absence of humic acid.

The results indicate the formation of ternary complexes of Al with humic acid, whereas the reaction of Eu concluded from Fig. 5.7 a represents formation of a binary

complex at pH 6.6. It is apparent from Fig. 5.7, that humic colloids are formed when metal ions do not saturate by complexation all available functional sites of humic acid which can thus remain stable in the hydrophilic state.

As shown in Fig. 5.7, when increasing pH to 7.8, the formation of humic colloids requires less humic acid concentrations than at pH 6.6. At pH 7.8, as indicated in the speciation diagram (Fig. 5.6 a), three different Eu species are possibly involved in the reaction with humic acid: Eu^{3+}, $Eu(OH)^{2+}$ and $Eu(OH)_2^{+}$. Previously published data regarding the complexation of Am and Cm with humic acid [65, 66, 134] reported the formation of binary humate and ternary An-hydroxohumate complexes in the same pH range as in the present experiment. In analogy with the stability constants derived in the above mentioned studies for the Am(Cm)-complexes, each of the Eu species present in solution at pH 7.8 is expected to have its own affinity towards complexation with humic acid. As shown in Fig. 5.7 c, the formation of humic colloids via complexation with Eu starts at 2.2 mg/L humic acid, progressing slowly at the beginning and then increasing abruptly for humic acid concentration ≥ 3.6 mg/L. This non-smooth correlation with the humic acid concentration describes the plausible reactions of different Eu species as can be correlated with Fig. 5.6 b. The ternary complexation of Eu forming its hydroxohumate species requires less humic acid according to the metal ion charge neutralization model [29, 67] where the metal ion occupies a number of proton sites equal to its effective charge. The present observation in Fig. 5.7 c follows closely this approach. As a result, formation of humic colloids progresses step-forwards via complexation of different Eu species. According to the speciation given in Fig. 5.6 a, the equivalent concentration of Eu species involved in complexation with humic acid can be estimated at pH 7.8:

$$Eu^{3+}(55\%) + Eu(OH)^{2+}(35\%) + Eu(OH)_2^{+}(10\%): 1x10^{-5}(3x0.55 + 2x0.35 + 1x0.1)$$
$$= 2.45x10^{-5}\ (eq/L)$$

The equivalent concentration of Eu species suggests that formation of humic colloids requires a concentration higher than 5 ($2.45x10^{-5}/4.8x10^{-3}$) mg/L humic acid to include all Eu species present in solution, concentration which is certainly lower than with Eu^{3+} alone observed at pH 6.6. The value > 5 mg/L corresponds well to the experimental results showed in Fig. 5.7.

In case of humic colloid formation in the presence of Al at pH 7.8, the colloids

formation starts at humic acid concentration of approximately 0.3 mg/L, as can be appreciated from Fig. 5.7 d. Referring to the speciation given in Fig. 5.6 b, the prevailing Al species at pH 7.8 appears to be $Al(OH)^-_4$, an anionic species which is less probable to interact with humic acid as we already discussed in section 5.1. The result given in Fig. 5.7 d indicates that more than $1.4x10^{-6}$ eq/L humic acid is required to form humic colloids. This means that a minor amount of $Al(OH)_3$ species present together with trace Am species is responsible for humic colloids formation. As speciation of Eu and Al as a function of pH varies largely from one another, the formation characteristics of humic colloids are different accordingly as concluded from the experiment.

Based on these results, the observed different patterns of humate-colloid-borne actinides formation associated with the actinide oxidation state, pH and HA concentration, as discussed for Fig. 5.5 b., might be correlated with changes in the metal ion hydrolysis species (i.e. the cation charge) present in solution depending on the specific experimental conditions.

The validity of this assumption for Th and U, is investigated by performing a similar experiment as for Am. For this purpose we carry out an experiment similar as for Fig. 5.5 b but Al is replaced in this case either by Th or U. Increasing amount of humic acid, up to 8 mg/L, are added to solutions containing the actinide tracer (either $5x10^{-8}$ M (^{234}Th+^{232}Th) or $8x10^{-7}$ M ^{233}U) and 10^{-5} M either ^{232}Th or ^{238}U. The equivalent of higher HA concentration is achieved by decreasing the actinide concentration in samples while HA concentration is maintained constant. Accordingly, keeping humic acid concentration at 6.5 mg/l, actinide concentration is decreased from $1x10^{-5}$ M to $5x10^{-8}$ M in case of Th and to $8x10^{-7}$ M for U. An overview of the results regarding colloidal fraction observed by actinide and ^{14}C-measurements is illustrated for pH 6.6 and 7.8 in Fig. 5.8 a, containing also the results for the formation of humate-colloid-borne Am(Eu) discussed above.

From Fig. 5.8 a we observe that with increasing the actinide tendency toward hydrolysis (i.e. from Am to Th or increasing pH), the HA concentration at which the humic-colloids are generated shifts toward lower values, as lower positive charge requires less humic acid for complexation. At pH 7.8, the generation of humate-colloid-borne U proceeds slowly and appears to be less favorable as for Am and Th. As one can see in Fig. 5.8, the curves describing the colloidal fractions from actinide activity measurements

a)

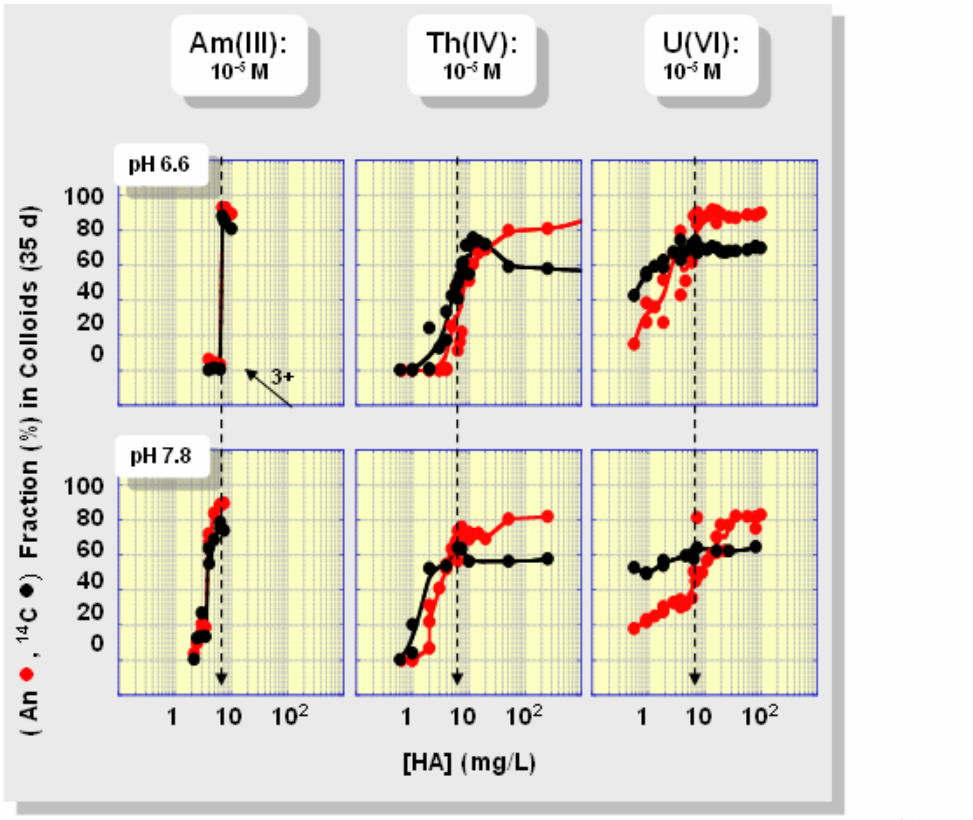

b)

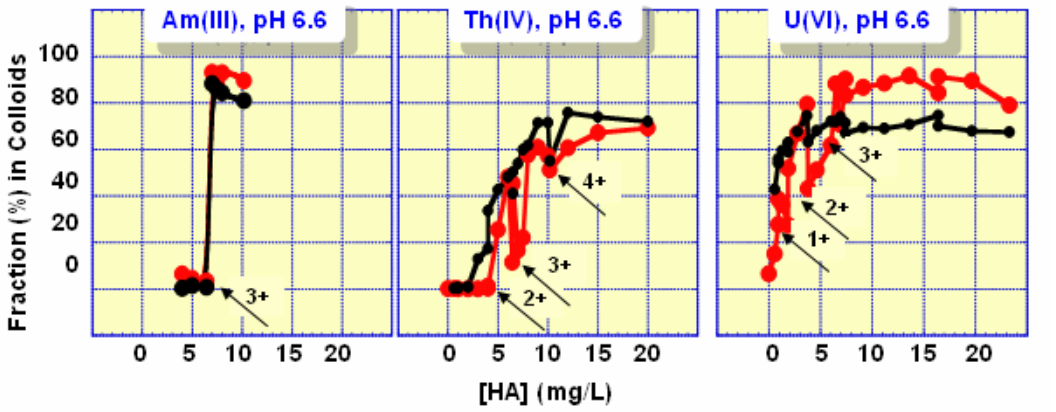

Fig. 5.8 a): a): Actinide and 14C activity fraction (%) as a function of humic acid concentration for samples at pH 6.6 and 7.8 and 35 days sample conditioning time. The samples are prepared at constant concentration (10^{-5} M) of either Eu, ^{232}Th or ^{238}U and ^{241}Am $5x10^{-8}$ M, ^{234}Th $1x10^{-12}$, ^{233}U $8x10^{-7}$ M and increasing HA concentration up to 8 mg/L and by further decreasing An concentration at HA concentration of 6.5 mg/L; b): Selected results for pH 6.6, indicating the charge of the actinide species suggested to be present in solution at the corresponding experimental conditions.

become equal and further exceed those from ^{14}C-measurements when increasing HA concentration or decreasing the An/HA concentration ratio, respectively. In association with the previous results for Am/Al, the changes in the relative position of the two curves might suggest an increasing affinity of Th/U species toward complexation with humic-colloids when the experimental conditions change as mentioned above. One can further observe from Fig. 5.8 a, that at pH 6.6, in case of both Th and U, the colloid fractions exhibits oscillations with several minima corresponding to HA concentration where the colloids begins to form out of the precipitate. The effect appears to be reproducible as observed at repeated experiments. Such minima could be taken as indicators of experimental conditions where distinct Th(U) ionic species are neutralized by humic acid. This hypothesis is analyzed in the followings for pH 6.6. For a better view, reference is made to the Fig. 5.8 b, illustrating the results for a limited HA concentration range, up to 20 mg/L.

Th concentration of 10^{-5} M is above the solubility limit of the amorphous $Th(OH)_4$ [135] and in absence of HA, Th activity fraction is found in the precipitate. As can be seen in Fig 5.8 b in the region of low HA concentration, there is no colloid formation, Th and HA remain in the precipitate phase. The generation of colloid-borne Th via complexation with HA starts at 4 mg/L HA, that is lower as needed as for the same concentration of Am(Eu) (species with charge 3+) at the same pH. We carry out similar calculation as in case of Am(Eu) for the reactant equivalent concentration involved in the complexation reaction. For 4 mg/L HA and its PEC of $4.8x10^{-3}$ (eq/g), the equivalent concentration is

Humic acid: $4.8x10^{-3}$ (eq/g) x $4.0x10^{-3}$ (g/L) $= \sim 1.9x10^{-5}$ (eq/L)

Taking this as equivalent concentration as in the neutralization reaction with the $Th(OH)_y^{4-y}$ species assumed to be present in solution at the concentration of 10^{-5} M a reverse calculation is carried out. This leads to a value of approximately 2 ($1.9x10^{-5}$ M /$1x10^{-5}$ M) for the charge of Th species involved in the complexation reaction. According to the speciation data, in absence of HA, the expected species in solution are $Th(OH)_4$ and $Th(OH)_3^+$ (Fig. 8.2 a). The result indicates that in presence of 4 mg/L HA, Th hydrolysis is inhibited and $Th(OH)_y^{4-y}$ species with charge 2+ should be the reactive species in solution. With increasing HA concentration formation of Th colloids proceeds rapidly. The next points (minima) associated with the formation of colloids from the precipitate are observed to occur at 6 and 8 mg/L HA. Similar calculations as described above suggest

that the equivalent HA concentrations correspond to the complexation (neutralization) of Th species with effective charge of approximately 3+ (2.9) and 4+ (3.8), respectively, with the latter value corresponding to the non-hydrolyzed Th^{4+}. The result suggests that with increasing the HA concentration, the complexation takes place with the less hydrolyzed species. The complexation of Th with HA in the neutral pH range is reported in the literature [74], but the available thermodynamic data are poor for the ternary complexation [11].

A similar pattern of colloid-formation is observed in case of U. At pH 6.6 the U concentration of $1x10^{-5}$ M is above the saturation concentration of the U(VI) hydroxide: metaschopite [61]. As can be seen in Fig. 5.8 b, in absence of humic acid U activity is present in the precipitate phase. Upon addition of humic acid, the formation of humate-colloid-borne U proceeds slowly. The first point associated to the colloid generation out of precipitate occurs at 2 mg/L HA. The speciation data shown in Fig. 8.2 b, indicate that in absence of HA at pH 6.6 the expected species in solution are $(UO_2)_3(OH)_5^+$ and UO_2OH^+. Based on the equivalent HA concentration and assuming the concentration of U reactive species in solution is 10^{-5} M, the charge of the U species involved in the reaction in this case is found to be approximately 1+, in agreement with the U speciation data in absence of HA. The literature documents the interaction of HA with the above mentioned species [7, 46]. Increasing HA concentration follows the minima at 4 and 6 mg/L HA, corresponding to reactive U species with charge 2+ and 3+, respectively. The charge 3+ for U(VI) is conceivable since it is known that in the linear structure of UO_2^{2+} the effective charge available for complexation (specific binding) is 3.2+ [46, 73]. The results indicate once more that increasing the humic acid concentration induces an inhibition of the actinide hydrolysis with preferential formation of higher positively charged species, with higher affinity towards complexation with humic colloid. For both Th and U we observe from Fig. 5.8 that at increasing the HA/An concentration ratio (decreasing An concentration), the An tend to be preferentially distributed to the colloidal phase.

5.4 Conclusions

The present results show that interaction of trace amount of actinides with humic colloids is very efficient in the neutral pH range 6.6-7.8. The complexation of An and Al

with the humic-colloids is correlated to their hydrolysis tendency. Hence, the generation of humate-colloid-borne species is distinctively favored for the non-hydrolyzed ionic species. Accordingly, among actinides present at tracer concentration, the less hydrolyzed Am(III) shows higher affinity as compared to Th(IV) and U(VI) for the formation of humate-colloid-borne species in the neutral pH range and for humic acid concentration at the average level of natural waters. Al, with higher tendency to hydrolyze is less favored at the interaction with humic colloids. However, apart from the element intrinsic hydrolysis behaviour, the prevailing species will be also influenced by the specific conditions: e.g., at increasing HA concentration the hydrolysis is expected to be suppressed by humate complexation.

6. Competitive interaction of actinide(III-VI) with aluminosilicate and humate colloids

The results discussed in chapters 4 and 5 have given a better insight on the interaction of actinides (An) either with the HAS or with HA. The study is continued for investigating the behaviour of Al and the actinides, either Am, Th or U, in the mixed system humic acid-aluminosilicate. Thus, the actinides may undergo complexation with humate colloids, conucleate with silicic acid with formation of An-HAS pseudocolloids, and interact with both HAS and HA with formation of mixed HAS-humic colloidal species or a mixture of An-HAS and An-humic colloids. The formation of colloid-borne An in the presence of both HAS and humic acid (^{14}C-HA) is examined within the neutral pH range 6.6 to 7.8. The pH range, for which the An-humate complexation has been discussed in chapter 5, is chosen to follow the low solubility regions of $Al(OH)_3$ and aluminosilicate minerals in which the HAS colloid formation is not pronounced due to precipitation [26, 27] and thus the eventual influence of HA on the colloid formation becomes visible. HAS solutions are prepared from both undersaturated and oversaturated silica to observe colloid formation from both monosilicic and polysilicic acid, respectively. Based on the results from section 5.2, humic acid concentration is kept constant at 6.5 mg/L appeared to be appropriate to appraise the humic acid effect. Trace amounts of actinides are used in the experiment: [^{241}Am]: $5x10^{-8}$ M, [^{234}Th + ^{232}Th]: $5x10^{-8}$ M and [^{233}U]**:** $8x10^{-7}$ M.

6.1 Complexation of Al and An(III) with silicic and humic acid

6.1.1 Formation of colloid-borne actinide(III): parameter screening

A parameter screening experiment is carried out to characterize the conditions for formation of colloid-borne Am in presence of both HAS and humic colloids for the above mentioned experimental conditions. Fig. 6.1 depicts the results for colloid formation ascertained by ^{241}Am and ^{14}C measurements. Colloidal fractions are distinguished after a sample conditioning time of 35 days as a function of the relevant parameters, namely pH, concentration and concentration ratio of Si and Al. The figure contains three contour diagrams for the interaction of Am with different colloid types: (a) HAS colloids synthesized from Si and Al; (b) humic colloids complexed with Al; (c) composite HAS and humate

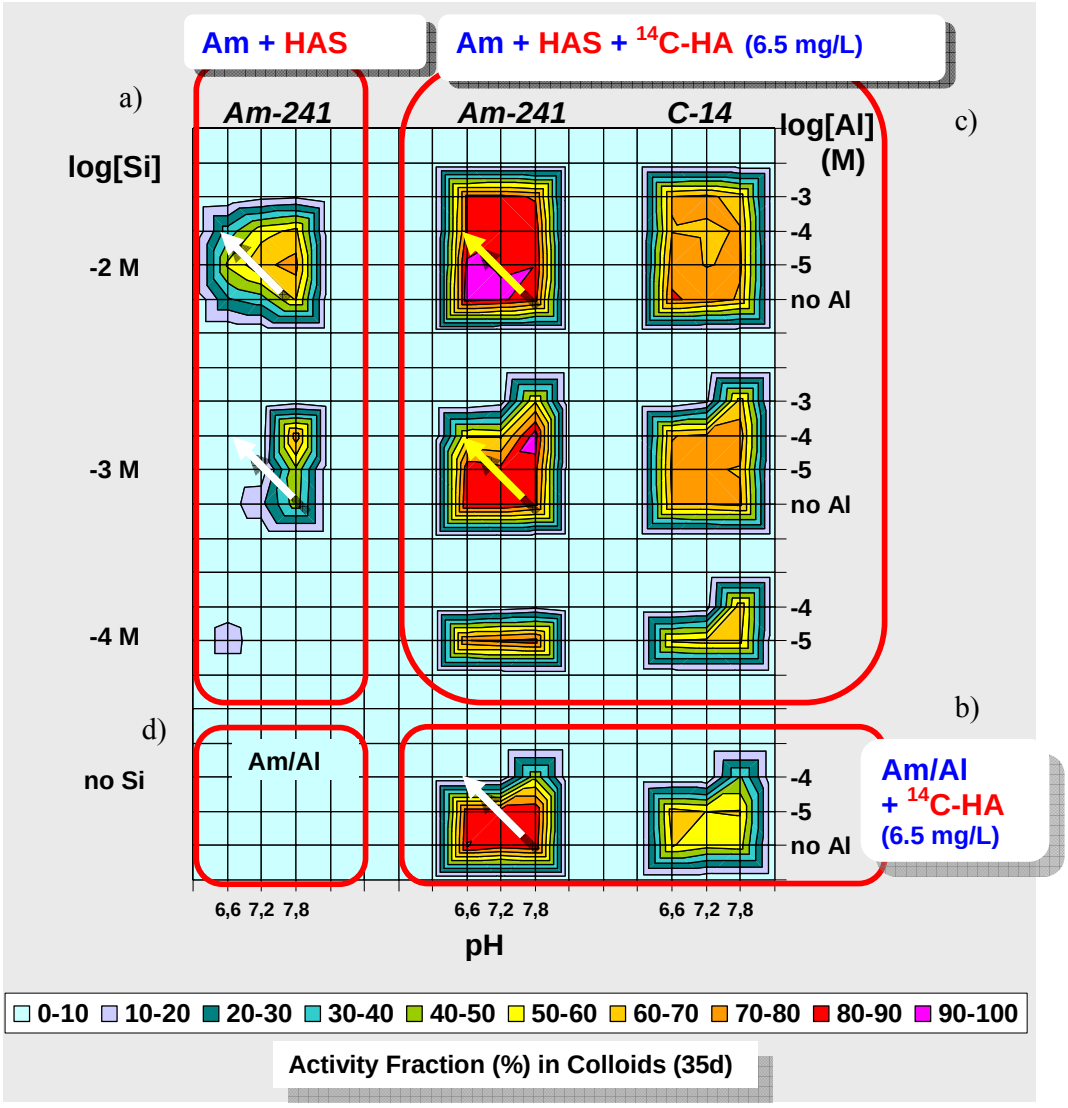

Fig. 6.1 Radiometric screening experiment for the formation of colloids from (a) HAS, (b) Al-humate and (c) HAS+Al-humate and d) Am/Al solutions as a function of pH, concentration of Si and Al. Contours indicate ^{241}Am and ^{14}C activity fraction in the colloidal phase as a function of pH, for samples after 35 days conditioning time. Samples are prepared with $5x10^{-8}$ M Am, variable concentration of Si (left axis) and Al (right axis) and in presence of 6.5 mg/L HA (b and c).

colloids generated from solutions containing Si, Al and humic acid. Contour diagram d) shows the colloidal activity fraction for samples containing only Am and Al. Contour profiles for the formation of HAS - colloid borne Am are shown in Fig. 6.1 a for both monosilicic and polysilicic acid. As outlined in section 4.2.1, the previous TRLFS studies

have shown that in the pH range of the current experiment, Cm binds to the HAS-colloids by coordination with the silicate ligand via partial or full displacement of water molecules of Cm. The formation depends whether the HAS are produced from monosilicic or polysilicic acid. Fractions of HAS-colloid borne Am are relatively low because of low solubilities of HAS in the present pH region.

Addition of humic acid converts precipitates to the colloids, as shown in Fig. 6.1 c, colloidal fractions are thus increased in broad ranges of Al concentration and pH. The increase of colloidal fractions by addition of HA (from Fig. 6.1 a to c) suggests a conversion of HAS precipitate to HAS-humic colloids. As shown in Fig. 6.1 c, the colloidal fractions measured by ^{241}Am (left part) are somewhat higher than those of humic colloids (right) although the patterns of colloids formation are similar for similar Al concentration and pH. These observations implicate that during conversion of HAS precipitate to HAS-humic colloids, Am appears to be preferentially incorporated into the colloidal fraction. Fig. 6.1 b shows contour profiles of the humic colloid formation in the presence of Al but without Si. Fractions of humic colloid-borne Am (left side) are again somewhat higher than those of humic colloids (right side) whereas both profiles are comparable. This preferential incorporation of Am into the colloidal phase at complexation with HA has been already mentioned in section 5.2. Once the silicic acid is present, the colloid formation patterns change (from 6.1 b to 6.1 c) and the colloid formation is overall enhanced. Both changes from Figs. 6.1 a, and 6.1 b to 6.1 c can be considered as synergic formation of HAS-humic colloids incorporating Am efficiently.

The behaviour of Am is further analyzed under particular conditions indicated in Fig. 6.1 by arrows, where the formation of colloid-borne Am depends sensitively on the individual components under consideration, Si, Al and HA. Concentration of 10^{-4} M Al is chosen because at this concentration level, the effects of Si and HA can be better compared for recognition of their ligand competition. Fig. 6.2 illustrates formation of colloid-borne Am under different conditions.

In blank Al(Am) solution (Fig. 6.2 a) Am is precipitated in the given pH range and no colloid formation is observed. Addition of HA results in the formation of a marginal fraction of humic colloid-borne Am only at pH 7.8. The result can be expected, because as discussed in the previous section, the formation of Am/Al-humate colloids at Al concentration of $1x10^{-5}$ M requires HA concentration of at least 1 mg/L HA at pH 6.6 (Fig. 5.7 b)

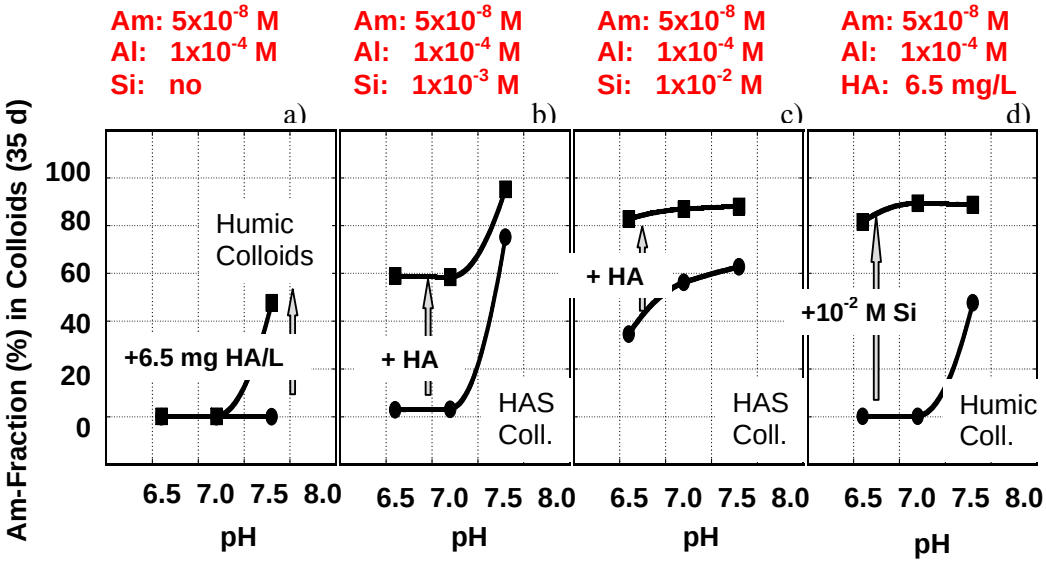

Fig. 6.2 Formation of colloid-borne Am as a function of pH after 35 d conditioning time for the following samples: a) Al (Am) + HA, b) Al (Am) + monosilicic acid + HA, c) Al (Am) + polysilicic acid + HA, d) Al(Am) + HA + polysilicic acid. Initial samples composition is indicated above each graph. HA or Si is added after 1 h conditioning time of the mother solution.

and more than 0.3 mg/L at pH 7.8 (Fig. 5.7 d). Accordingly, the offered amount of humic acid available in the present experiment is, depending on pH, below and above the required one, since at pH 6.6 more than 10 (10x1) mg/L and at pH 7.8 more than 3 (10x0.3) mg/L humic acid are needed. The HAS-colloid generation can be observed in Fig. 6.2 b by addition of 10^{-3} M monosilicic acid, only at pH 7.8. The colloid formation is then enhanced by addition of HA following the conversion of the precipitate to colloids.

Upon increasing Si concentration to 10^{-2} M (Fig. 6.2 c) in which polysilicic acid prevails, the formation of HAS-colloid-borne Am becomes significant even at lower pH. At the same time, humic acid further enhances the colloid formation under identical conditions.

Fig. 6.2 d depicts the results obtained for samples with the same final composition as in Fig. 6.2 c, but prepared in different sequence of component addition, i.e. 10^{-2} M Si is added to the Al/Am-humate. As can be seen, both experiments lead to the same final results, indicating that different order of component addition does not affect the formation of colloid-borne Am and the equilibrium is reached. These observations suggest that under the given experimental conditions, the partially hydrolyzed Am ionic species bind to

to both humic acid and HAS colloids and moreover imply that polysilicic and humic acid have similar binding affinity toward Am. As a result, the presence of humic acid in the process of HAS-colloid formation activates a synergic action of HAS and humic colloids for stable incorporation of Am into the colloidal phase.

6.1.2 Spectroscopic speciation of colloid-borne Cm(III)

For obtaining a further insight into the possible synergic effect for formation of HAS-An-humic colloids, TRLFS is applied by Kim et al. [136] in order to ascertain the binding state of Am within such colloids. As for the previous investigations based on TRLFS, the optically sensitive Cm is chosen as a chemical analogue of Am.

Speciation is conducted measuring the fluorescence emission by exciting at two different wavelengths: 370 nm and 383 nm. At the excitation wavelength of 370 nm, the light absorption of Cm is minimal and mainly the humic acid absorbs. On the other hand at the excitation wavelength of 383 nm, the light is absorbed primarily by Cm and to a less extent by humic acid. Speciation is carried out for three different colloid samples prepared as in case of the radiometric experiment but in presence of $5x10^{-8}$ M Cm: Cm + HAS and Cm + HA as reference samples, and a sample containing Cm + HAS +HA. The speciation results are illustrated in Fig. 6.3.

As can be seen in Fig. 6.3 a, for the reference sample Cm+HA, the Cm species excited at the two different excitation wavelengths generates two consistent emission peaks at 602.7 nm with comparable intensities at ratio I(370)/I(383) of 1.09. This ratio indicates that an indirect excitation via humic acid results in a slightly higher fluorescence emission. The emission peak at 602.7 nm corresponds to the ternary humate complex of Cm(OH)HA, as confirmed in previous study [66].

The HAS-colloid-borne Cm species shown in Fig. 6.3 b reveals emission bands with identical peak positions at 606.9 nm but distinctively different emission intensities: for direct excitation at 383 nm and indirect excitation at 370 nm. The clear difference in the heights of the two emission bands from direct and indirect excitations and the emission peak position at 606.9, together with the considerably long emission lifetime of 518± 25 µs imply the incorporation of Cm into the HAS colloids. These spectroscopic characteristics agree with those observed in the previous study [27].

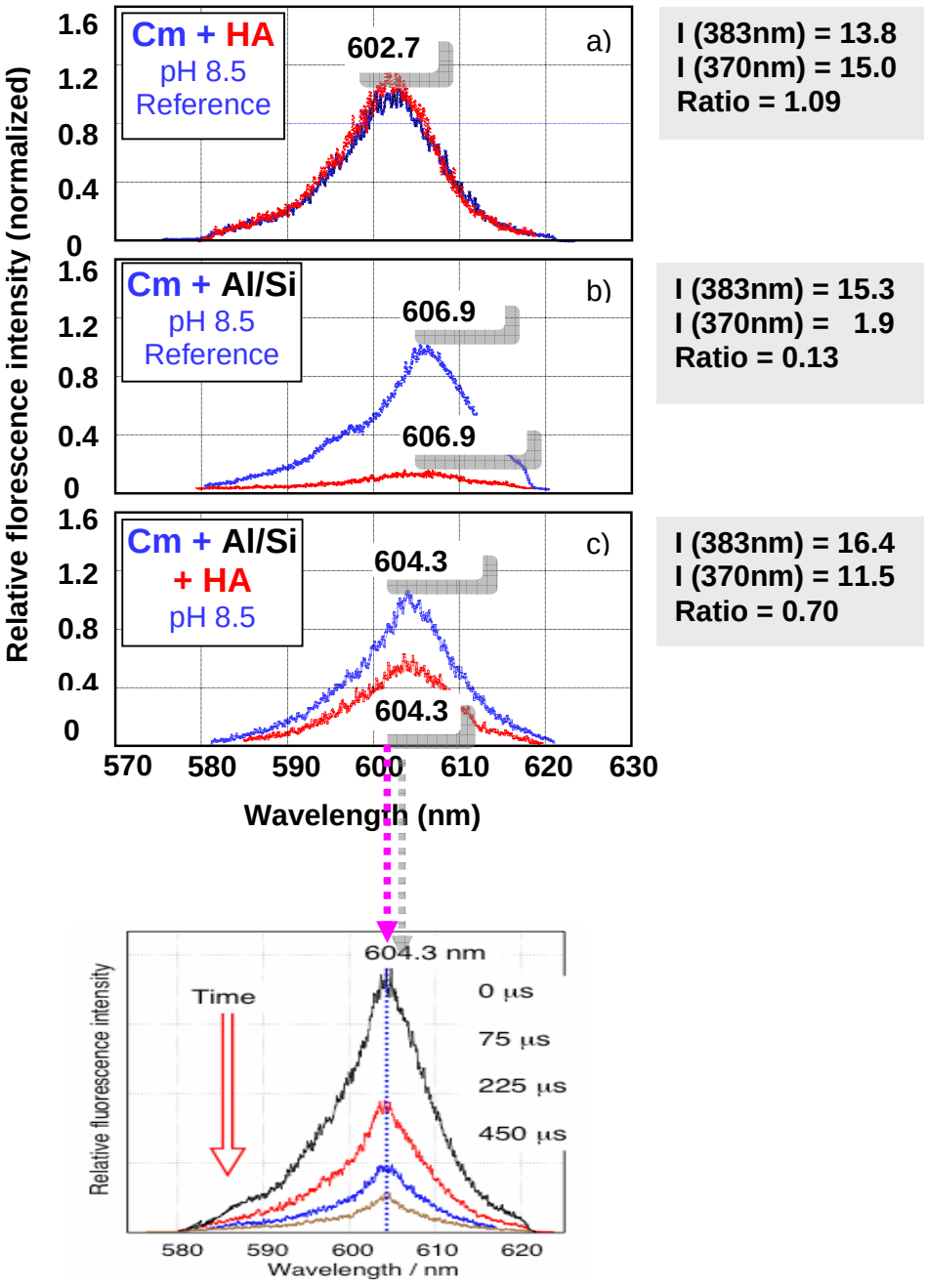

Fig. 6.3 TRLFS speciation of Cm(III) in different solutions. Figures a-c show the fluorescence emission by direct (blue) and indirect (red) excitation of Cm in the following samples: a) humate-colloid-borne Cm in a sample containing 10^{-4} M Al and 10 mg/L HA, b): HAS colloid-borne Cm in a sample containing 10^{-4} M Al and 10^{-2} M Si, c): HAS-humate colloid-borne Cm in a sample containing 10^{-4} M Al, 10^{-2} M Si and 10 mg/L HA. Samples are prepared at pH 8.5 with 4.9 x10^{-8} M Cm. The graph in the lower part shows the emission spectra measured at different delay time as indicated on the right part of the graph.

The chemical state of HAS-colloid-borne Cm is different in presence of humic acid, as shown in Fig. 6.3 c. The emission peak position shifts to 604.3 nm, which is different from those corresponding to humic-colloid-borne Cm (602.7 nm) and HAS–colloid-borne Cm (606.9 nm). The emission intensity from indirect excitation is 70% of the value corresponding to direct excitation. The life time of the emission, although not shown here, has been also found to change: from 518 ± 25 μs for the HAS-colloid-borne Cm (606.9 nm) to 329±15 μs in presence of humic acid (604.3 nm). The life time value observed in the mixed colloid sample is however longer than that corresponding to the humate-colloid-borne Cm of 106 μs [137]. Moreover, one can observe that the position of the emission peak does not change at increasing the delay times during the lifetime measurements. If a mixture of the two species, i.e. the humate-borne Cm and the HAS-borne Cm would be present in the solution, than the short lived humate–borne Cm would be no longer detected during the measurements at longer delay time and one would observe an emission peak at higher wavelength characteristic to the HAS-borne Cm. The fact that this is not observed in the composite sample together with the previously mentioned characteristics regarding the emission intensity, peak position and fluorescence life time, prove that Cm, initially incorporated in the HAS-colloids undergoes partially chemical bonding to humic acid, hence forming a composite structure of the HAS-humic colloid-borne species.

6.1.3 Kinetics of actinide(III) incorporation into the colloid mixture

The kinetics of the formation of colloid-borne Am is examined for the parameter screening experiment described in section 6.1.1. Formation of the colloid-borne Am at different conditioning times of the mother solutions between 3h to 35 d is illustrated in Fig. 6.4. The colloid formation in presence of both HAS and HA is compared with the case when only one of the components is present, either HAS or HA. The general observation is that for samples containing only HA (Fig. 6.4 a) or only HAS (c, e), the fraction of colloid-borne Am decreases generally with time and is accompanied by the activity transfer to the precipitate. In contrast, in samples containing both HAS and HA (Fig. 6.4 b, d), the colloid-borne Am fraction increases within the observation time of 35 d. The effect is more evident for samples generated in presence of polysilicic acid and 10^{-4}-10^{-3} M Al at pH 6.6-7.8, conditions indicated by the white lines in Fig. 6.4 d.

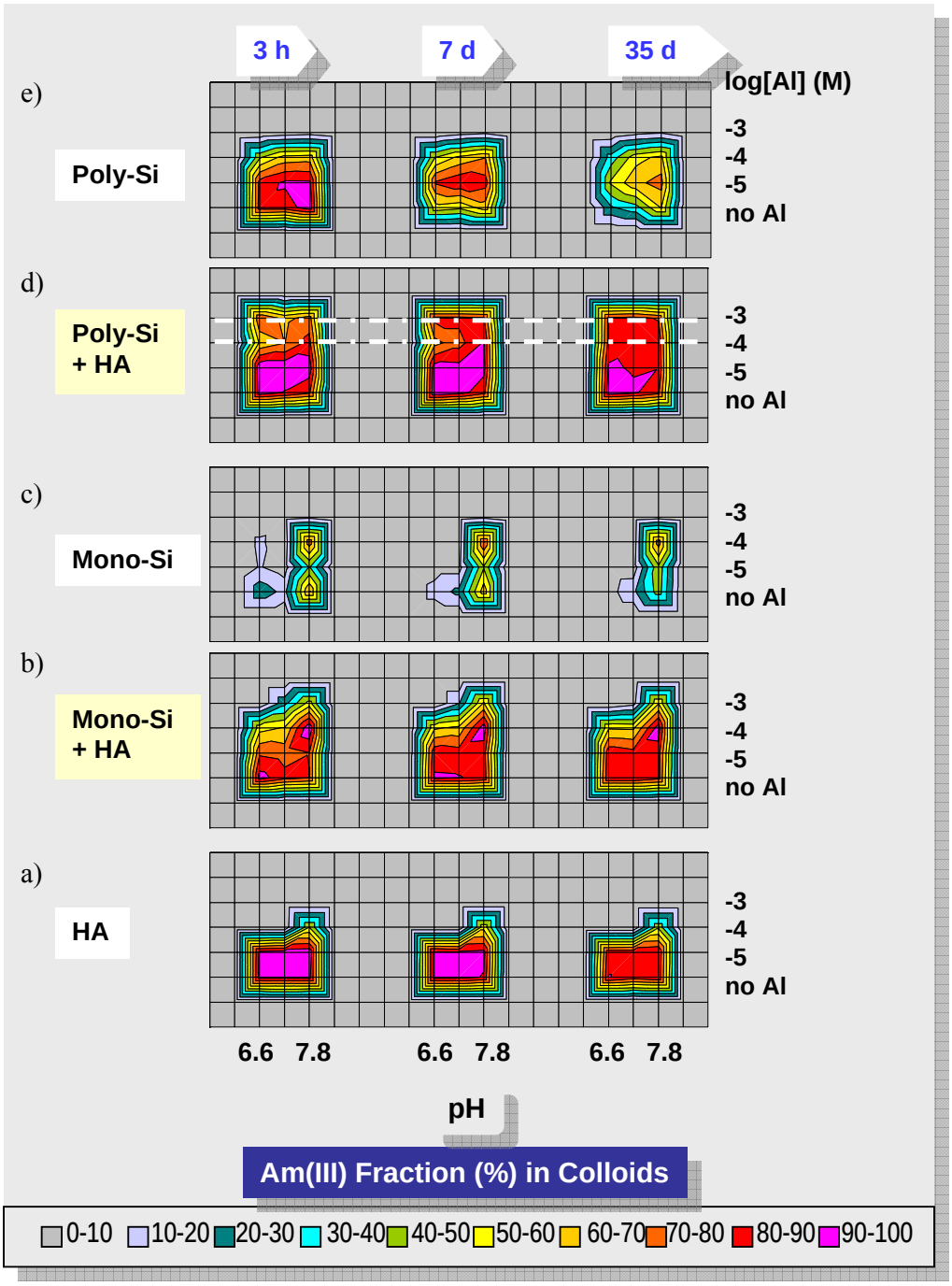

Fig. 6.4 Actinide activity fraction (%) in the colloidal phase as a function of pH after sample conditioning time from 3h to 35 days. Samples are prepared with $5x10^{-8}$ M Am in solutions containing $1x10^{-2}$ M Si (polysilicic acid) and $1x10^{-3}$ M Si (monosilicic acid) and variable Al concentration (right axis) in presence of 6.5 mg/L HA (marked by the yellow boxes). Results for reference samples (without HA or without Si) are indicated by the white labels.

For example, in solutions containing HA and polysilicic acid /10^{-4} M Al, the initial Am fraction in the colloidal phase is approximately 60% and increases to more than 80 % after 35 d sample conditioning time.

Kinetics effects have been also observed during the TRLFS measurements for speciation of Cm in HAS/HA solutions as described in section 6.1.2. In Fig. 6.5, the graph in the lower part depicts the results for the colloid-borne Cm species formed in the solution obtained by mixing all reactants at the same time [137]. In this case, the spectra obtained immediately after the sample preparation correspond to those already discussed and indicate the formation of a mixed humic-HAS-colloid-borne species. It is evident that the position of the emission peaks obtained at direct and indirect excitation of Cm, and their intensity ratio does not change significantly within 20 d observation time. This fact suggests that the species equilibrium is rapidly attained in this case, as Cm has similar binding affinity for both ligands, HAS and HA, which are added simultaneously in solution.

The graph in the upper part of Fig. 6.5 shows the results obtained at direct and indirect excitation of Cm in the mixed colloid sample generated by addition of HA to the preformed HAS-colloid-borne Cm, which is the order of reactant addition corresponding to the radiometric experiment discussed above. Immediately after the sample preparation, as can be seen in Fig. 6.5 the upper left, the colloid-borne Cm species present in the solutions show two distinct emission peaks at 605.5 and 606.9 nm and with different intensities at a ratio of 0.23. Since the most intense peak at 606.9 obtained at direct excitation corresponds to the HAS-Cm, as outlined in section 6.1.2, the results suggest that the HAS-Cm species dominates in the solution immediately after preparation of sample. After 20 d conditioning time of the mother solution, the spectrum reveals the emission peak at approximately 604 nm corresponding to the mixed HAS-humate-colloid-borne Cm. Also, the intensity of the emission corresponding to indirect excitation of Cm increases leading to a peaks intensity ratio of 0.59. The results indicate the progressive complexation of Cm with HA and the formation of a prevailing mixed humic-HAS species. Thus, the kinetic effect appears to be associated with the equilibration time necessary for the process of HAS partial displacement by HA from the already formed HAS-Am, followed by the formation of the mixed colloid species. The results of the fluorescence lifetime measurements (not shown here) also indicate a similar trend [137].

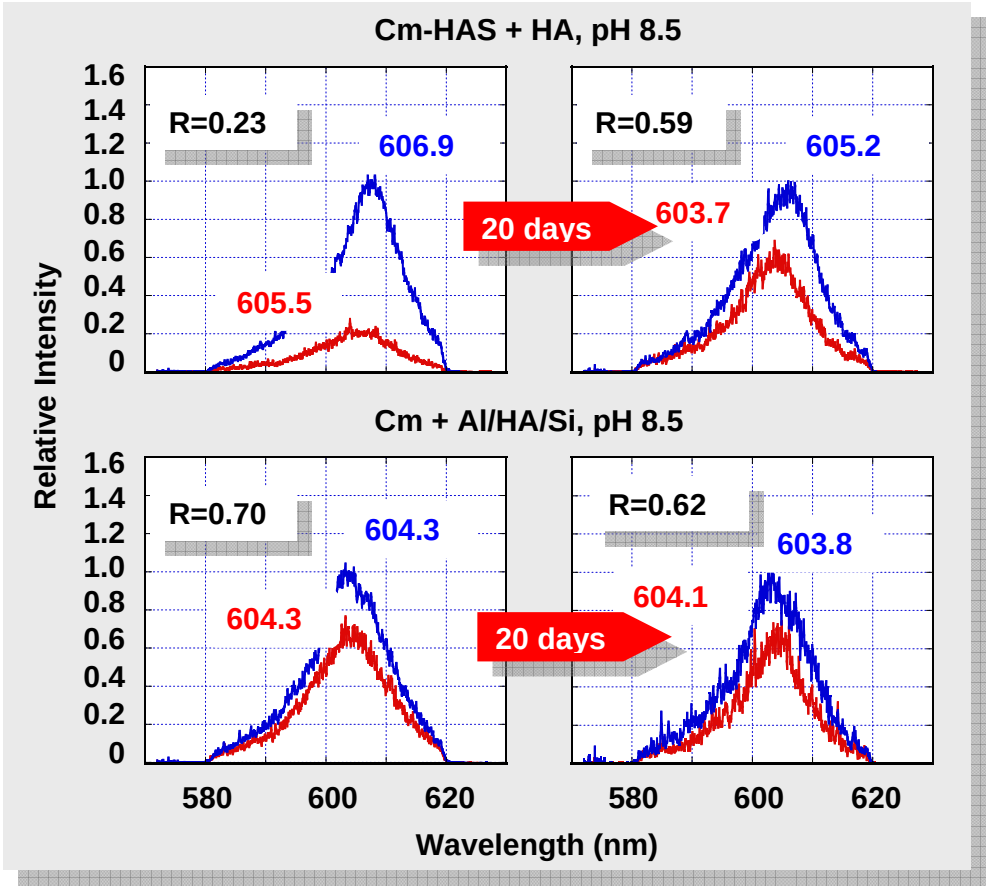

Fig. 6.5. Florescence emission spectra of Cm ($4.9x10^{-8}$ M) at direct (blue) and indirect excitation (red) immediately (left) and after 20 d (right) sample conditioning time. Upper part of figure: samples prepared by addition of HA to a Cm-HAS solution; Lower part: all reactants (Cm, Al, Si, HA) are added at the same time; R= intensity ratio [137].

Hence, immediately after sample preparation different life times are measured depending on the order of reactant addition, whereas after 20 d conditioning the values are quite close, irrespective the order of reactant addition, indicating the equilibrium to be reached.

6.2 Complexation of Al and actinide(III)/(IV)/(VI) with silicic and humic acid: comparison

A similar parameter screening experiment as described in section 6.1.1 for Am, is conducted in order to investigate formation of colloid-borne-Th (U) in presence of silicic and humic acid. Trace amounts of $5x10^{-8}$ M Th and $8x10^{-7}$ M U are introduced in the sam-

ples. Fig. 6.6 gives an overview of the colloid formation for actinides interacting with the different colloid types: HAS colloids (left side of each diagram), composite of HAS and humic colloids generated in solutions containing silicic acid, Al and HA (right side, the upper and middle contours) and humic colloids complexed with Al (right side, the lowest contours). Reference samples, containing only the actinide are also indicated (left side, lowest contours). The contours show the actinide incorporation into the colloidal phase separated by ultrafiltration.

From the contour profiles for formation of HAS-colloid borne actinides (left parts of Fig. 6.6) one can observe that Th and U colloidal fractions are abundant for the entire pH range in presence of polysilicic acid. As outlined in section 4.3, as compared with Am, Th and U have been shown to have higher affinity towards polysilicic acid. However, even in this case, Al concentration of 10^{-3} M destabilizes the HAS colloids and the actinides precipitate. In HAS solutions formed from monosilicic acid the actinde fraction in the colloids is generally poor, except for Am and Th at pH 7.8. In presence of humic acid, as illustrated by the contours on the right side of the diagram, one can observe an enhanced activity fraction in the colloidal phase. As previously discussed for Am, addition of HA converts the precipitated An-HAS to colloids. The formation of colloid-borne actinides becomes promoted for the entire pH range and Al concentration range.

In presence of humic colloids and Al but without silicic acid (the contours at the bottom of the right side diagram), formation of colloid-borne actinides is favored except for Al concentration exceeding the proton exchange capacity of HA. These conditions occur for 10^{-4}-10^{-3} M Al, for which the An/Al-humate complexes precipitate.

At addition of silicic acid we observe the incorporation patterns change (from the lowest part contours to those at the top and middle part of the diagram). Hence, formation of colloid-borne actinides is enhanced under all conditions mentioned above causing initial precipitation of actinides. Only in case of U, the presence of both HAS-monosilicic acid (10^{-3} M Si/ 10^{-5} M Al) and humic colloids appears to be less favorable for colloids formation as compared to the reaction with humate colloids. As discussed in the previous section (Fig. 5.4), in absence of HAS, U complexation with humic colloids is favorable at these HA and Al concentration. The presence of monosilicic acid, which does not favor formation of colloid-borne U, leads to a decrease of the fraction of colloid-borne U. However, as in case of Am, the results for Th and U show that the simultaneous presence of both HAS and HA enhances generally the actinide colloid fractions. As discussed in the

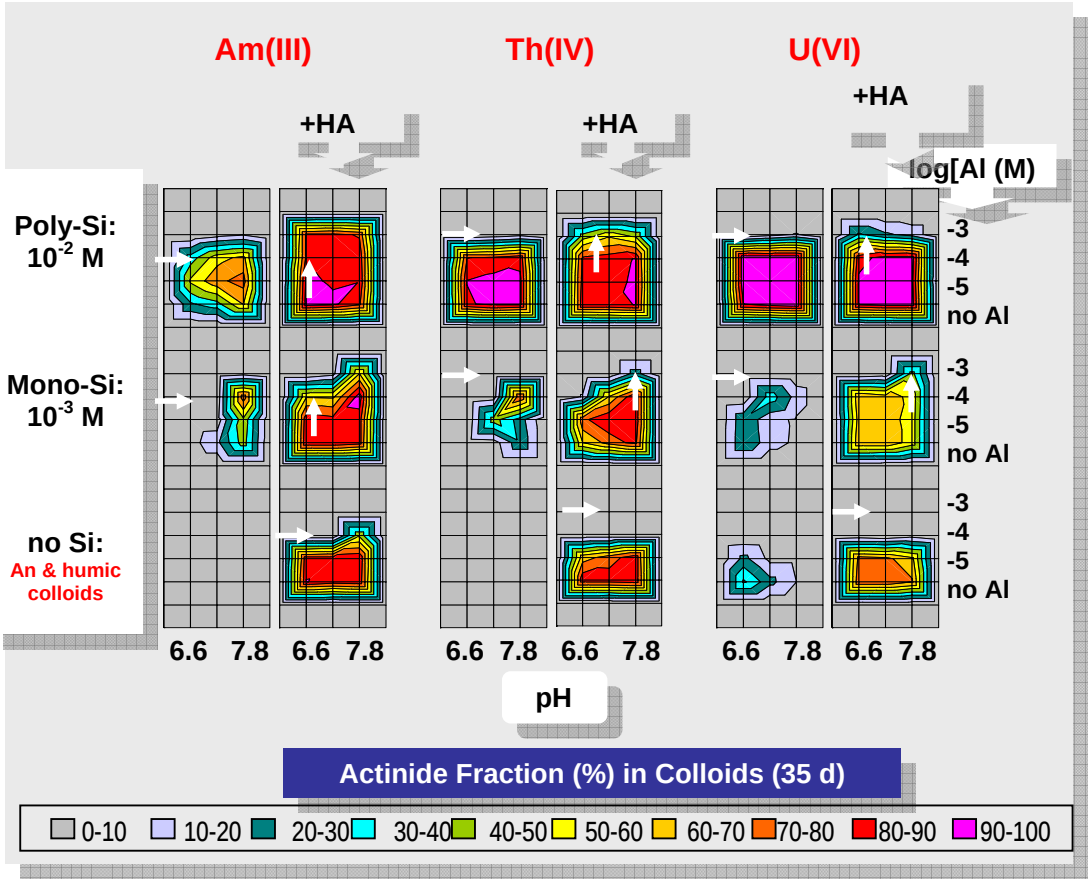

Fig. 6.6 Actinide activity fraction (%) in the colloidal phase as a function of pH after 35 days sample conditioning time, for the following samples: HAS-colloids generated from polysilicic and mononosilicic acid (left part of the graphs-top and middle contours); HAS-humic colloids (right part of the graphs-top and middle contours); humic colloids (right part of the graph-the contours at the bottom), in solutions containing only the An (left part-the contours at the bottom). Actinide concentration in the samples is $5x10^{-8}$ M Am / $5x10^{-8}$ M Th / $8x10^{-7}$ M U. HA concentration is 6.5 mg/L.

previous section, spectroscopic speciation of Cm has proved this effect to be due to a synergic formation of mixed HAS-humic colloids. Thus, the spectroscopic and radiometric results for Am support the assumption of formation of mixed colloids also in case of Th and U under the specified experimental conditions.

The behaviour of Th and U in mixed HAS/HA solutions is examined in more detail at different sequence of component addition. The abundant colloid formation in presence of polysilicic acid and 10^{-4} M Al, prevents the observation of synergic effect. Therefore, the experimental conditions are chosen so that the competing effect of silicic and humic acid can be better evidenced, namely for samples with 10^{-3} M Al. The results are

depicted in Fig. 6.7.

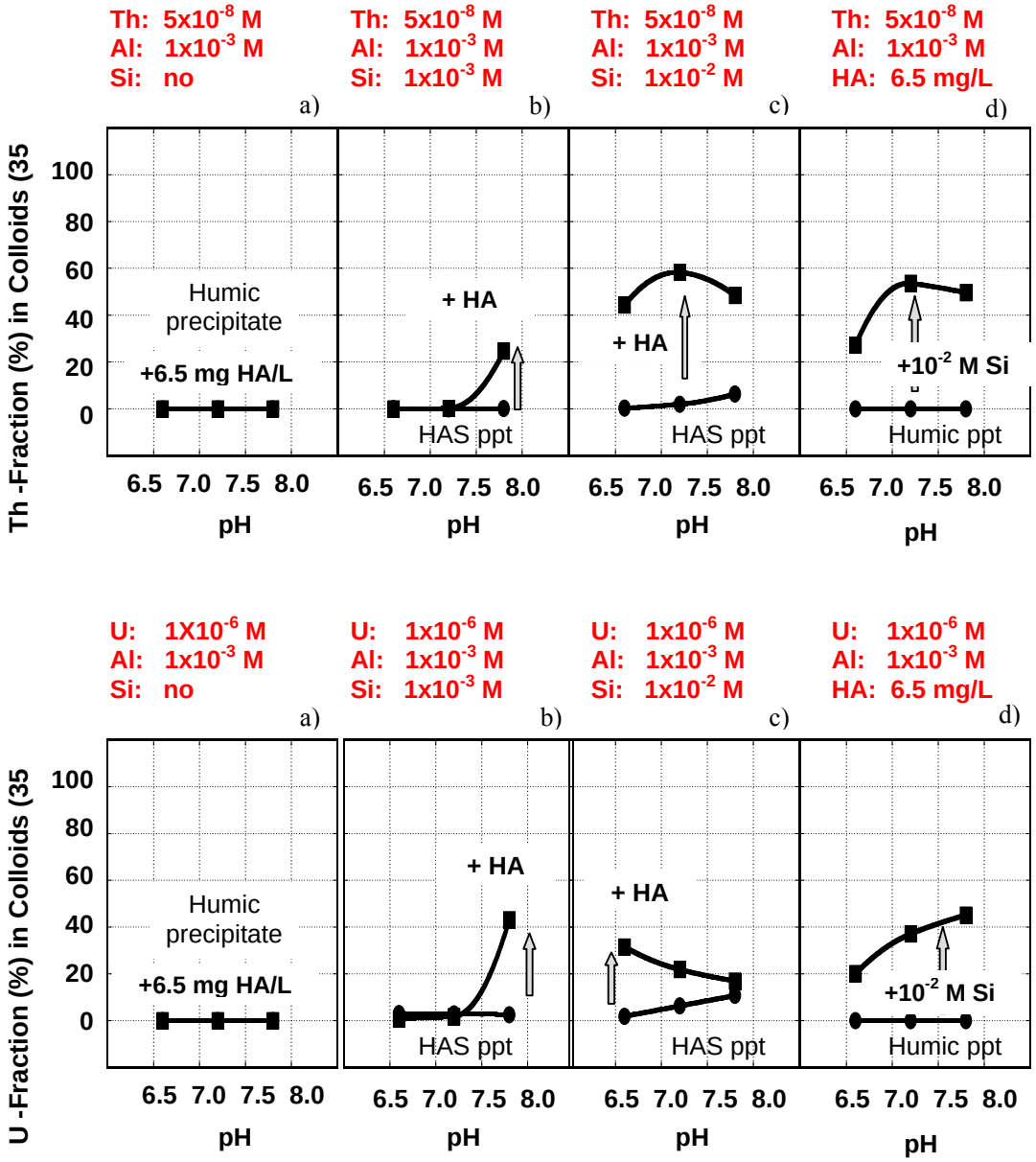

Fig. 6.7 Formation of colloid-borne Th (upper part) and U (lower part) as a function of pH after 35 d conditioning time for the following samples: a) Al (An) + HA, b) Al (An) + monosilicic acid + HA, c) Al (An) + polysilicic acid + HA, d) Al(An) + HA + polysilicic acid. Initial samples composition is indicated above each graph. HA or Si is added after 1 h conditioning time of the mother solution.

In the blank samples containing Al/Th (U) (Fig. 6.7 a) the actinides are in the precipitate phase and after addition of HA the actinides remain as humate precipitate. As discussed in section 5.2.2 (Fig. 5.5), the offered HA concentration of 6.5 mg/L is much below the required one for the formation of Al/Th(U)-humate colloids at the present Al concentration.

In HAS solutions prepared out of monosilicic acid (Fig. 6.7 b) Th(U)-HAS are precipitated. After addition of HA, the conversion of the precipitate to colloid-borne actinide species can be observed for both Th and U at pH 7.8. In HAS solutions prepared from polysilicic acid (Fig. 6.7 c), minor fractions of colloids form only at pH 7.8. HA addition enhances significantly the fraction of colloid-borne Th in the entire pH range. In case of U, the HA effect is pronounced only at pH 6.6. The results indicate the synergic action of HAS and HA at binding the actinide.

Fig. 6.7 d illustrates the results obtained for the experimental solutions having the same final composition as those described in 6.7 c but prepared by reverse sequence of reactant addition. The initial precipitated Al/Th(U)-humate are partially converted to colloids by addition of polysilcic acid. At this point a different behaviour of Th and U can be distinguished. In case of Th, as can be seen from the upper graphs of the Fig. 6.7 c and d, the increase of the colloid-borne Th fraction appears to be generally the same irrespective the sequence of reactant addition. In contrast, in case of U, the order of reactant addition appears to affect the formation of colloids at pH 7.2 and 7.8. Under these conditions, the fraction of colloid-borne U is larger at addition of polysilicic acid to the humic precipitate. This indicates that for U the equilibrium of the colloid formation is not attained within the 35 d observation time. The reason might be a slow kinetics associated to the conversion of the precipitate to the colloids.

However, in all other cases the process of actinide colloid formation appears no to be affected by the order of reactant addition and supports the hypothesis of formation of mixed HAS-humic colloid species under the present experimental conditions.

Consequently, the formation of mixed HAS-humic-colloidal Th(U), further supports the results of section 5.2.2 suggesting the formation under the selected experimental conditions of partially hydrolyzed Th(U) species, interacting with both HAS and HA.

6.3 Colloid stability and average particle size

The mixed HAS-humic colloids have been analyzed by LIBD [136] for monitoring their average size and number density as a function of time. HAS colloids are generated with or without addition of Eu in a solution containing $1x10^{-4}$ M Al, $1x10^{-2}$ M Si and 8 mg/L HA at pH 8.5, following the conditions applied for generating composite colloids as proved by TRLFS. The average size of the predominant colloids is found to be of approximately 20 nm immediately after generation, either with or without Eu. After 10 days colloids become dispersed somewhat as the average size decreased slightly to about 10 nm which remains nearly consistent up to 58 days. According to these results, trivalent actinides incorporated into such composed colloids are expected to remain stable in aquifer system.

6.4 Conclusions

The simultaneous presence of HA and HAS is found to enlarge the region of colloids stability. The observed fact can be ascribed to different and complementary mechanisms of HAS and HA for binding the An. The type of the colloid-borne An species which forms is determined by the An hydrolysis behaviour. Accordingly, An can be incorporated into HAS colloids of aluminosilicate composition via co-nucleation of hydrolyzed species (Al, An and Si) or bound to humic colloids made of humic acid via complexation with the ionic species metal/An. Eventually, partially-hydrolyzed metal(An) ion species can be simultaneously bound to HAS-humic colloids through synergic bond coupling with humic molecules and HAS colloids. Nevertheless the equilibrium between the non-hydrolyzed ionic and hydrolyzed actinide species, determining which kind of colloid-borne species forms is finally governed by the specific conditions, i.e. the oxidation state of the An and its concentration together with the environmental characteristics (e.g. pH). The synergic colloid effect is mostly pronounced if the conditions of pH, concentration of Al, An and humic acid are such that Al is fully hydrolyzed, whereas the An becomes partially hydrolyzed, thus conucleating with Si and Al (HAS colloids) on the one side and complexing with humic colloids on the other side. A schematic illustration for the proposed behaviour of An at the interaction with HAS and humic colloids is shown in Fig. 6.8.

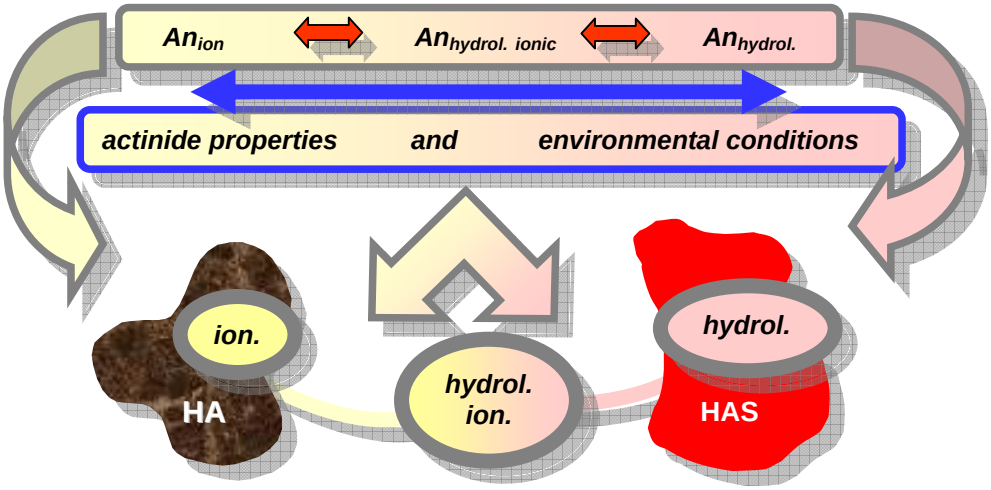

Fig. 6.8 Schematic illustration of expected (proposed) behaviour of An in an aquatic environment containing both HAS and HA.

7. Conclusions

The formation and stability of the HAS-colloid-borne actinides is maximum at neutral and slightly alkaline pH in the presence of polysilicic acid. Under these conditions, the tendency for the co-nucleation with the HAS is higher for the more hydrolyzed actinides ions.

The formation of humate-colloid-borne actinide species is very efficient for trace amount of actinides species in the neutral pH range and at HA concentration at the average level encountered in natural waters. In contrast to the case of HAS colloids, the generation of humate-colloid-borne actinide species is distinctively favored for the non-hydrolyzed ionic species.

In the presence of both HAS and HA colloids, the stability region of the actinide colloid-borne species is enlarged as far as the pH and the concentration range of Al and Si are concerned. This enhanced stability is due to the formation of mixed HAS-humic colloids leading to a synergic effect in binding the actinides. Such synergic effects can be explained by the different but complementary mechanisms of interaction between the actinide with HAS and HA colloids.

As the actinides exist mainly as hydrolyzed cationic species under the relevant conditions encountered in natural waters, the formation of stable mixed HAS-humic colloid-borne actinide species is therefore expected in case of waters containing both HAS and HA. Since in natural waters HAS and humic colloids are always present to some extent as representative for inorganic and organic colloids, in natural aquatic systems the actinides will play an important role as colloid-borne species, with high potential for migration in geosphere.

Apart from trying an approach to the complex natural conditions, the study provides also a better understanding of the underlying mechanisms of aquatic actinide colloids formation.

8. Appendix

Figures

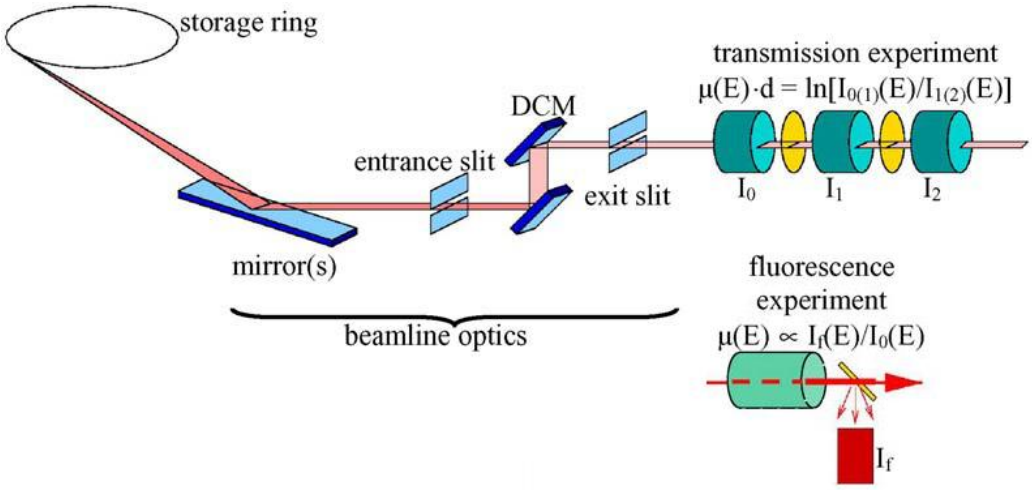

Fig. 8.1 Sketch of a generic X-ray absorption experiment using synchrotron radiation and standard transmission geometry. Inserted: schematic representation of fluorescence detection mode [83].

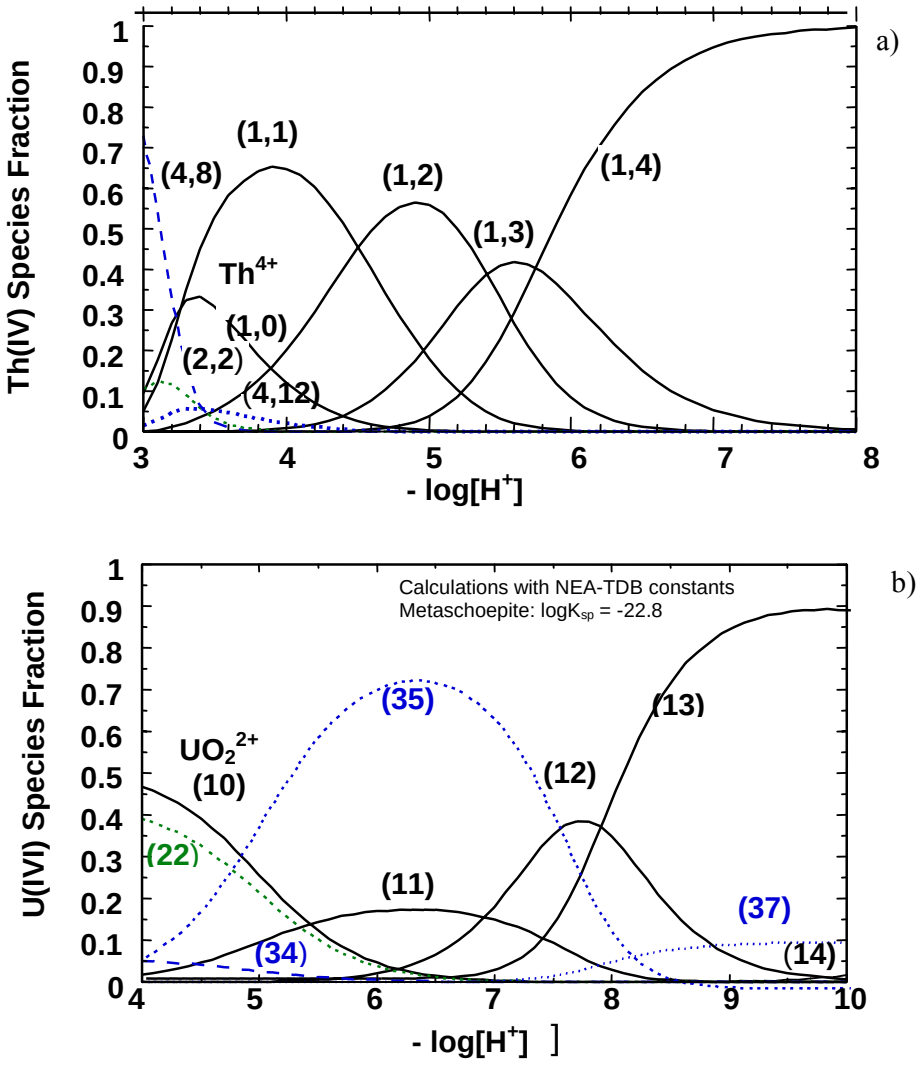

Fig. 8.2 Distribution of solution species at 25°C in carbonate-free solution for: a): Th(IV) in a saturated solution of 0.5 M $NaClO_4$: (x,y)=$Th_x(OH)_y^{4x-y}$ and b): $(UO_2)_x(OH)_y^{2x-y}$ species in a 0.1 M $NaClO_4$ solution saturated relative to the metaschoepite [92].

Tables

Table 8.1 Literature data regarding the stability constants for the complexation of EDTA with different cations, at 25^0C and 0.1 M ionic strength.

Reaction	Log K
$EDTA^{4-} + H^+ = HEDTA^{3-}$	10.23 [126]
$EDTA^{4-} + 2H^+ = H_2\ EDTA^{2-}$	16.36
$EDTA^{4-} + 3H^+ = H_3EDTA^-$	19.05
$EDTA^{4-} + 4H^+ = EDTA^{4-}$	21.05
$Al^{3+} + EDTA^{4-} = AlEDTA^-$	16.5
$Al^{3+} + H_2O + EDTA^{4-} = AlOHEDTA^{2-} + H^+$	10.67
$Am^{3+} + EDTA^{4-} = AmEDTA^-$	17 [127]
$UO_2^{2+} + EDTA^{4-} = (UO_2)EDTA^{2-}$	13.0 [128]
$UO_2^{2+} + H_2O + EDTA^{4-} = (UO_2)(OH)EDTA^{3-} + H^+$	5.9 [128]
$Th^{4+} + EDTA^{4-} = ThEDTA$	23.2 [129]

Table 8.2 Distribution of Th activity fraction (%) normalized to the input activity between the precipitate, colloids and solution as a function of EDTA contact time. Samples with initial composition of $8x10^{-6}$ M Th in 0.03 M NaCl at pH 5, 7 and 9 are conditioned for 1 day before EDTA ($1x10^{-3}$ M) addition.

Time (days)	pH 5			pH 7			pH 9		
	Precipit.	Coll.	Solut.	Precipit.	Coll.	Solut.	Precipit.	Coll.	Solut.
0.14	33	0.2	66	9.0	5.0	86	65	20	15
1.91	15	0.5	84	4.8	2.4	93	3.9	2.8	93
5.94	13	1.5	86	5.1	2.5	92	2.6	1.2	96
19.9	11	0.9	88	4.2	2.8	95	2.1	2.8	95
40.9	9.5	0.8	90	4.4	1.0	95	2.5	0.6	97

Table 8.3 U activity fraction (%) normalized to the input activity in the precipitate, colloids and solution as a function of EDTA contact time. Samples with initial composition of $8x10^{-6}$ M Th in 0.03 M NaCl at pH 5 and 9 are conditioned for 1 day before EDTA ($1x10^{-3}$ M) addition.

Time (days)	pH 5			pH 9		
	Precipit.	Colloids	Solution	Precipit.	Colloids	Solution
0.08	2.2	3.9	94	3.2	27	70
1.08	2.8	3.1	94	3.3	8.3	88
9.0	4.3	0.2	96	21	2.8	76
15.1	4.4	0.8	95	24	7.8	69
41.2	4.2	0.7	95	26	5.1	69

Table 8.4 Am activity fraction (%) normalized to the input activity, in the precipitate, colloids and solution as a function of EDTA contact time. The samples with initial composition ($8x10^{-6}$ M Am, $1.5x10^{-4}$ M Al and $1.3x10^{-2}$ M Si, at pH 7 and 9) are conditioned for 1 day before addition of EDTA ($1x10^{-3}$ M). Time 0 marks the moment before EDTA addition.

Time (days)	pH 7			pH 9		
	Precipit.	Colloids	Solution	Precipit.	Colloids	Solution
0	8.6	90	1.1	2.5	96	1.9
0.14	7.5	37	56	3.1	63	34
1.14	7.2	16	77	3.4	32	65
1.90	7.4	11	82	3.1	23	74
2.90	7.9	8.4	84	4.1	15	81
6.80	8.9	5.3	86	2.9	11	86
9.90	9.0	3.9	87	2.5	7.3	90
16.1	8.2	3.3	89	2.8	4.6	93
22.9	8.2	2.8	89	2.6	3.7	94
29.9	7.8	2.4	90	2.6	2.7	95

Table 8.5 Th activity fraction (%) normalized to the input activity, in the precipitate, colloids and solution as a function of EDTA contact time. The samples with initial composition ($8x10^{-6}$ M Th, $1.5x10^{-4}$ M Al and $1.3x10^{-2}$ M Si, at pH 7 and 9) are conditioned for 1 day before addition of EDTA with final concentration $1x10^{-3}$ M. Time 0 marks the moment before EDTA addition.

Time (days)	pH 7			pH 9		
	Precipit.	Colloids	Solution	Precipit.	Colloids	Solution
0	0.3	58	42	2.5	80	17
0.16	0.6	60	40	4.5	80	15
0.95	0.4	61	38	2.3	87	8.7
1.95	1.0	62	37	4.3	88	6.1
4.90	1.2	61	38	5.3	92	4.1
8.90	0.5	62	37	4.4	93	3.3
15.1	0.8	65	34	3.5	93	3.2
22.0	0.3	68	31	3.4	94	3.0
29.0	0.4	69	31	2.8	94	3.4

Table 8.6 U activity fraction (%) normalized to the input activity in the precipitate, colloids and solution as a function of EDTA contact time. The samples with initial composition ($8x10^{-6}$ M U, $1.5x10^{-4}$ M Al and $1.3x10^{-2}$ M Si, at pH 7 and 9) are conditioned for 1 day before addition of EDTA ($1x10^{-3}$ M). Time 0 marks the moment before EDTA addition.

Time (days)	pH 7			pH 9		
	Precipit.	Colloids	Solution	Precipit.	Colloids	Solution
0	2.9	97	0.9	1.5	97	1.6
0.15	2.5	95	2.7	2.0	96	1.8
1.14	2.3	96	2.5	2.0	97	1.5
1.90	1.1	96	2.5	1.1	98	1.4
6.0	2.8	95	2.4	1.6	97	1.3
9.9	1.6	96	2.2	0.5	98	1.9
16.1	1.7	96	2.3	1.5	97	1.2
23.0	1.3	96	2.2	0.6	98	1.2
30.0	1.3	96	2.5	0.8	98	1.4

Table 8.7 Am activity fraction (%) normalized to the input activity in the precipitate, colloids and solution as a function of EDTA contact time. Initial samples composition: $8x10^{-6}$ M (Am+Eu) spiked to 7 days aged HAS ($1.5x10^{-4}$ M Al and $1.3x10^{-2}$ M Si, at pH 5, 7 and 9). EDTA ($1x10^{-3}$ M final) addition after 5 days conditioning time of the HAS solution with Am. Time 0 marks the moment before EDTA addition.

Time (days)	pH 5			pH 7			pH 9		
	Precipit.	Coll.	Solut.	Precipit.	Coll.	Solut.	Precipit.	Coll.	Solut.
0	7.9	21	72	12	78	9.8	5.5	95	0.1
0.17	6.7	0.7	93	8.0	1.2	91	4.8	71	24
1.9	5.5	0.8	94	7.1	2.7	90	4.9	29	66
3.1	6.7	1.0	92	8.0	2.0	90	5.8	20	74
6.0	6.6	0.9	93	7.3	2.0	91	5.6	11	83
7.9	6.9	1.3	92	8.9	1.3	90	6.2	9.0	85
9.9	7.7	0.9	92	9.0	0.9	91	6.6	6.1	87
15.0	9.0	0.3	91	11	0.4	89	7.5	4.3	88
24.0	9.5	0.7	90	11	0.6	89	7.2	4.0	89
30.0	10	0.1	90	13	0.0	88	7.8	4.2	88

Table 8.8 Th activity fraction(%) normalized to the input activity, in the precipitate, colloids and solution as a function of EDTA contact time. Initial samples composition: $8x10^{-6}$ M Th spiked to 7 days aged HAS ($1.5x10^{-4}$ M Al and $1.3x10^{-2}$ M Si, at pH 5, 7 and 9). EDTA ($1x10^{-3}$ M final) addition after 5 days conditioning time of the HAS solution with Th. Time 0 marks the moment before EDTA addition.

Time (days)	pH 5			pH 7			pH 9		
	Precipit.	Coll.	Solut.	Precipit.	Coll.	Solut.	Precipit.	Coll.	Solut.
0	4.4	96	0.1	3.3	97	0	1.1	92	6.7
0.07	2.8	20	78	3.5	94	2.6	1.1	91	8.0
0.66	2.5	18	79	2.5	95	3.0	0.4	91	8.5
3.78	1.9	22	76	3.0	94	3.3	1.3	91	8.0
9.7	3.3	27	69	2.6	94	3.4	9.5	88	11
16.8	1.4	35	64	2.4	94	3.4	0.7	91	8.5
23.0	1.8	39	59	3.6	92	3.8	1.1	89	9.0
31.0	1.9	42	57	2.4	93	3.8	0.3	91	8.9

Table 8.9 Distribution of U activity fraction (%) normalized to the input activity between the precipitate, colloids and solution as a function of EDTA contact time. Initial samples composition: $8x10^{-6}$ M U spiked to 7 days aged HAS ($1.5x10^{-4}$ M Al and $1.3x10^{-2}$ M Si, at pH 5, 7 and 9). EDTA ($1x10^{-3}$ M final) addition after 5 days conditioning time of the HAS solution with U. Time 0 marks the moment before EDTA addition.

Time (days)	pH 5			pH 7			pH 9		
	Precipit.	Coll.	Solut.	Precipit.	Coll.	Solut.	Precipit.	Coll.	Solut.
0	3.1	84	13	2.2	96	0.4	3.7	96	0.4
0.08	0.6	14	86	1.3	95	3.3	3.3	96	1.1
0.70	1.5	15	84	1.3	95	4.1	3.8	95	1.1
3.80	1.4	19	80	1.5	94	4.1	3.5	95	1.2
6.70	1.4	24	75	2.2	94	4.0	3.7	95	1.2
13.7	0.1	32	68	2.7	94	3.6	4.0	95	1.2
16.7	1.2	34	65	1.7	95	3.6	3.8	95	1.2
23.0	1.3	37	62	1.4	95	3.5	3.4	95	1.2
30.0	1.2	40	59	1.9	64	3.7	3.3	95	1.3

Nomenclature

AFM	Atomic Force Microscopy
An	Actinide
Da	Dalton
DLVO theory	Derjaguin-Landau-Verwey-Overback theory
d	day
E	photon energy
E_0	ionization energy
EDTA	Ethylenediamine tetraacetic acid
EDX	Energy dispersive X-ray
E_h	Redox potential
EXAFS	Extended X-ray absorption fine structure
FT	Fourier transform
g	gravitational accelaration
h	hour
HA	Humic acid
HAS	Hydroxyaluminosilicate
HS	Humic substances
I_0, I	Intensity of incident and transmitted light
IEP	Isoelectric point
IIIF	Institut für Interdisziplinäre Isotopen Forschung
INE	Institut für Nukleare Entsorgung
k	photoelectron wave number
LC	Loading capacity
LIBD	Laser Induced Breakdown Detection

LSC	Liquid Scintillation Counting
MOPS	3-[N-morpholino] propanesulfonic acid
MS	multiple scattering
Nd:YAG-Laser	Solid corp laser with Nd-dotted Ytrium-Aluminium-Granat Wirtskristall ($Y_3Al_5O_{12}$)
N	coordination number
PEC	proton exchange capacity
ppb	parts per billion (10^{-9}g/g)
ppm	parts per million (10^{-6}g/g)
ppt	parts per trillion (10^{-12} g/g)
pH_{pzc}	pH value (-log[H^+]) at zero surface charge
PCS	photon correlation spectroscopy
R	interatomic distance
S	supersaturation
SEM	scanning electron microscopy
SPC	single particle counting
SS	single scattering
TEM	transmitted electron microscopy
TRLFS	time resolved laser fluorescence spectroscopy
UV-VIS	Ultraviolet-Visible domain of light
V	molecular volume
XANES	X-ray absorbtion near edge structure
z	ionic charge
y	year

Greek symbols

Å	Ångstrøm; 1 Å = 10^{-10} m
λ	wavelength
λ(k)	photoelectron mean free path
μ	absorption coefficient
μ_0	absorption coefficient of an isolated atom
σ^2	mean square average displacement (Debye-Waller factor)
χ(k)	EXAFS function
Φ(k, R)	total phase shift

9. Figures captions:

Fig. 4.6 Polymerization kinetics of monosilicic acid.

Fig. 4.7 Actinide activity fraction in the colloidal phase as a function of actinide concentration at different pH for different samples: blank, HAS- monosilicic acid colloids and HAS-polysilicic acid colloids.

Fig. 4.8 a): Am activity fraction in the colloidal phase in HAS or blank samples; b):Cm(III) species distribution in HAS-polysilicic acid solution by TRLFS.

Fig. 4.9 Illustration of colloid-borne Cm species forming in HAS solutions depending on the experimental conditions.

Fig. 4.10 Th L_{III} edge k^3-weighted EXAFS spectra and the corresponding FTs for Th in: a) and b) aluminosilicate solution and c) in silicate solution

Fig. 4.11 Th L_{III} edge k^3-weighted EXAFS spectra and the corresponding FT for Th precipitated with $Al(OH)_3$.

Fig. 4.12 Np L_{III} edge k^3-weighted EXAFS spectra and the corresponding FT for Np in HAS solution of pH 12.

Fig. 4.13 U L_{III} edge k^2-weighted EXAFS spectra and the corresponding FTs for U in HAS and silicate solution of pH 8.5.

Fig. 4.14 FTs of the actinide L_{III} edge k^n-weighted EXAFS spectra (overview) and the EXAFS derived structural parameters for Eu, Th, Np and U in HAS solutions.

Fig. 4.15 a) Cm species distribution as a function of pH upon decreasing pH of a HAS – polysilicic acid mother solution from 9 to 2; b) Fraction of Cm-HAS(III) species as a function of time at different pH values; c) Fraction of Al remaining in the HAS-polysilicic acid colloids upon decreasing the solution pH.

Fig. 4.16 Activity fraction of Am, Th and U in the colloidal phase as a function of time upon contact of the HAS-polysilicic acid solution of pH 9 with EDTA.

Fig. 4.17 Fraction of Al remaining in the HAS colloids as a function of contact time with EDTA. a), b): HAS solutions prepared from polysilicic acid at pH 5 and 9; c), d): HAS solutions prepared from monosilicic acid at pH 5 and 9.

Fig. 4.18 Activity fraction of Am, Th and U in the colloidal phase as a function of time upon contact of the 7 days aged HAS mother solutions of pH 5, 7 and 9 with EDTA.

Fig. 5.1 Partition of [^{14}C]-HA between the precipitate, colloids and solution as function of pH.

Fig. 5.2 Partition of [^{14}C]-HA between the precipitate, colloids and solution as function of the HA concentration in presence of 10^{-5} M Al at pH 6.6.

10. References

[1] Stumm, W and Morgan, J., Aquatic Chemistry, John Wiley & Sons, New York, 1981.

[2] Degueldre, C., Grauer, M., Laube, A., Oess, A., Silby, H., Appl. Geochem. 11 (1996) 697.

[3] Kim, J.I., Mater. Res. Soc. Symp. Proc. 294 (1993) 3.

[4] Duan, J., Gregory, J., Colloids Surf. A: Physicochem. Eng. Aspects 107 (1996) 309.

[5] Degueldre, C., Triay, I., Kim, J.I., Vilks, P., Laaksoharju, M., Miekeley, N., Appl. Geochem. 15 (2000) 1043.

[6] Kim, J.I, Rhee, D.S., Buckau, G., Morgenstern, A., Radiochim. Acta 79 (1997) 173.

[7] Kim, J.I, Zeh, P., Delakowitz, B., Radiochim. Acta 58/59 (1992) 147.

[8] Runde, W., Los Alamos Science 26 (2000) 412.

[9] Kim, J.I, Radiochim. Acta 52/52 (1991) 71.

[10] Kim, J. I., MRS Bulletin, December 1994, 47.

[11] Kim, J.I., Nucl. Eng. Des. 202 (2000) 143.

[12] McCarthy, J.F., McKay, L.D., Vadose Zone Journal 3 (2004) 326.

[13] Kersting, A.B., Efurd, D. W., Finnegan, D. L., Rokop, D. J., Smith, D. K.Thompson, J.L., Nature 397 (1999) 56.

[14] Litaor, M.I., Health Physics 76 (1999) 171.

[15] Stumpf, Th., Bauer, A., Coppin, F., Environ. Sci. Technol. 35 (2001) 3691.

[16] Rabung, Th., Stumpf, Th., Geckeis, H., Klenze, R., Kim, J.I., Radiochim. Acta 88 (2000) 711.

[17] Geckeis, H., Klenze, R., Kim, J.I., Radiochim. Acta 87 (1999) 13.

[18] Artinger, R., Schüßler, W., Schäfer, T., Kim, J.I., Environ. Sci. Technol. 36 (2002) 4358.

[19] Artinger, R., Rabung, Th., Kim, J.I., Sachs, S., Schmeide, K., Heise, K.H., Bernhard, G., Nitsche, H., J. Contam. Hydrol. 58 (2002) 1.

[20] Moulin, V. and Moulin, Ch., Radiochim. Acta 89 (2001) 773.

[21] Geckeis, H., Rabung, Th., Ngo Manh, T., Kim, J.I., Beck, H.P., Environ. Sci. Technol. 36 (2002) 2946.

[22] Doucet, F., Schneider, C., Bones, S. J., Kretchmer, A., Moss, I., Tekely, P., Exley, Ch., Geochim. Cosmochim. Acta 65(15) (2001) 2461.

[23] Doucet, F., Rotov, M., Exley, Ch., J. Inorg. Biochem. 87 (2001) 71.

[24] Swaddle, Th., Coord. Chem. Rev. 219-221 (2001) 665.

[25] Kim, M.A., Panak, P.J., Yun, J.I., Kim, J.I., Priemyshev, A., Köhler, K., Abschlussbericht, RCM 012004.

[26] Kim, M.A., Panak, P.J., Yun, J.I., Kim, J.I., Klenze, R., Köhler, K., Coll. Surf. A: Physiochem. Eng. Aspects 216 (2003) 97.

[27] Kim, M.A., Panak, P.J., Yun, J.I., Priemyshev, J.I., Kim., Coll. Surf. A: Physiochem. Eng. Aspects 254 (2005) 137.

[28] Panak, P. J., Kim, M.A., Yun, J.I., Kim, J.I, Fanghänel, Th., Radiochim. Acta 93 (2005) 133.

[29] Jones, M.N., Bryan, N.D., Advances in Colloid and Interf. Sci. 78 (1998) 48.

[30] Silva, R.J. and Nitsche, H., Radiochim. Acta 70/71 (1995) 377.

[31] Choppin, G., Liljenzin, J-O., Rydberg, J., Radiochemistry and Nuclear Chemistry, Butterworth Heinemann, USA, 2002.

[32] Shaw, D. J., Introduction to Colloid and Surface Chemistry, Butterworth, London, 1970.

[33] Stumpf, Th., Henning, C., Bauer, A., Denecke, M.A., Fanghänel, Th., Radiochim. Acta 92 (2004) 133.

[34] Farmer, V.C., Adams, M.J., Fraser, A.R., Palmieri, F., Clay Miner. 18 (1983) 459.

[35] Arai, Y., McBeath, M., Bargar, J.R., Joye, J., Davis, J.A., Geochim. Cosmochim. Acta 70 (2006) 2492.

[36] North, M., and Swaddle, Th., Inorg. Chem. 39 (2000) 2661.

[37] Taylor, P., Jugdaohsingh, R., Powell, J. J., J. Am. Chem. Soc. 119 (1997) 8852.

[38] Iler, R.K., The chemistry of silica. Solubility, polymerization, colloid and surface properties and biochemistry. J.W. Sons, Wiley-Interscience, 1979.

[39] Dietzel, M., Geochim. Cosmochim. Acta 64 (19) (2000) 3275.

[40] Kim, J.I., Grambow, B. Eng. Geol. 52 (1999) 221.

[41] Hur, J., Schlautman, M.A., J. Colloid Interf. Sci. 264 (2003) 313.

[42] Buckau, G. FZKA-Report 6969, Forschungszentrum Karlsruhe, 2004.

[43] Kerner, M., Hohenberg, H., Ertl, S., Reckermann, M., Spitzy, A., Nature 422 (2003) 150.

[44] Beckett, R., Zhang, J., Giddings, J., Environ. Sci. Technol. 21 (1987) 289.

[45] Sutton, R., and Sposito, G., Environ. Sci. Technol. 39/23 (2005) 9009.

[46] Zeh, P., Czerwinski, K. R., Kim, J.I., Radiochim. Acta 76 (1997) 37.

[47] Van De Weerd, H., Van Riemsdijk, W.H., Leijnse, A., Environ. Sci. Technol. 33 (1999) 1675.

[48] Zeh, P. Ph.D Thesis. Institut für Radiochemie der Technischen Universität München, 1993.

[49] Labonne-Wall, N., Moulin, V., Vilarem, J.P., Radiochim. Acta 79 (1997) 37.

[50] Rothe, J., Plaschke, M., Denecke, M.A., J. Phys. IV France 104 (2003) 421.

[51] Marquardt, C.M., FZKA-Report 6999, Forschungszentrum Karlsruhe, 2004

[52] Sutheimer, S.H., Cabaniss, S.E., Geochim. Cosmochim. Acta 61(1) (1997) 1.

[53] Fairhurst, A., Warwick, P., Richardson, S., Colloids Surf. A: Physicochem. Eng. Aspects 99 (1995) 187.

[54] Heidmann, I., Christl., I., Kretzschmar, R., Environ. Sci. Technol. 39 (2005) 807.

[55] Righetto, L., Bidoglio, G., Azimonti, G., Bellobone, I.R., Environ. Sci. Tchnol. 25 (11) (1991) 1913.

[56] Righetto, L., Bidoglio, G., Marcandalli, B., Bellobone, I.R., Radiochim. Acta 44/45 (1988) 73.

[57] Bouby, M., Ngo Manh, T., Geckeis, H., Scherbaum, F., Kim, J.I., Radiochim. Acta 90 (2002) 727.

[58] Stevenson, F.J., Humus Chemistry, Wiley, New York, 1982.

[59] Mansel, A., to be published.

[60] Klenze, R., Fanghänel, Th., Langzeitsicherheit der Endlagerung: Aquatische Chemie der Actiniden, Nachrichten aus der Chemie 53 (2005) 1004.

[61] Fanghänel, Th., Pure Appl. Chem. 74 (10) (2002) 1895.

[62] Yun, J.I., Kim, M.A., Panak, P.J., Kim, J.I., Fanghänel, Th. J. Phys. Chem. B 110 (2006) 5416.

[63] Nagasaki, S., Tanaka, S., Suzuki, A., Colloids Surf. A: Physicochem. Eng. Aspects 155 (1999) 137.

[64] Wang, X., Zhou, X., Du, J., Hu, W., Chen, Ch., Chen, Y., Surface Science 600 (2006) 478.

[65] Panak, P.J., Klenze, R., Kim, J.I., Radiochim. Acta 74 (1996) 141.

[66] Morgenstern, M., Klenze, R., Kim, J.I., Radiochim. Acta 88 (2000) 7.

[67] Kim, J.I., Czerwinski, K.R., Radiochim. Acta 73 (1996) 5.

[68] Singhal, R.K., J., Radioanal. Nucl. Chem. 265(3) (2005) 405.

[69] Murphy, R.J., Lenhart, J., Honeyman, D., Colloids Surf. A: Physicochem. Eng. Aspects 157 (1999) 47.

[70] Quigley, M., Santschi, P.H., Guo, L., Honeymann, B.D., Marine Chemistry 76 (2001) 27.

[71] Marquardt, C., Kim, J.I., Radiochim. Acta 80 (1998) 129.

[72] Seibert, A., Mansel, A., Marquardt, C.M., Keller, H., Kratz, J.V., Trautman, V., Radiochim. Acta 89 (2001) 505.

[73] Rao, L., Choppin, G., Clark, S.B., Radiochim. Acta 66/67 (1994) 141.

[74] Reiller, P., Moulin, V., Casanova, F., Dautel, Ch., Radiochim. Acta 91 (2003) 513.

[75] Reiller, P., Moulin, V., Casanova, F., Dautel, Ch., Appl. Geochem. 17 (2002) 1551.

[76] Scherbaum, F.J., Knopp, R., Kim, J.I., Appl. Phys. B 63 (1996) 299.

[77] Passo, C.J, Cook, G. Handbook of Environmental Liquid Scintillation Spectrometry. Packard Instrument Company, USA 1995.

[78] Panak, P, Klenze, R., Kim, J.I., Wimmer, H., J. Alloys Compd. 225 (1995) 261.

[79] Kim, J.I., Klenze, R., Wimmer, H. J. Solid State Inorg. Chem. 28 (1991) 347.

[80] Fanghänel, Th., Kim, J.I., J. Alloys. Compd. 271-273 (1998) 728.

[81] Kitamura, A., Yamamura, T., Hase, H., Yamamoto, T**.,** Radiochim. Acta 82 (1998) 147.

[82] Monsalier, J., Choppin, G.R., Radiochim. Acta 91 (2003) 135.

[83] Denecke, M.A., Coord. Chem. Rev. 250 (2006) 730.

[84] Vlaic, G, Olivi, L., Croatica Chemica Acta CCACAA 77 (3) (2004) 427.

[85] Newville, M. Fundamentals of EXAFS, An internet tutorial, 2004.

[86] EXAFS: material available at www.p-g.si/~arcon/xas/exafs/exafs.htm.

[87] Walther, C., Colloids Surf. A: Physicochem. Eng. Aspects 217 (2003) 81.

[88] Kim, M.A., RCM-Report 2006, in preparation.

[89] Denecke, M.A., Physika Scripta XX (2006).

[90] Hudson, E.A., Allen, P.G., Terminello, L.J., Physical Review B, 54 (1) (1996) 156.

[91] Neck, V., Runde, W, Kim, J.I., Kanellakopoulos, B., Radiochim. Acta 65 (1994) 29.

[92] Guillaumont, R., Fanghänel, Th., Fuger, J., Grenthe, I., Neck, W., Palmer, D.A., Rand, M.H. OECD-NEA TDB, Update on the chemical thermodynamics of Uranium, Neptunium, Plutonium, Americium and Technetium, Elsevier, 2003.

[93] Meinrath, G., Kato, Y., Kimura, T., Yoshida, Z., Radiochim. Acta 75 (1996) 159.

[94] Prikryl, J.D., Jain, A., Turner, D.R., Pabalan, R. T. J., Contam. Hydrol. 47 (2001) 241.

[95] Gabriel, U., Charlet, L., Schläpfer, C.W., Vial, C.V., Brachmann, A., Geipel, G.J., Colloid Interf. Sci. 239 (2001) 358.

[96] Geipel, G., Coord. Chem. Rev. 250 (2006) 844.

[97] Panak, P. J., Kim, M.A., Yun, J.I., Kim, J.I., Colloids Surf. A: Physiochem. Eng. Aspects 227 (2003) 93.

[98] P.J. Panak, P. Loiseau, P., K. Dardenne, J. Rothe, M.A. Denecke, R. Klenze, M.A. Kim, J.I. Kim, Th. Fanghänel, ANKA/FZK Annual Report 2003, 51.

[99] Farges, F., Geochimica et Cosmochimica Acta 11(55) (1991) 3303.

[100] Oesthols, E., Manceau, A., Farges, F., Charlet, L. J., Coll. Interf. Sci. 194 (1997) 10.

[101] Dähn, R., Scheidegger, A. M., Manceau, A., Baeyens, B., Bradbury, M.H. Proceedings of the 1-st ACTINIDE-XAS-2000 Workshop on Speciation, Technologies and Facilities of Radioactive Materials at Synchrotron Light Sources, Grenoble, France, 2000, 75.

[102] Petit-Maire, D., Petiau, J., Calas, G., Jacquet-Francillon, M., Physica B 158 (1989) 56.

[103] Brown, J.E. Jr., Farges, F., Bargar, J.R., Thompson Berbeco, H. Proceedings of the 1-st ACTINIDE-XAS-2000 Workshop on Speciation, Technologies and Facilities of Radioactive Materials at Synchrotron Light Sources, Grenoble, France, 2000, 15.

[104] Hennig, C., Reich, T., Dähn, R., Scheidegger, A.M., Radiochim. Acta 90 (2002) 653.

[105] Rai, D., Yui, M., Hess, N., Felmy, A.R., Moore, D.A., Radiochim. Acta 93 (2005) 443.

[106] Rothe, J., Denecke, M.A., Neck, W., Müller, R. Kim, J.I., Inorg. Chem. 41 (2002) 249.

[107] Denecke, M.A., Rothe, J., Dardenne, K., Lindquist-Reis, P., Phys. Chem. Chem. Phys. 5 (2003) 939.

[108] Giaquinta, D.M., Soderholm, L., Yuchs, S.E., Wasserman, S.R., J., Alloys Compd**.** 249 (1997) 142.

[109] Reich, T., Bernhard, G., Geipel, G., Funke, H., Hennig, C., Rossberg, A., Matz, W., Schell, N., Nitsche, H., Radiochim. Acta 88 (2000) 633.

[110] Reich, T., Amayri, S., Reich, Ta., Drebert, J., Jermolajev, A., Thoerle, P., Trautmann, N., Hennig, C., Sachs, S. Annual Report 2004, Forschungszentrum Rossendorf.

[111] Combes, J-M., Chisholm-Brause, Brown, G.E. Jr., Parks, G.A., Environ. Sci. Technol. 26 (1992) 376.

[112] Allen, P.G., Shuh, D.K., Bucher, J.J., Edelstein, N.M., Reich, T., Denecke, M.A., Nitsche, H., Inorg. Chem. 36 (1997) 4676.

[113] Denecke, M.A., Marquardt, Ch.M., Rothe, J., Dardenne, K., Jensen, M. J., Nucl. Sci. Technol., Suppl. 3 (2002) 410.

[114] Neck, W., Kim, J.I., Kanellakopoulos, B., Radiochim. Acta 56 (1992) 25.

[115] Duff, M.C., Hunter, D.B., Oji, L.N., Wilmarth, W.R. Characterization of uranium solids precipitated with aluminosilicates, WM'04 Conference, 29 Febr-4 March 2004, Tuscon, Arizona, available at at http://www.osti.gov/bridge.

[116] Sylwester, E.E., Hudson, E.A., Allen, P.G., Geochim. Cosmochim. Acta, 64(14) (2000) 2431.

[117] Reich, T., Moll, H., Arnold, T., Denecke, M.A., Hennig, C., Geipel, G., Bernhard, G., Nitsche, H., Allen, P.G., Bucher, J.J., Edelstein, N.M., Shuh, D.K., J. Electron Spectroscopy and Related Phenomena 96 (1998) 237.

[118] Reich, T., Moll, H., Denecke, M.A., Geipel, G., Bernhard, G., Nitsche, H., Allen, P.G., Bucher, J.J., Kaltsoyannis, N., Edelstein, N.M., Shuh, D.K., Radiochim. Acta 74 (1996) 219.

[119] Wahlgren, U., Moll, H., Schimmelpfennig, B., Maron, L., Vallet, V., Gropen, O.J., Phys. Chem. A 103 (1999) 8257.

[120] Allen, P.G., Shuh, D.K., Bucher, J.J., Edelstein, N.M., Palmer, C.E.A., Silva, R.J., Nguyen, S.N., Marquez, L.N., Hudson, E.A., Radiochim. Acta 75 (1996) 47.

[121] Allard, T., Ildefonse, P., Beaucaire, C., Calas, G., Chem. Geology 158 (1999) 81.

[122] Farges, F., Ponader, C.W., Calas, G., Brown, G.E. Jr., Geochim. Cosmochim. Acta 56 (12) (1992) 4205.

[123] Walter, M., Arnold, Th., Geipel, G., Scheinost, A., Bernhard, G. J., Colloid Interf. Sci. 282(2) (2005) 293.

[124] Moyes, L.N., Parkman, R., Charnock, J.M., Vaughan, D.J., Livens, F.R., Hughes, C.R., Braithwaite, A. Environ. Sci. Technol. 34 (2000) 1062.

[125] Bargar, J.R., Reitmeyer, R., Lenhart, J.J., Davis, J.A., Geochim. Cosmochim. Acta 64 (16) (2000) 2737.

[126] Kent, D.B., Davis, J.A., Anderson, L., Rea, B., Coston, J., Geochim. Cosmochim. Acta 66/17 (2002) 3017.

[127] Cernochova, K, Mathur, J., Choppin, G.R., Radiochim. Acta 93 (2005) 733.

[128] Read, D., Ross, D., Sims R.J., J. Contam. Hydrol. 35 (1998) 235.

[129] Katz, J.J., Seaborg, G.T., Morss, L.R. The Chemistry of the Actinide Elements, Vol.1., Chapmann and Hall Ltd, London 1986.

[130] Nagy, N. M., Konya, J., Wazelischen-Kun, G., Coll. Surf. A: Physicochem. Eng. Eng.Aspects 152 (1999) 245.

[131] Lindsay, W.I. Chemical Equilibria in Soils, Wiley-Interscience, New York, 1979.

[132] Plaschke, M., Roemer, J., Klenze, R., Kim, J.I., Surf. Interface Anal. 30 (2000) 297.

[133] Neck, V., Fanghänel, Th., Kim, J.I, Aquatische Chemie und Thermodynamische Modellierung von trivalenten Actiniden, FZKA-Report 6110, Forschungszentrum Karlsruhe, 1998.

[134] Sakuragi, T, Stao, S., Kozaki, T., Mitsugashira, T., Hara, M., Suzuki, Y., J. Radioanal. Nucl. Chem. 265(3) (2005) 349.

[135] Neck, V., Kim, J.I., Radiochim. Acta 89 (2001) 1.

[136] Kim, M.A., Panak, P.J., Breban, D., Priemyshev, A., Yun, J.I., Kim., J.I., submitted to Coll. Surf. A: Physiochem. Eng. Aspects.

[137] Panak, P.J., Kim, M.A., Yun, J.I., Kim., J.I., Fanghänel, Th. 10th International Conference on Chemistry and Migration Behaviour of Actinides and Fission Products in the Geosphere, Avignon, France, 18-23 September 2005.

Eidesstattliche Erklärung

Ich erkläre hiermit, dass ich die vorgelegte Dissertation selbst verfasst und mich keiner anderen als der von mir ausdrücklich bezeichnerten Quellen und Hilfen bedient habe.

Domnica Cristina Breban